Report No. IITRI-U6003-19
(Final Report)

INVESTIGATION OF LIGHT SCATTERING IN HIGHLY REFLECTING PIGMENTED COATINGS

Volume 2

National Aeronautics
and Space Administration

Report No. IITRI-U6003-19
(Final Report)

INVESTIGATION OF LIGHT SCATTERING IN HIGHLY REFLECTING PIGMENTED COATINGS

Volume 2
CLASSICAL INVESTIGATIONS; THEORETICAL AND EXPERIMENTAL

May 1, 1966, to September 30, 1966

Contract No. NASr-65(07)
IITRI Project U6003

G. A. Zerlaut, S. Katz,
V. Raziunas, and M. Jackson

of

IIT RESEARCH INSTITUTE
Technology Center
Chicago, Illinois 60616

for

National Aeronautics and Space Administration
Office of Advanced Research and Technology
Washington 25, D.C.

Copy No. ____

October 1966

FOREWORD

This is Volume II of three volumes of Report No. IITRI-U6003-19 (Final Report) of IITRI Project U6003, Contract NASr-65(07), entitled "Investigation of Light Scattering in Highly Reflecting Pigmented Coatings." This report covers the period from May 1, 1963, to September 30, 1966.

The following Quarterly Reports were issued:

IITRI-C6018-3	October 11, 1963
IITRI-C6018-6	January 29, 1964
IITRI-C6018-8	May 5, 1964
IITRI-C6018-11	September 5, 1964
IITRI-C6018-12	December 21, 1964
IITRI-C6018-13	March 10, 1965
IITRI-C6018-14	May 13, 1965
IITRI-C6018-15	August 9, 1965
IITRI-U6003-16	November 9, 1965
IITRI-U6003-17	February 28, 1966
IITRI-U6003-18	May 3, 1966

Because of a divisional reorganization and the accompanying administrative changes, the IITRI number designating this project was changed from C6018 to U6003 on September 1, 1965. The Quarterly Report issued on November 9, 1965 was the first report to bear the new number. Project administration and technical organization were not affected in this change.

The project was under the technical direction of the Research Projects Laboratory of the George C. Marshall Space Flight Center, and Mr. Daniel W. Gates was the cognizant technical manager. The contract was administered by Mr. James J. Gangler of the Office of Advanced Research and Technology, National Aeronautics and Space Administration.

Major contributors to the program were: G. A. Zerlaut, project leader; Dr. S. Katz, theoretical (classical) light-scattering studies; Dr. B. H. Kaye, theoretical Monte Carlo and statistical studies; V. Raziunas, experimental (classical) studies on silver bromide suspensions; M. R. Jackson, experimental studies and statistical analyses; and H. Iglarsh,

preparation of random models. Administrative supervision was provided by Dr. T. H. Meltzer, Manager, Polymer Research.

Experimental data are recorded in Logbooks C13906, C14085, C14644, C16369, and C16765.

Respectfully submitted,

G. A. Zerlaut
Group Leader
Polymer Research

Approved by:

T. H. Meltzer
Manager
Polymer Research

GAZ/rmc

ABSTRACT

INVESTIGATION OF LIGHT SCATTERING
IN HIGHLY REFLECTING PIGMENTED COATINGS
Volume 2
CLASSICAL INVESTIGATIONS; THEORETICAL AND EXPERIMENTAL

The light-scattering theory pertinent to three basic types of "pigmented" systems was reviewed: (a) systems with real refractive indices in which $k = 0$, $n^* = n$, and the particle is transparent at that wavelength (k is proportional to the absorption coefficient), (b) systems with complex refractive indices in which both k and n are finite numbers and the particle both absorbs and scatters incident light, and (c) systems in which the complex refractive index, n^*, approaches infinity according to either $n \to \infty$ or $k \to \infty$ and the surface is perfectly reflecting at that wavelength. Application of classical theory to the multiple-scattering problem was essentially confined to theoretical films of spherical particles of real refractive index. Models were therefore proposed and tested by using applicable theory.

Experimental studies of silver bromide dispersions were attempted in order to establish relationships between both inherent (refractive index, etc.) and induced (film thickness, concentration, etc.) optical properties of the films. The experiments were limited to reflectance and transmittance measurements of various silver bromide suspensions (i.e., both liquid and solid suspensions).

Optical properties of suspensions of particles having narrow size distributions were compared with bimodal mixtures of these sizes. The data indicated that (a) particles of two sizes (a bimodal mixture) acted as independent scatterers in dilute solutions, (b) particles within thin concentrated films (of up to four layers) tended to act as independent scatterers, (c) an actual increase in transmittance at wavelengths corresponding to the first scattering maximum occured with increasing concentration of particles in dilute gelatin suspensions,

(d) the optical properties predicted from single-particle size measurements were in general agreement with those observed experimentally on bimodal mixtures in concentrated films, (e) the back-scatter coefficient of thin films tended to be slightly higher than that of thicker ones, and (f) the back-scatter intensity obtained from bimodal mixtures was less than that predicted from measurements of monodisperse films.

These last observations tend to support the "ideal" coating model that was subsequently proposed. This model, which consists of several layers of ever-decreasing particle size, was not tested because of difficulties in obtaining colorless sized fractions of model pigments.

TABLE OF CONTENTS

		Page
I.	Introduction	1
II.	Classical Light-Scattering Theory	2
	A. Introduction	2
	B. Concept of Light Scattering by Particles	2
	1. Transparent Isotropic Particles	3
	2. Partially Absorbing Spheres	8
	3. Totally Reflecting Spheres	13
	C. Application of Classical Theory to Multiple Scattering	15
	1. Introduction	15
	2. General Considerations	17
	3. Theoretical Films of Spherical Particles of Infinite Refractive Index	18
	4. Theoretical Films of Spherical Particles of Real Refractive Index	22
III.	Experimental Studies of Silver Bromide Dispersions	29
	A. Introduction	29
	B. Experimental Procedures	30
	1. Apparatus	30
	2. Preparation of Monodisperse AgBr Precipitates	30
	C. Results and Discussion	39
	1. Measurements of Particle Size and Concentration	39
	2. Secondary Oscillations in Scattering by Polystyrene Spheres	44
	3. Transmittance of Suspensions Containing Two Particle Sizes	44
	4. Transmittance of Concentrated Monodisperse Suspensions in Thin Films	50
	5. Transmittance and Reflectance Properties of Concentrated Bimodal Suspensions in Thin Films	59
	6. Optical Properties of Films of Various Thicknesses	68
	7. Optical Properties of Flocculated Dispersions	77
	D. Summary and Conclusions	77

IV. Verification of Multilayer Model of Paint Film 83

V. Characterization of Optical Properties of Mixed Powders 85

A. Description of the Reflectometer 85

B. Preparation of Mixed Powders 85

C. Experimental Results 89

D. Discussion 92

References 95

LIST OF TABLES

TABLE		Page
1	Light-Scattering Parameters for Totally Reflecting Spheres	19
2	Attenuation of Light by a Film of Particles of 1-μ Radius and Infinite Refractive Index at a Concentration of $6.7 \times 10^8/cm^2$	20
3	Conditions for Maximum Scattering by 1-μ Transparent Particles	26
4	Scattering Properties of 1-μ Particles of Various Refractive Indices at Wavelengths Corresponding to Maximum Scattering Cross Sections	28
5	Concentration of 1-μ Particles and Film Thickness Required to Attenuate the Incident Signal to 1%	28
6	Preparation of AgBr Suspensions	32
7	Concentration Measurements in Water Suspensions	43
8	Amplitude of the Scattering Extrema as a Function of Path Length	57
9	Thickness and Concentration of AgBr Films	60
10	Reflection from Titanium Dioxide on White Filters	89
11	Reflection from Titanium Dioxide on Black Filters	90

LIST OF FIGURES

FIGURE		Page
1	Total Mie Scattering Coefficient for Refractive Indices of 1.33 and 1.48	7
2	Radial Distribution of Intensity of Light Scattered by Spherical Particles	9
3	Extinction (K_e), Absorption (K_a), and Scattering (K_x) Coefficients for $m = 1.27-1.37^a i$	12
4	Variation of Extinction Coefficient for a Spherical Particle as the Imaginary Part of the Refractive Index is Varied for $m = 1.29(1 - ik)$	12
5	Radial Scattering Diagram for Very Small Totally Reflecting Spheres	14
6	Total Scattering Diagram for Totally Reflecting Spheres	14
7	Transmission for 1-μ-Radius Spheres When $m = \infty$	21
8	Limits of Forward- and Back-Scatter in Films	23
9	Crystal-Growth Apparatus	31
10	Electron Micrographs of AgBr Particles	33
11	Particle-Size Distribution for Batch 25	34
12	Particle-Size Distribution for Batch 26	35
13	Particle-Size Distribution for Batch 28	36
14	Particle-Size Distribution for Batch 30	37
15	Particle-Size Distribution for Batch 31	38
16	Transmittance of AgBr Suspensions in Water	41
17	Particle-Size Measurements from Light Scattering	42
18	Electron Micrographs of Monodisperse Polystyrene Spheres	45
19	Transmittance of Polystyrene Spheres in Suspensions of Various Refractive Indices	46
20	Transmittance of Dilute Suspensions of AgBr Mixtures (Batches 28 and 30)	47
21	Transmittance of Dilute Suspensions of AgBr Mixtures (Batches 25 and 30)	48
22	Transmittance of Dilute Suspensions of AgBr Mixtures (Batches 26 and 30)	49
23	Schematic Representation of Particle Packing in Gelatin Layers at Various Concentrations	52

FIGURE		Page
24	Scattering Extrema versus Thickness of Gelatin Suspensions	54
25	Transmittance of Concentrated Gelatin Films	55
26	Transmittance of Concentrated Gelatin Films	56
27	Schematic Diagram of the Overlap of Radial Intensity Functions	58
28	Optical Density of AgBr Suspensions (Batches 25 and 26)	61
29	Optical Density of AgBr Suspensions (Batches 25 and 30)	62
30	Theoretical (Mie) Density of AgBr Coatings	64
31	Optical Density of a Mixture of Batches 26 and 30	65
32	Back-scatter Intensity of AgBr Suspensions (Batches 25 and 26)	66
33	Back-scatter Intensity of AgBr Suspensions (Batches 25 and 30)	67
34	Optical Density at Various Thicknesses	69
35	Back-scatter Intensity at Various Thicknesses	70
36	Back-scatter Coefficient at Various Thicknesses	71
37	Thickness versus Back-scatter Intensity (Batch 25)	72
38	Back-scatter Intensity at Various Thicknesses (Batch 26)	73
39	Back-scatter Intensity at Various Thicknesses (Batch 30)	74
40	Thickness versus Back-scatter Intensity (Batch 26)	75
41	Thickness versus Back-scatter Intensity (Batch 30)	76
42	Optical Density of a Flocculated Coating	78
43	Back-scatter Coefficient of a Flocculated Coating	79
44	Schematic of Multilayer Coating and Resultant Optical Density of Layers	82
45	Optical Bench Reflectometer	86
46	Schematic Diagram of the Reflectometer	87
47	Schematic Diagram of the Detection Circuit	88
48	Reflectance of Rutile and Graphite Mixtures on a Nominally White Surface	91
49	Relationship between Angle α of Photocell and Visible Area of Deposit	93

INVESTIGATION OF LIGHT SCATTERING
IN HIGHLY REFLECTING PIGMENTED COATINGS
Volume 2
CLASSICAL INVESTIGATIONS; THEORETICAL AND EXPERIMENTAL

I. INTRODUCTION

The principal objective of this program was to apply light-scattering theory to particle arrays in order to explain the scattering behavior of polydisperse pigmented coatings, especially highly reflecting pigmented coatings. The program was aimed at a definition of light-scattering parameters associated with the maximum reflection of solar radiation.

This report, which is Volume 2 of the three-volume final report on the subject program, is concerned with that portion of the research dealing with classical light-scattering investigations. Both theoretical and experimental studies were performed during this phase of the work. This report and Volume 3, "Monte Carlo and Other Statistical Investigations," are summarized in Volume 1, "Summary Report."

The work reported in this volume consists of (a) a review of pertinent light-scattering theory, (b) an attempt to adapt classical methods to the study of theoretical films in order to elucidate the multiple-scattering problem, and (c) the generation of experimental data on the optical properties of carefully prepared arrays of silver bromide particles dispersed in a matrix (also aimed at the multiple-scattering problem).

The results of the studies that are within the scope of the classical investigations are discussed in this volume, while the significance of the results within the context of the overal program is discussed in Volume 1.

II. CLASSICAL LIGHT-SCATTERING THEORY

A. Introduction

The purpose of this portion of the study was to define the parameters controlling the scatter of light by small particles and thus to assist in the selection of optimum pigment materials for control of reflective and emissive properties of surfaces.

B. Concept of Light Scattering by Particles

When light or a related electromagnetic radiation impinges on a particle, the interaction leads to a redistribution of the radiant energy. The resulting radiation, which may be regarded as originating at the particle, is the light scattered by the particle. The particle is differentiated from the medium in which it resides by its refractive index. This refractive index may be real or complex -- a concept requiring further consideration.

Solution of the electromagnetic wave equation for transparent and absorbing material leads to a generalized expression for the refractive index. The expression includes terms for both refraction and absorption. For greatest generality, the refractive index is written as a complex number; the real part corresponds to the refractive index as it is usually written, and the imaginary part is related to the absorbing properties of the scatterer. The complex refractive index, n^*, is defined by:

$$n^* = n(1 - ik) \tag{1}$$

For a substance whose absorption coefficient is μ, it is shown (ref. 1) that K in Equation 1 is defined by:

$$\mu = \frac{4\pi k}{\lambda} \tag{1a}$$

where λ is the wavelength of light.

The n in Equation 1 is not analogous to the refractive index defined by Snell's law. Snell's law is not obeyed for transmitting media with absorption (ref. 2). In the limit,

as the absorption diminishes to zero and the medium becomes transparent, n^* becomes equal to n and Snell's law applies.

In addition to systems with real and complex refractive indices, a third case exists, that of a perfectly reflecting surface. Expressed in terms of electromagnetic theory, this condition can be described (ref. 3) as the upper limiting value of n, i.e., $n \to \infty$

Three special cases can therefore be considered:

(A) When $k = 0$, $n^* = n$, and the particle is transparent at that wavelength.

(B) When k is a finite number, the particle both scatters and absorbs incident light. The absorption coefficient, μ, is related to k:

$$k = \frac{\lambda\mu}{4\pi}$$

(C) n^* can approach infinity by one of two routes:

$$n \to \infty$$

or

$$k \to \infty$$

The total scattering of light by spherical particles is therefore a function of three parameters: the particle size, the refractive index of the particle in relation to the surrounding medium, and the wavelength of the light.

Throughout the discussion, incoherent unpolarized incident light is considered and the scattering is limited to light with the same wavelength as that of the incident light.

1. Transparent Isotropic Particles

Historically, the scattering of light by small particles was first discussed quantitatively by Rayleigh (ref. 4). He considered the case of spherical particles much smaller than the wavelength of the scattered light. For these transparent spherical particles, the amount of light of wavelength λ scattered by a sphere of radius r per unit intensity of illumination (unit energy/unit area of cross section) is:

$$S = 24\pi^3 \left(\frac{n^2 - 1}{n^2 + 2}\right)^2 \frac{V^2}{\lambda^4} \qquad (2)$$

where

V is the volume of the particle

n is the refractive index of the particle

S is the effective scattering area or the scattering cross section of one sphere.

Equation 2 applies to very small particles of molecular dimensions without regard to shape. It is applicable to spherical particles when $r < 0.1\ \lambda$. The familiar relationships for Rayleigh scattering, which state that the scattered energy of small particles varies directly as the sixth power of the particle radius and inversely as the fourth power of the wavelength, are evident in Equation 2.

Mie (ref. 5) examined the general problem in which no restriction is applied to the particle size. His analysis employed classical electromagnetic theory to examine the diffraction of a plane wave by a sphere of any composition. In Mie's treatment, the possibility of conductivity or absorption in both the external medium and the sphere is considered by assigning to each a complex index of refraction. We shall follow the usual practice and consider only a real refractive index in the external medium. The discussion here is limited to spheres of real finite refractive index. Other cases will be examined later.

When a beam of light passes through a monodisperse suspension of spherical particles of radius r, the transmission, T, is:

$$T = e^{-K\pi r^2 nL} \qquad (3)$$

where

n is the particle concentration per unit volume

L is the path length.

K is the energy scattered per unit area of particle cross section per second. K is equal to the scattering area, S, divided by πr^2. It is described by various authors as the effective scattering cross section, the total Mie coefficient, and the extinction cross section. The extinction cross section is a somewhat more general term than the scattering cross section, and only in the case of nonabsorbing particles is it equivalent to the scattering cross section.

Mie's analysis defined K as the sum of a convergent series:

$$K(\alpha,n) = \frac{2}{\alpha^2} \sum_{m=1}^{\infty} (2m + 1) \left[|a_m|^2 + |b_m|^2 \right] \qquad (4)$$

where

n is the refractive index of the particle in the medium

$\alpha = \frac{2\pi r}{\lambda}$, a size parameter

$\beta = n\alpha$

r is particle radius

λ is the wavelength of light.

The vertical lines in Equation 4 indicate that the absolute value of the complex argument is to be used; a_m and b_m are complex numbers termed amplitude functions. They are:

$$a_m = (-1)^{m+1/2} \frac{S'(\beta)\ S(\alpha) - nS'(\alpha)\ S(\beta)}{S'(\beta)\ \phi(\alpha) - n\phi'(\alpha)\ S(\beta)} \qquad (4a)$$

$$b_m = (-1)^{m+3/2} \frac{nS'(\beta)\ S(\alpha) - S'(\alpha)\ S(\beta)}{nS'(\beta)\ \phi(\alpha) - \phi'(\alpha)\ S(\beta)} \qquad (4b)$$

where

$$S(Z) = \frac{\pi Z}{2}^{1/2} J_{m+1/2}(Z)$$

$$\phi(Z) = S(Z) + iC(Z)$$

$$C(Z) = (-1)^m \frac{\pi Z}{2}^{1/2} J_{-m-1/2}(Z)$$

J represents a Bessel function of the indicated order, and the primed terms is the derivative with respect to Z.

It can be shown that Equation 4 reduces to Equation 2 for very small values of r; i.e., Rayleigh scattering is a limiting case of Mie scattering.

Representative plots of the total Mie coefficient, K, with respect to the parameter α for two refractive indices are reproduced in Figure 1. The first maximum is higher and is displaced toward the origin with increasing n.

A number of tabulations of K are available. Both Van de Hulst (ref. 3) and Penndorf (ref. 6) list compilations of data and also have extensive bibliographies of source material.

For many applications, the angular or radical distribution of the scattered energy is required. For unpolarized incident radiation of intensity, I_0, the radiation scattered in the direction θ (the angle between the incident and the scattered beam), is:

$$I(\theta,n) = \frac{I_0}{2}(i_1 + i_2) \tag{5}$$

The quantities i_1 and i_2 are intensity functions. They are proportional to the two mutually perpendicular plane polarized components of the light scattered by the particle in the direction θ. The intensity functions are:

$$i_1 = \left| \sum_{m=1}^{\infty} \frac{2m + 1}{m(m + 1)} \left(a_m \pi_m + b_m \tau_m\right) \right|^2 \tag{5a}$$

and

$$i_2 = \left| \sum_{m=1}^{\infty} \frac{2m + 1}{m(m + 1)} \left(a_m \tau_m + b_m \pi_m\right) \right|^2 \tag{5b}$$

Again, the vertical lines indicate that the absolute values of the complex arguments are to be used (a_m and b_m have the same values as before). π_m and τ_m are derivative functions of the corresponding Legendre polynomial, P_m, of order m.

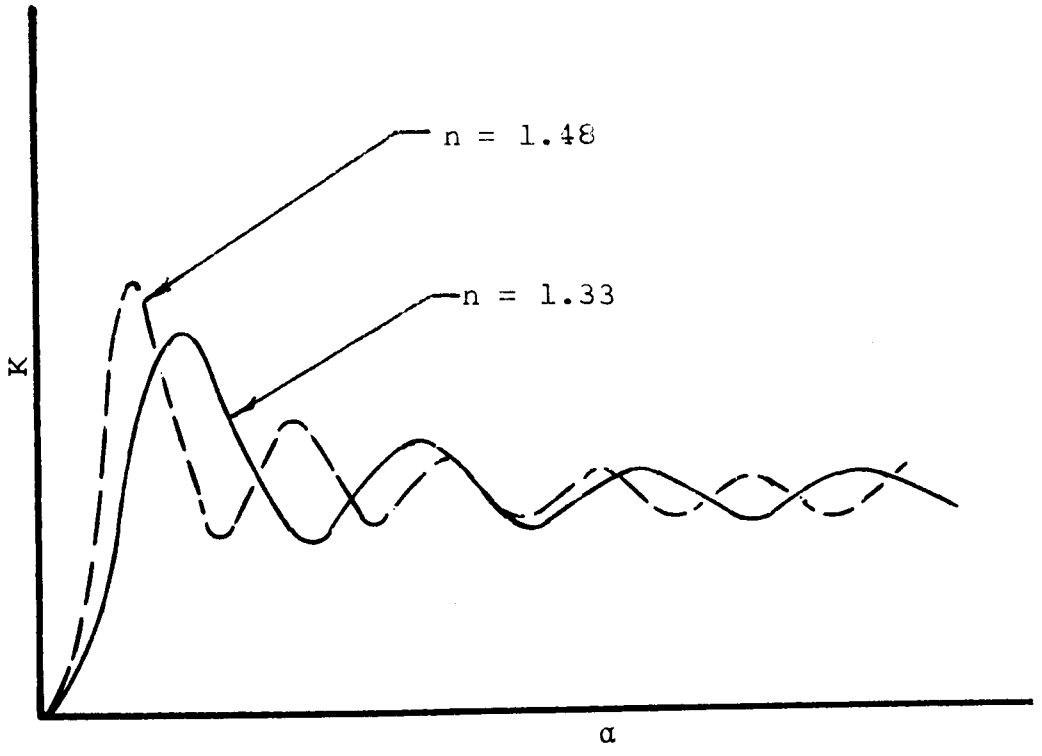

Figure 1

TOTAL MIE SCATTERING COEFFICIENT
FOR REFRACTIVE INDICES OF 1.33 and 1.48

Thus,

$$\pi_m = \frac{dP_m}{dx} \tag{5c}$$

and

$$\tau_m = \pi_m x - (1 - x^2)\pi'_m \tag{5d}$$

where $x = \cos\theta$.

Tables of amplitude functions have been prepared by Penndorf (ref. 6), Gumprecht and Sliepcevich (ref. 7), and others. Many authors, including Lowan (ref. 8), have tabulated the angular scattering functions for various values of the parameter α and various refractive indices. In the case of transparent scatterers, certain characteristics are noted. Maxima always occur in the forward- and back-scattered directions, and the intensities of these maxima are the same for both of the polarized components of scattering. Also, as the size of the particle increases with respect to the wavelength of the scattered light, the scattering in the forward direction increases very rapidly. Some representative angular scattering patterns are shown in Figure 2.

2. Partially Absorbing Spheres

The total scattering coefficient for a plane wave incident on a spherical particle is given by Mie as the sum of the convergent series:

$$K_s(\alpha,n) = \frac{2}{\alpha^2}\sum_{m=1}^{\infty}(2m+1)\left[|a_m|^2 + |b_m|^2\right] \tag{6}$$

Equations 6 and 4 are identical except for the use of subscripts with K, to emphasize the distinction between transparent and partially absorbing spheres. The total Mie extinction coefficient is:

$$K_e(\alpha,n) = \frac{2}{\alpha^2}\,\mathrm{Re}\sum_{m=1}^{\infty}(2m+1)\left(a_m + b_m\right) \tag{7}$$

Only the real parts of the amplitude functions, a_m and b_m, contribute to the extinction.

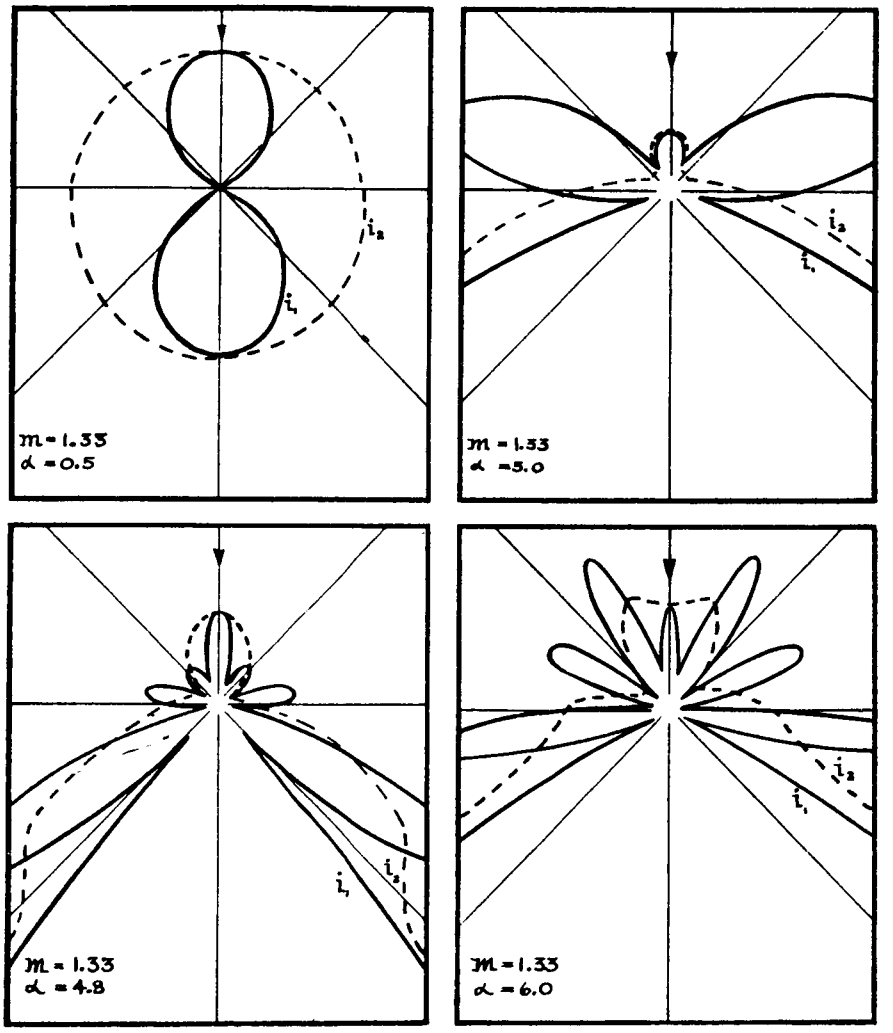

Figure 2

RADIAL DISTRIBUTION OF INTENSITY
OF LIGHT SCATTERED BY SPHERICAL PARTICLES

The extinction defines the attenuation of the incident beam by all causes. In the present case, the extinction includes both absorption and scattering, i.e., $K_e = K_s + K_a$, where K_a is the absorption coefficient. If the particle is a pure scatterer with no absorption, $K_e = K_s = K$, where K is the scattering coefficient of a transparent particle.

It is of interest to consider Equations 6 and 7 further. The influence of the complex term on the scattering properties of the particle is of importance. In addition, the physical significance of the complex number requires some examination. There are a number of compilations of the scattering of light by complex scatterers, and a few publications describe the effect of progressive change in the complex term of the scattering cross section. Some numerical magnitudes of the complex term for several materials will be discussed first.

A moderately absorbing material, such as a tinted glass, has a very small imaginery term. A fairly dense black glass, which transmits only 8% of the incident intensity through 1-mm thickness, has a refractive index of 1.5-0.001 i. This absorption is so slight for particles in the micron size range that the absorption can be neglected. Metals at optical frequencies have refractive indices whose coefficients are both near unity. Thus, the refractive index of iron in the visible region, at $\lambda = 0.44\ \mu$, is 1.27-1.37 i. At longer wavelengths the refractive index terms of metals become very large and almost equal. In the infrared, at 10 μ, the refractive index of platinum is 37-41 i. This is almost a totally reflecting material. Penndorf (ref. 9) has compiled a bibliography of numerical computations on the scattering and absorption of electromagnetic radiation for spherical particles.

The complex attenuation by water in the infrared was studied by Johnson and his associates (ref. 10) and by Stephens (ref. 11), among others. Stephens examined the total attenuation, the scattering, and the absorption cross sections of particles of diameters between 1.0 and 10 μ in the wavelength range between 4 and 90 μ.

There are very few compilations of radial scattering data for substances with complex refractive indices. Kerker (ref. 12) describes the total and radial scattering of light by mercury droplets whose refractive index at 0.546 μ is 1.46-4.30 i.

In Figure 3, plots of scattering, absorption, and total extinction cross sections for iron particles at 0.44 μ are shown. It was noted that the complex refractive index of iron at this wavelength is 1.27-1.37 i. This plot is of interest because it shows the relative contributions of scattering and absorption to the total attenuation. At small values of α, absorption is the principal contributor to total attenuation. At $\alpha = 2$, the attenuations due to absorption and scattering are about equal, and beyond that, scattering predominates. Since $\alpha = 2\pi\ r/\lambda$, scattering predominates at a wavelength of about 0.5 μ for particles greater than 0.3-μ diameter.

The effect of the gradual variation of the imaginary part of the complex refractive index on the total extinction coefficient has been computed by Johnson, Eldrige, and Terrell (ref. 10). Figure 4 shows a portion of their calculations at low values of α for a series of refractive indices of the form $1.29(1 - ik)$ as K varies from 0 to ∞. The progressive changes in the extinction coefficient, K_e, with the changes in the imaginary part of the refractive index are clearly illustrated. In their extended analysis, Johnson, Eldrige, and Terrell noted that when the imaginary coefficient, k, is less than 0.10, the extinction curve oscillates as α increases. This recalls the scattering coefficient for nonabsorbing particles (Figure 1), which is the limiting case as $k \to 0$. At higher values of k, the oscillations after the first maximum disappear and the extinction coefficient converges smoothly to the asymptotic value.

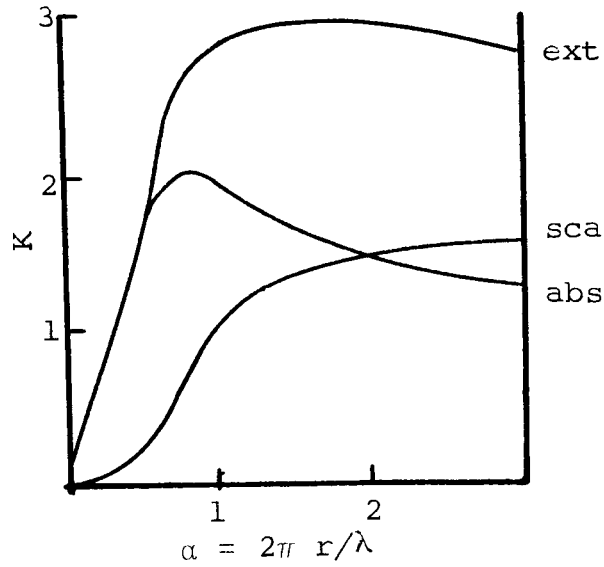

Figure 3

EXTINCTION (K_e), ABSORPTION (K_a), AND SCATTERING (K_x) COEFFICIENTS FOR m = 1.27-1.37 i

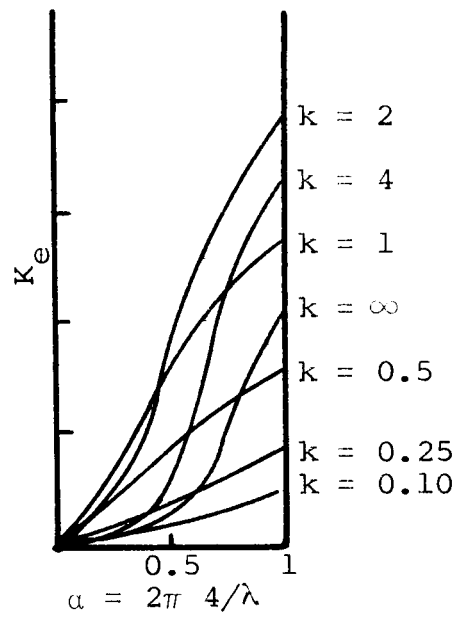

Figure 4

VARIATION OF EXTINCTION COEFFICIENT FOR A SPHERICAL PARTICLE AS THE IMAGINARY PART OF THE REFRACTIVE INDEX IS VARIED FOR m = 1.29(1 - ik)

Kerker's data (ref. 12) give the radial scattering intensities between 30 and 150°. Aden (ref. 13) has analyzed the back-scattering of electromagnetic waves from spheres with complex refractive indices. Aden's procedure, which is especially adaptable to materials with complex refractive indices, includes a comparison of theoretical scattering in the region $0.74 \geq \alpha \geq 5.90$ and experimental data obtained on water droplets at microwave frequencies.

3. Totally Reflecting Spheres

The case of spheres whose refractive index, m, equals infinity has been studied thoroughly because of its relative simplicity compared to the cases considered previously. The physical meaning of an infinite refractive index is that there is no penetration of the medium by light. The problem can be considered as the limiting value either as the real or as the imaginary part of the refractive index increases to infinity; the results are the same in both cases.

Since a total reflector inplies no penetration of the particle by incident rediation, Rayleigh scattering does not apply for even the smallest particles. The radial scatter for very small particles is shown in Figure 5. The backscattered intensity predominates over the forward scatter by a factor of 9/1.* Radial scattering data for total reflectors for values of α between 0.5 and 10 are given by van de Hulst (ref. 3). At larger values of α, above about 1.4, the usual predominance of forward scatter over back scatter is noted.

The total scatter of light by particles with infinite refractive index is shown in Figure 6. The scattering, or extinction, coefficient, which is the same in the absence of absorption, reaches a maximum slightly greater than the asymptotic value.

---

*One characteristic of true Rayleigh scattering is the equal intensity of the forward- and backscattered radiation.

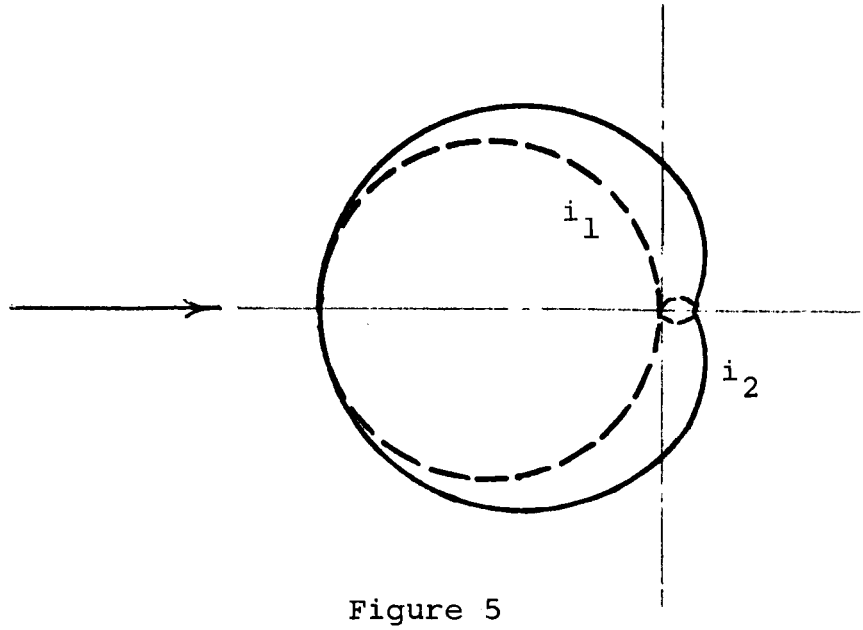

Figure 5

RADIAL SCATTERING DIAGRAM
FOR VERY SMALL TOTALLY REFLECTING SPHERES

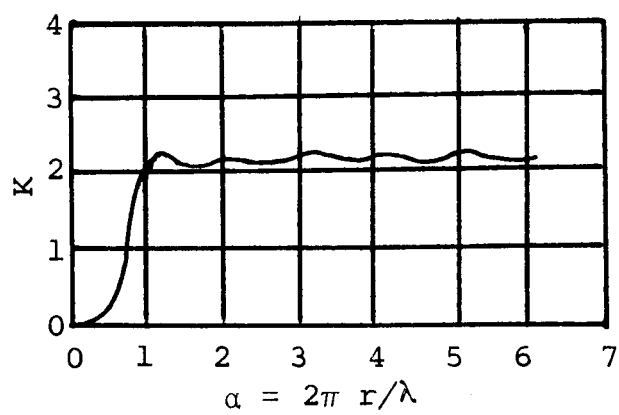

Figure 6

TOTAL SCATTERING DIAGRAM
FOR TOTALLY REFLECTING SPHERES

Very small particles with infinite refractive indices are not true Rayleigh scatterers. The radial distribution of the scattered intensity is never symmetrical, but instead the back-scattered intensity at 180° from the forward direction is nine times the intensity of the forward-scattered light. This is a desirable condition for back-scattering, of course. Unfortunately, very small totally reflecting particles have small effective cross sections and are not much more efficient light scatterers than are Rayleigh scatterers of comparable size. With increasing particle size, the total scattering efficiency increases to a maximum slightly in excess of 2 as $\alpha(2\pi\ r/\lambda)$ approaches unity and remains near that value as α increases (Figure 6).

Radial scattering data for larger totally reflecting particles have been given by van de Hulst. The strong attenuation of the back-scattered signal that characterizes transparent particles is not present here and, as might be expected, a large component of energy is present in the back-scattered radiation (ref. 3). In comparison with transparent particles, therefore, an array of totally reflecting particles should produce a substantial attenuation with a relatively small concentration.

For the present application the optimum particle appears to be a particle with an infinite refractive index. In the next sections, experimental approximations to such materials are discussed, and an attempt has been made to construct a theoretical pigment film designed for selective transmission or rejection of different spectral regions.

C. Application of Classical Theory to Multiple Scattering

1. Introduction

In previous sections, we have discussed light-scattering theory with reference to single particles. Single-particle theory can be used to describe the light-scattering characteristics of a colloidal or aerosol suspension in which the

particles are very widely dispersed. For the present application of scattering theory to the design of a coating material, it becomes necessary to attempt to set a lower limit to the separation distance that still permits application of scattering theory.

The theoretical problem of computing the scattering of light by a multiple array of particles in terms of the interaction of an electromagnetic wave on a multiple discontinuity does not appear to have been analyzed rigorously. Van de Hulst (ref. 14) noted the problem in 1946 and commented then on its complexity. A number of references in the literature give an empirical or an estimated partial solution of the problem. Sinclair (ref. 15) suggested a spacing of 10 or preferably 100 times the radius of the particle for independent scattering. However, Berry (ref. 16) studied the scattering of light by cubic silver bromide crystals embedded in gelatin and reported that the approximation to single independent scattering appears to be quite satisfactory when the separation of the grain centers is more than about twice the grain size.

In previous reports, we defined the term S as the effective scattering area of a single particle. K, the scattering coefficient per unit cross-sectional area of the particle, is therefore equal to $S/\pi r^2$. Figure 1 (Section II-B-1) is a plot of K against the parameter $\alpha = 2\pi r/\lambda$ for several real refractive indices.

In the absence of a more exact procedure, it is proposed that for particles whose scattering coefficient, K, is greater than unity, the scattering cross section, S, governs the limit of particle spacing for effective application of light-scattering theory. The electromagnetic fields that define the scattering cross sections will interfere if the particles are spaced more closely. Also, in the case of very small particles when K is less than unity, the scattering cross section is smaller than the geometric cross section and the physical dimensions of the particle will dictate the limits of particle spacing.

2. General Considerations

We shall next consider the formation of a theoretical film consisting of a transparent matrix in which the light-scattering particles are embedded. Since the system is theoretical, it is possible to visualize such convenient factors as fully monodisperse particle assemblies, complete freedom of choice of refractive index, etc. The analysis is handicapped by the limited availability of numerical data. Total and radial scattering data are available for transparent spherical particles over a wide range of conditions. On the other hand, the information for fully reflecting particles with infinite refractive index is fragmentary, and only a few cases involving complex refractive indices have been computed. Practically no data exist for nonspherical particles, although a number of these appear to have some value in the present context.

In formulating this model, one should note that the Mie theory of light scattering was developed for the case of a parallel light beam impinging on an isolated particle. It has often been stated that the argument is applicable to particle clouds in which the separation distance is "large," and it has also been noted that the viewing optics must be located at "infinity." The second condition is realized adequately when the viewing distance is a few tens of wave-length equivalents separated from the scatterer. The first, the separation distance, is a problem of some magnitude in the present context, where we are attempting to replace a diffuse cloud with a close-packed array. This reservation emphasizes the necessity of careful scrutiny of the following operations, especially those involving the application of Mie theory to closely spaced arrays.

Some general relations of use here are noted:

Extinction per Single Particle. If I_0 is the intensity of the incident light, in watts per unit area, a sphere will intercept $K\pi r^2 I_0$ watts from the incident beam, where K, as before, is the scattering or scattering plus absorbing cross section of the particle and r is the radius of the particle. As noted previously, K is a function of the refractive index of the particle and of the wavelength of the light.

Scattering per Single Particle. The scattered intensity at a distance R from the particle in direction θ is equal to:

$$I_\theta = \frac{I_0 \lambda^2 (i_1 + i_2)}{8\pi^2 R^2} \tag{8}$$

where i_1 and i_2 are the polarized radial components of the scattered light as usually tabulated. In a medium containing n particles per unit volume, the scatter per unit volume is nI. The attenuation of the incident beam as it passes through a particulate array containing n particles per unit volume is:

$$I = I_0 e^{-K\pi r^2 nL} \tag{9}$$

where L is the length of the path through the particle cloud.

3. Theoretical Films of Spherical Particles of Infinite Refractive Index

The first system will consist of a suspension of spherical particles of refractive index $m = \infty$, i.e., perfectly reflecting surfaces. It should be recalled (Section II-C-1) that particles for which the ratio r/λ is very small have a very low effective cross section. At the other extreme, large particles show the usual preponderance of forward scatter over back scatter. Blumer (ref. 17) has computed the total and radial scatter for a number of cases. We shall examine the extinction conditions for the case where $\alpha = 0.5$.

$\alpha = 0.5$. The ratio of the back-scattered intensity of a single particle to the forward scatter is 9:1. Thus extinction of the incident beam in the forward direction is only slightly

compensated by forward scatter, so we shall omit consideration of forward scatter.

The values for α and K for totally reflecting spheres as cited by Blumer (ref. 17) are shown in Table 1.

Table 1

LIGHT-SCATTERING PARAMETERS FOR TOTALLY REFLECTING SYSTEMS

α	K
0.4	0.086
0.5	0.22
0.6	0.47
0.8	1.26
1.0	2.04
1.2	2.28

Equation 9 will be used for the case of an array of 1-μ-radius spheres. Since $\alpha = 2\pi r/\lambda$, then $\lambda = 12.5\ \mu$ when $\alpha = 0.5$.

Restating Equation 9 yields:

$$2.303 \log I_0/I = K\pi r^2 N \qquad (9a)$$

where N = nI. By replacing K and r with their indicated values and assigning I_0/I a value of 100, we can compute N, the number of particles, per unit area, required to attenuate the beam to 1%.

$$2.303 \log 100 = 0.218\pi(10^{-4})^2 N$$

Solving for N, we obtain:

$$N = 6.7 \times 10^8 \text{ particles/cm}^2$$

In a volume of 1 ml, this would correspond to an uniform lattice of particles with center-to-center distances of 10 μ. If we use a particle spacing of 4 μ in direction 1, i.e., 2 diameters, as suggested by Berry (ref. 16) as the limit for the application of scattering theory to closely spaced systems, the films would be 4 mm thick.

The calculation can be carried a stage further by determining the attenuation of light of other wavelengths by this film. By substituting the values for K corresponding to various wavelengths while keeping r equal to 1 μ, it is possible to determine I/I_0. Some representative values are shown in Table 2. It is seen that a film containing, per square centimeter, 6.7×10^8 particles of 1-μ radius and infinite refractive index will back-scatter all radiation below 12.5 μ and will be highly transparent to wavelengths at 21 μ and longer.

Table 2

ATTENUATION OF LIGHT BY A FILM OF PARTICLES OF 1-μ-RADIUS AND INFINITE REFRACTIVE INDEX AT A CONCENTRATION OF $6.7 \times 10^8/cm^2$

α	r, μ	K	I/I_0
0.3	21.0	0.028	0.48
0.4	15.6	0.086	0.16
0.5	12.5	0.22	0.01
0.6	10.4	0.47	1.6×10^{-5}
0.8	7.8	1.26	2.0×10^{-16}

A number of other systems have been computed, by using as the reference point the particle concentrations for α = 0.3, 0.8, and 1.0, at which the transmission is 1%. The results are shown in Figure 7. When α = 1, a film of 7.2×10^7 1-μ-radius particles/cm^2 will back-scatter 99% of the 6.28-μ wavelength radiation. All shorter wavelengths will be back-scattered, and the film will be transparent to longer wavelengths.

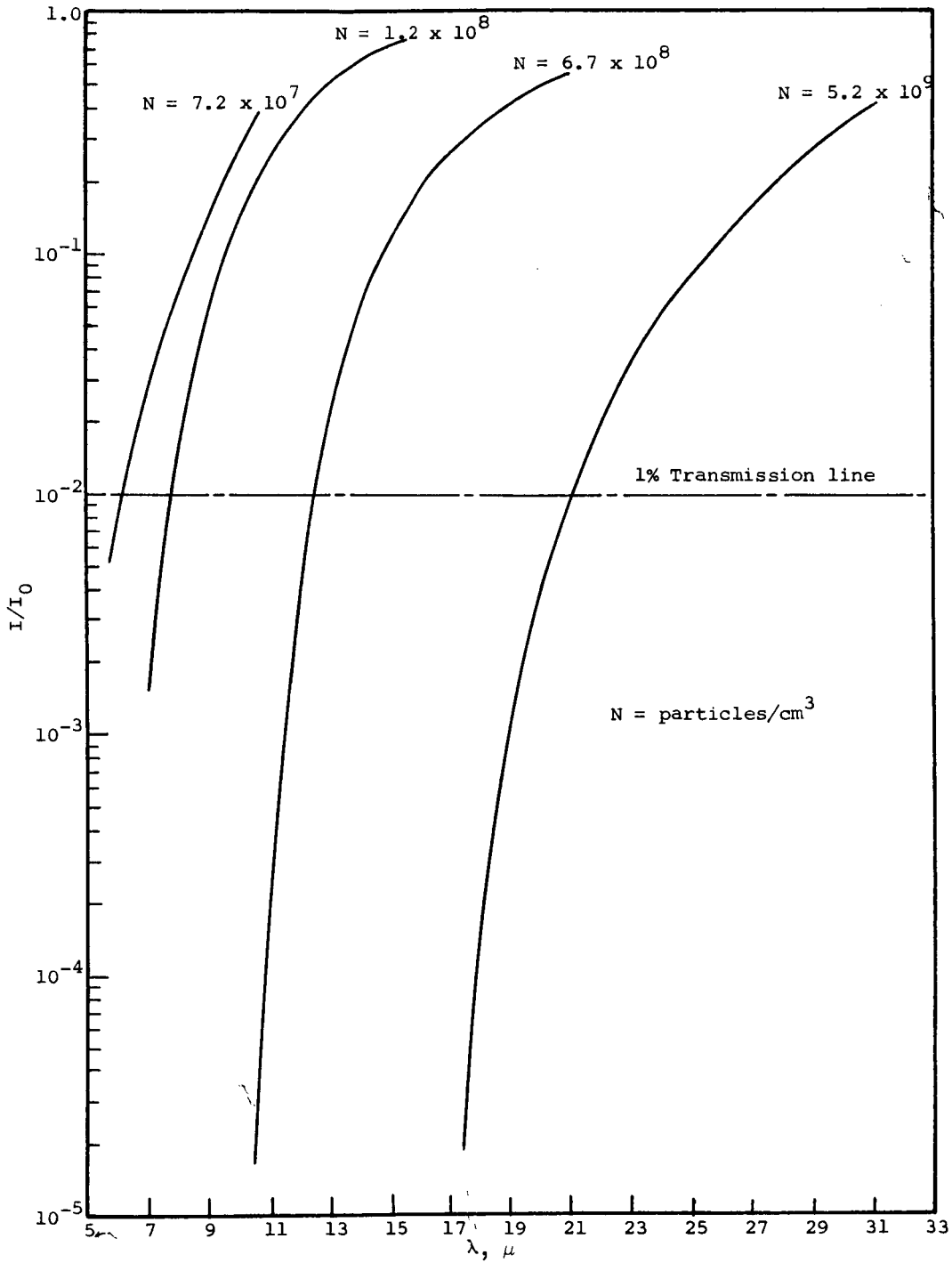

Figure 7

TRANSMISSION FOR 1-μ-RADIUS SPHERES WHEN m = ∞

4. Theoretical Films of Spherical Particles of Real Refractive Index

The system consisting of an array of monodisperse particles of infinite refractive index represents a theoretical limit that is approached but never reached in real systems. We will next present a parallel analysis of particle systems with real refractive index; i.e., all incident light energy is scattered, and none is retained by absorption.

The radial scattering intensity and the attenuation per individual particle are:

$$I_\theta = \frac{I_0 \lambda^2 (i_1 + i_2)}{8\pi^2 R^2} \tag{8}$$

$$I = I_0 e^{-K\pi r^2 N} \tag{10}$$

In the case of highly reflecting particles, only a small part of the energy incident on the particle undergoes forward scatter, and Equation 10 describes this attenuation very well. However, a large fraction of the energy is scattered in the forward direction by transparent particles. Equation 10 is satisfactory for attenuation of the forward beam in a long path with near-parallel optics, but in the case of a thin film all the energy in the forward direction within the critical angle (the angle of total reflection) is transmitted. This is illustrated in Figure 8, in which the index of refraction* is $1/\sin\theta$, and all light outside the cone subtended by the angle 2θ undergoes either back scatter or total reflection.

An exact determination of the forward-scatter component is obtained by integration of the radial scattering function over the solid angle of forward scatter. This is a formidable task, and we will not undertake its rigorous solution. Instead, approximation methods will be used by employing averaged values of the radial scattering terms. Lowan's modified form of Figure 8 is:

---

*Note that this is the refractive index between the film and air, not the refractive index of the particle.

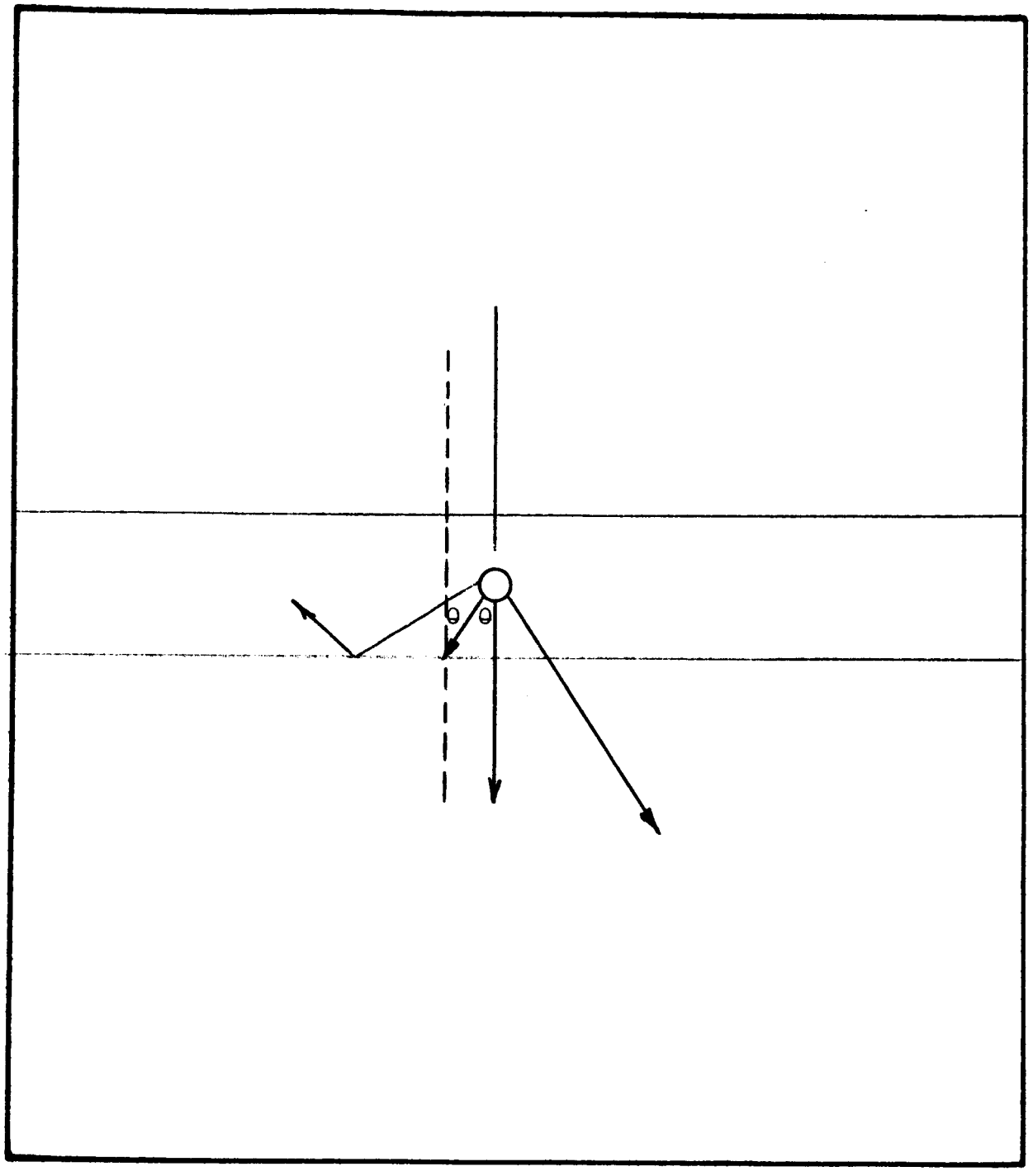

Figure 8

LIMITS OF FORWARD- AND BACK-SCATTER IN FILMS

$$I_\theta = \frac{I_0 \lambda^2 \ (i_1 + i_2)}{8\pi^2} \qquad (8a)$$

where

I_0 is the incident energy per unit area

I_θ is the scattered intensity per unit solid angle in the direction θ

i_1 and i_2 are the angular distribution functions for the two plane polarized components scattered by a transparent particle illuminated by natural light.

Consider first a system of particle embedded in a film. The refractive index of the particles in the medium is 1.44, and the angle of total reflection (Figure 8) is 45°. The forward-scattered cone will therefore subtend an angle of 90°, i.e., a solid angle of 1.84 steradians. The following parameters apply.

The scattering cross section, K, has its maximum value of 4.0 when $\alpha = 4.8$ and $m = 1.44$ (ref. 1). Consider the case for spheres of 1-μ radius: since $\alpha = 2\pi \ r/\lambda$, then $\lambda = 1.31 \ \mu$. By applying a weighted average to the radial scattering data of Lowan (ref. 8), the averaged value for i_1 and i_2 in the forward solid angle of 1.84 steradians is about 260. Then, from Equation 8a, the scattered intensity per unit solid angle in the forward cone is 5.6×10^{-8}, where the incident energy is unity per unit area, or 10.3×10^{-7} for a solid angle of 1.84.

Also, the scattering cross section of a particle of 1-μ radius is $K\pi r^2 = 12.6 \times 10^{-8}$ cm^2, and the total scattered intensity is therefore 12.6×10^{-8} energy units. Then the back-scattered energy by one particle of 3.14×10^{-8} cm^2 cross section will be $(12.6 - 10.3) \times 10^{-8} = 2.3 \times 10^{-8}$.

Thus K, the attenuation cross section of a particle for <u>all</u> energy, which is not the same as the cross section for the incident beam alone, is given by $\left(2.3 \times 10^{-8} \ / \ 3.4 \times 10^{-8}\right)$ and, in this case, is 0.73. This low figure emphasizes the preponderance of forward-scatter with this material.

Now the attenuation of an incident beam by a multiple array of particles can be computed. The parameters are the same as those used above, and no interference by adjacent particles is assumed. Then the attenuation is:

$$2.303 \log I_0/I = K \pi r^2 N$$

By replacing K and r by their indicated values (0.73 and 1, respectively), we can determine N, the number of particles per unit area required to attenuate the incident beam to 1%:

$$2.303 \log 100 = 0.73(10^{-4})\pi^2 N$$

Solving:

$$N = 2.0 \times 10^8 \text{ particles/cm}^2$$

In a film of 1-cm^2 area with a mean particle spacing of 10 μ, i.e., 5 particle diameters spacing between adjacent particles, the film will be about 2.0 mm thick.*

In the application of this method, the refractive index of the particles is referred to the surrounding medium, which is the film material. The critical angle for total reflection is a function of the refractive index of the film in its surrounding medium, i.e., air or vacuum. In the example discussed in the previous paragraph, the critical angle of the film was 45°, and spherical particles of 1-μ radius had a refractive index of 1.44 in the medium. Here the effect of changing the refractive index of the particles and leaving all other parameters unchanged is discussed. Thus:

Angle of total reflection is 45°.

Forward-scattering cone subtends 1.84 steradians.

Particle radius is 1 μ.

The maximum scattering cases, in which m = 1.33, 1.55, and 2.00, is examined by using the radial scattering data of Lowan (ref. 8). The case in which m = 1.44 is also reviewed.

---

*This calculation was made with no attempt to correct for the boundary condition in which particles are very close to the totally reflecting surface.

Conditions for maximum scatter as a function of the parameter $\alpha = 2\pi r/\lambda$ have been given by Sinclair and LaMer (ref. 1). For the cases indicated, the conditions shown in Table 3 apply.

Table 3

CONDITIONS FOR MAXIMUM SCATTERING BY 1-μ TRANSPARENT PARTICLES

Refractive Index, m	Maximum Scattering Cross Section, K	$2\pi r/\lambda$ (μ)	λ, m
1.33	3.9	6.3	1.0
1.44*	4.0	4.8	1.31
1.55	4.4	3.6	1.74
2.00	5.2	2.4	2.62

*The data of Section II-C-4 were recalculated from comparison in the present series.

The radial scattering intensity is:

$$I_\theta = \frac{I_0 \lambda^2 (i_1 + i_2)}{8\pi^2 R^2} \tag{8}$$

where

I_0 is the incident energy per unit area

I_θ is the scattered intensity per unit solid angle

i_1 and i_2 are the angular distribution functions for the two plane polarized components scattered by a transparent particle illuminated by incoherent light of wavelength λ.

By using Lowan's data, the scattered intensities in the forward-directed cone of 90° included angle were integrated numerically by minimizing the average intensities of the scattered light in the 10° zones between 0 and 50°. These scattered intensities correspond to the i_1 and i_2 term of Equation 8 and can be applied in Equation 8 to determine the fraction of incident energy if scattered into the forward cone.

By comparison with the total scattering cross section, the back-scatter for one particle is determined; and the attenuation, K_a, can be determined as a function of the particle's true cross section. All these calculations have been made and are tabulated in Table 4.

The attenuation cross sections, K_a, are then used to determine the concentration needed to attenuate an incident source by a standard amount. A multiple array of particles that do not interfere with each other is assumed.

The attenuation of a number of particles is:

$$I = I_0 e^{-K_a \cdot \pi r^2 N} \tag{11}$$

where I is the intensity of the emergent beam and the other terms are as defined previously. Equation 11 is conveniently stated in the form:

$$2.303 \log I_0/I = K_a \pi r^2 N \tag{11a}$$

For a given attenuation, N is determined when the appropriate values are assigned to K_a and r. By using the data of Table 4 and assigning a value of 100 to I_0/I, i.e., attenuating the source to 1%, the values shown in Table 5 are obtained. The tabulated data emphasize the increased attenuation efficiency of particles with high refractive indices.

Table 4

SCATTERING PROPERTIES OF 1-μ PARTICLES OF VARIOUS REFRACTIVE INDICES AT WAVELENGTHS CORRESPONDING TO MAXIMUM SCATTERING CROSS SECTIONS

Refractive Index, m	Scattering Cross Section, K	λ, μ	$i_1 + i_2$	$I_f \times 10^8$	Total Scattered Intensity, $\times 10^8$	Back-Scattered Intensity, $\times 10^8$	Attenuation Cross Section, K
1.33	3.9	1.0	440	10.2	12.3	2.1	0.67
1.44	4.0	1.3	260	10.3	12.6	2.3	0.73
1.55	4.4	1.7	155	10.9	13.8	2.9	0.92
2.00	5.2	2.6	43	6.9	16.4	9.5	3.0

Table 5

CONCENTRATION OF 1-μ PARTICLES AND FILM THICKNESS REQUIRED TO ATTENUATE THE INCIDENT SIGNAL TO 1%

Refractive Index, m	Attenuation Cross Section, K_a	Particle Radius, μ	Particles/cm^2, N	Film Thickness,[a] mm
1.33	0.67	1	2.2×10^8	2.0
1.44	0.73	1	2.0×10^8	2.0
1.55	0.92	1	1.46×10^8	1.5
2.00	2.00	1	7.3×10^7	0.7

[a]Film thickness for an idealized system of noninterfering particles spaced 10 μ apart.

III. EXPERIMENTAL STUDIES OF SILVER BROMIDE DISPERSIONS

A. Introduction

Methods of preparing monodisperse silver bromide (AgBr) precipitates have been reported by a number of workers. Berry and co-workers (ref. 16 and 18) prepared monodisperse AgBr precipitates and reported turbidity measurements of dilute suspensions and transmittance measurements of thin films. The radial distribution of the intensity of scattered light and methods of preparation of AgBr have been discussed by Napier and Ottewill (ref. 19).

The studies reported here consisted of attempts to establish quantitative relationships between both inherent (refractive index) and induced (film thickness) physical and optical properties of the films. The experiments were limited to transmittance and reflectance measurements of various particle-suspension media configurations. It is hoped that this study will be useful in elucidating the radiative interactions that occur in highly pigmented reflective coatings. In the design of such coatings it is important to know when the single particle (Mie) theory begins to fail and multiple interactions become dominant.

General references to light-scattering theory and notation throughout the following paragraph were taken from publications by Van de Hulst (ref. 3) and Penndorf (ref. 6). The optical densities given are to the base of natural log.

B. Experimental Procedures

1. Apparatus

A Cary model 14 recording spectrophotometer was used for the transmittance and reflectance measurements. The transmittance measurements were made with the film facing the detector. A quartz plate with a thin layer of gelatin was held in the reference beam as a blank to compensate for Fressnel reflection. For the dilute suspensions, 1-, 2-, and 5-cm path length cells were used. Reflectances were measured against a magnesium carbonate block standard.

2. Preparation of Monodisperse AgBr Precipitates

The AgBr precipitates were made by using procedures similar to those described by Berry (ref. 16). In order to keep the supersaturation as uniform as possible, the reagents (2N silver nitrate and 2N potassium bromide) were added simultaneously into a reaction vessel containing 3 g of gelatin and 100 ml of water; 25 ml of each reagent was added during the precipitation. The double-infusion apparatus for preparation of sols is shown in Figure 9. The data summarizing precipitation conditions are given in Table 6.

The particle diameters were obtained from the geometric mean of electron micrograph counts. The electron micrographs were made with a Hitachi type HS-6 electron microscope. The electron micrographs and particle-size distributions of several batches of particles are given in Figures 10 through 15.

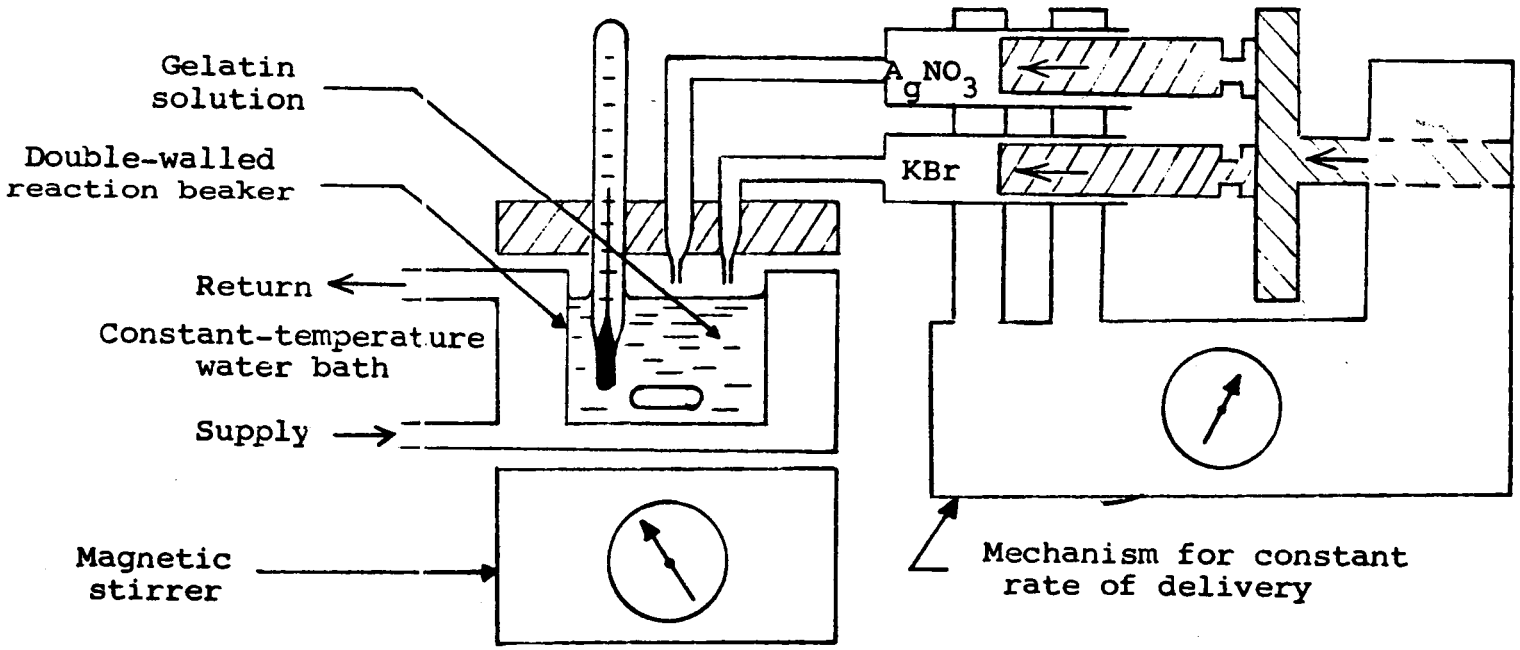

Figure 9

CRYSTAL-GROWTH APPARATUS

Table 6

PREPARATION OF AgBr SUSPENSIONS

Batch No.	Diam., μ	Normality of KCl and $AgNO_3$	Addition Rate, ml/min	Reaction Conditions		Excess KCl, ml
				Temp., °C	pH of NH_3	
25	0.78	2	0.8	58	9.6	2
26	0.64	2	2.0	50	9.7	2
27	0.92	2	2.0	55	9.9	2
28	0.88	2	2.0	55	9.7	2
29	0.92	2	2.0	55	9.9	2
30	0.40	2	2.0	50	9.5	2
31	0.68	2	2.0	50	9.7	2

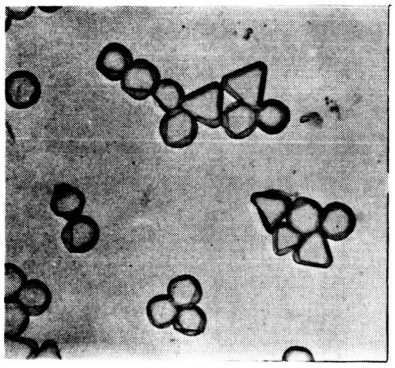

Batch 25
0.78-μ Diameter
(5000x)

Batch 26
0.64-μ Diameter
(5000x)

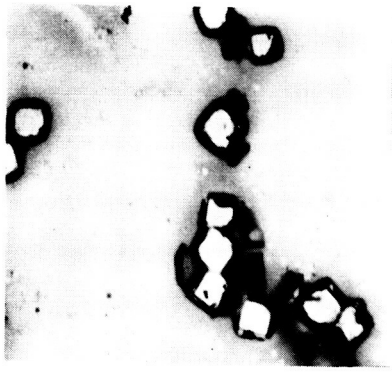

Batch 29
0.92-μ Diameter
(5000x)

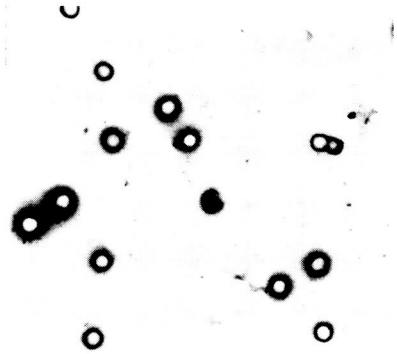

Batch 30
0.40-μ Diameter
(5000x)

Figure 10

ELECTRON MICROGRAPHS OF AgBr PARTICLES

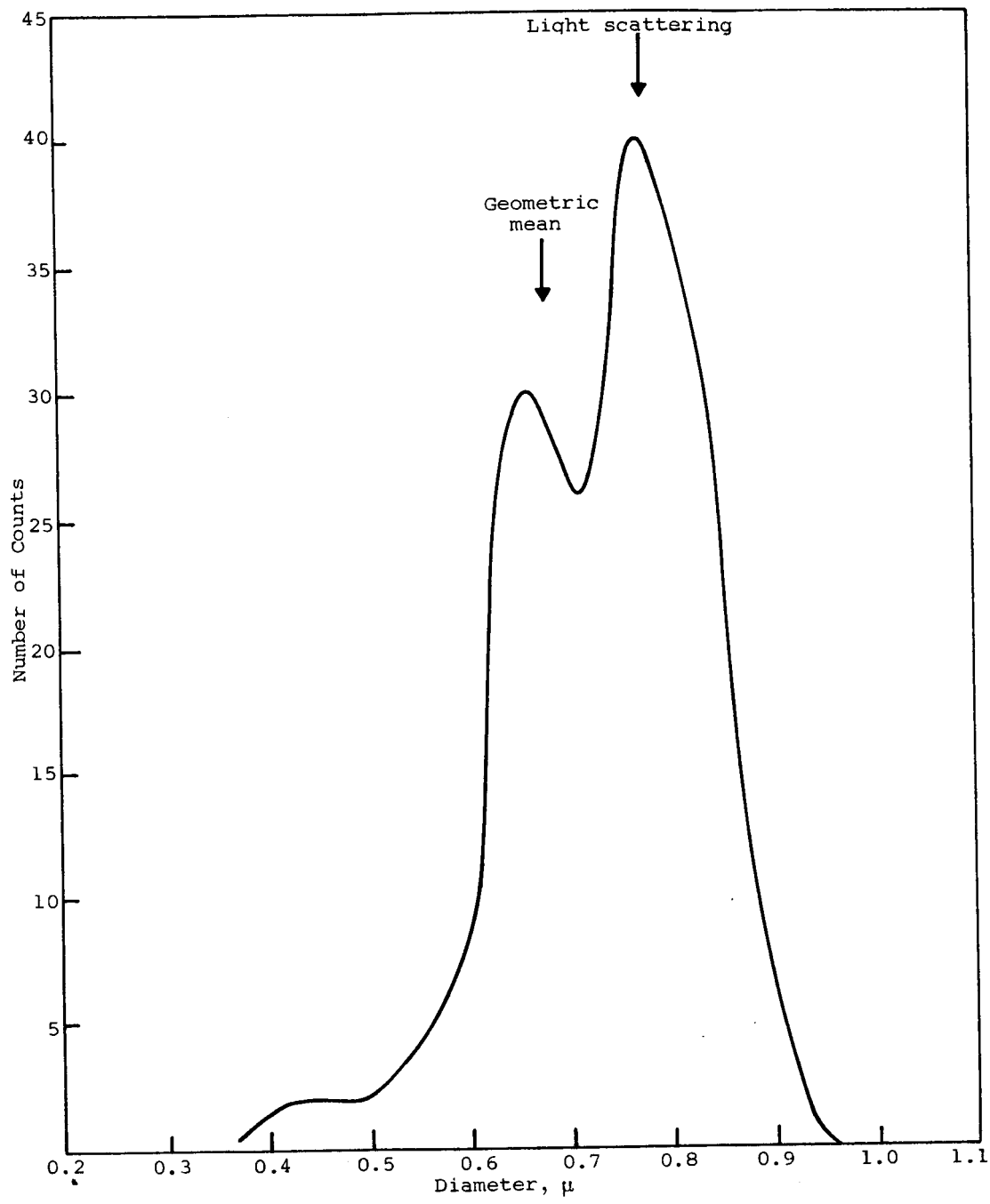

Figure 11

PARTICLE-SIZE DISTRIBUTION FOR BATCH 25

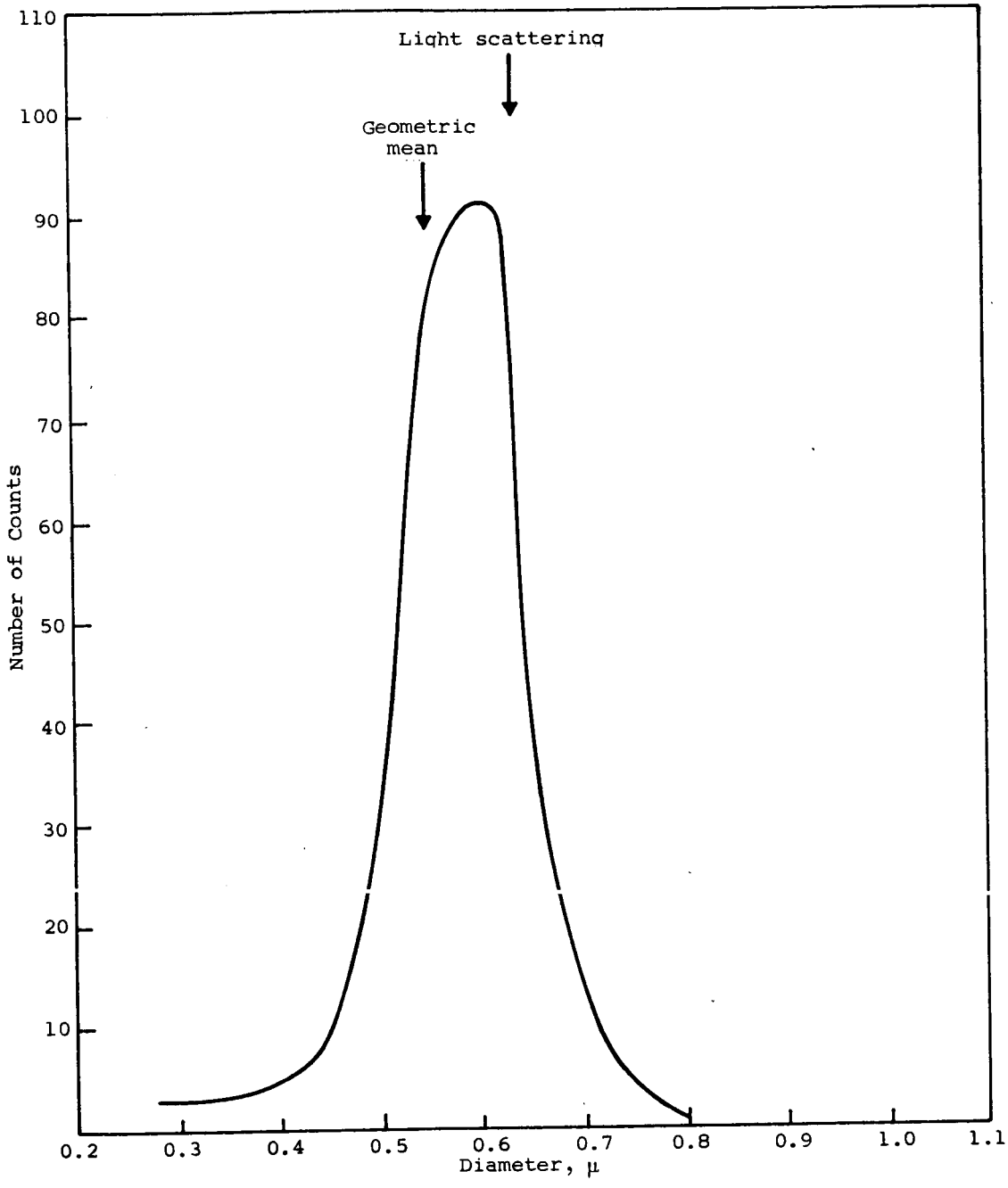

Figure 12

PARTICLE-SIZE DISTRIBUTION FOR BATCH 26

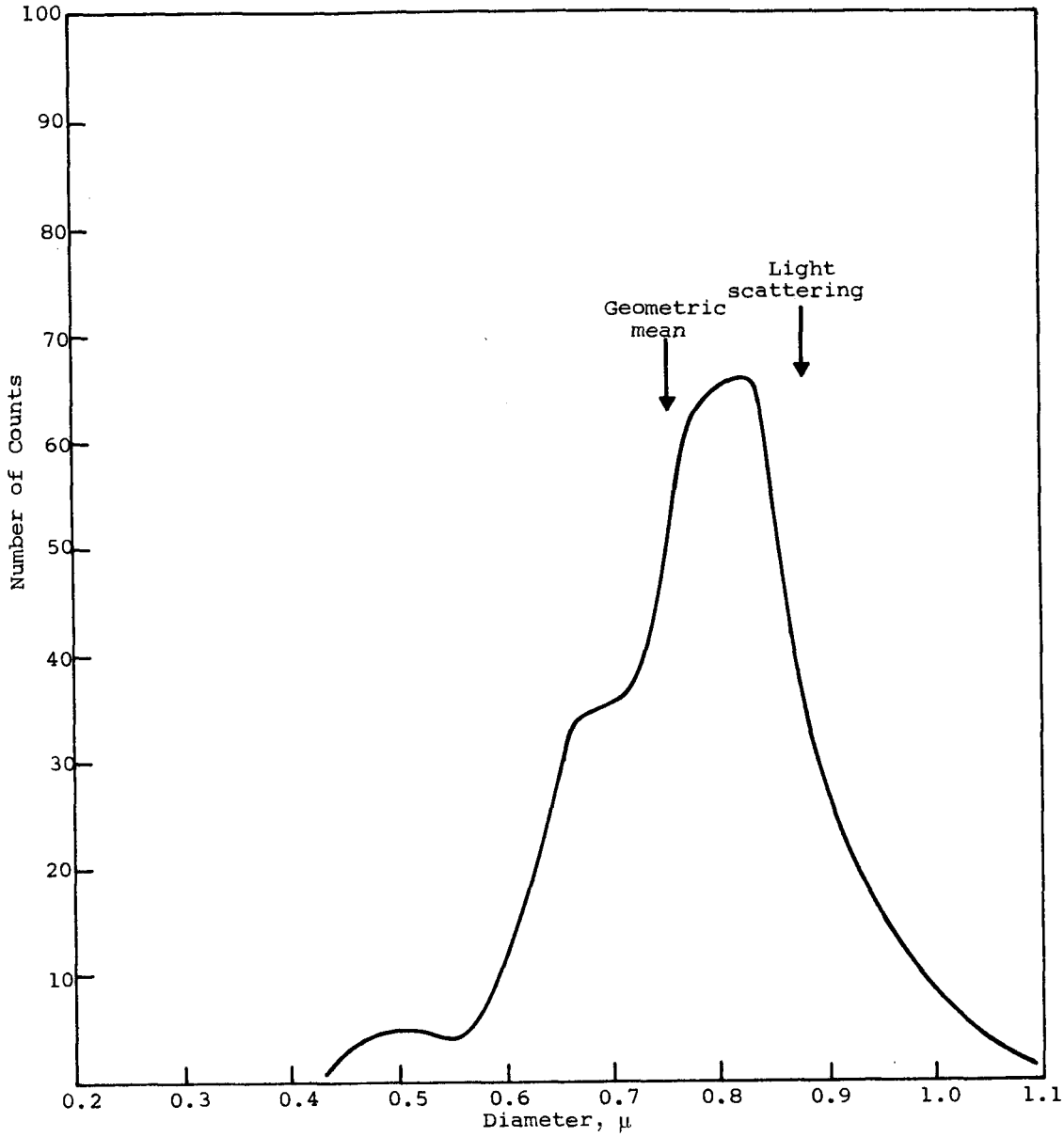

Figure 13

PARTICLE-SIZE DISTRIBUTION FOR BATCH 28

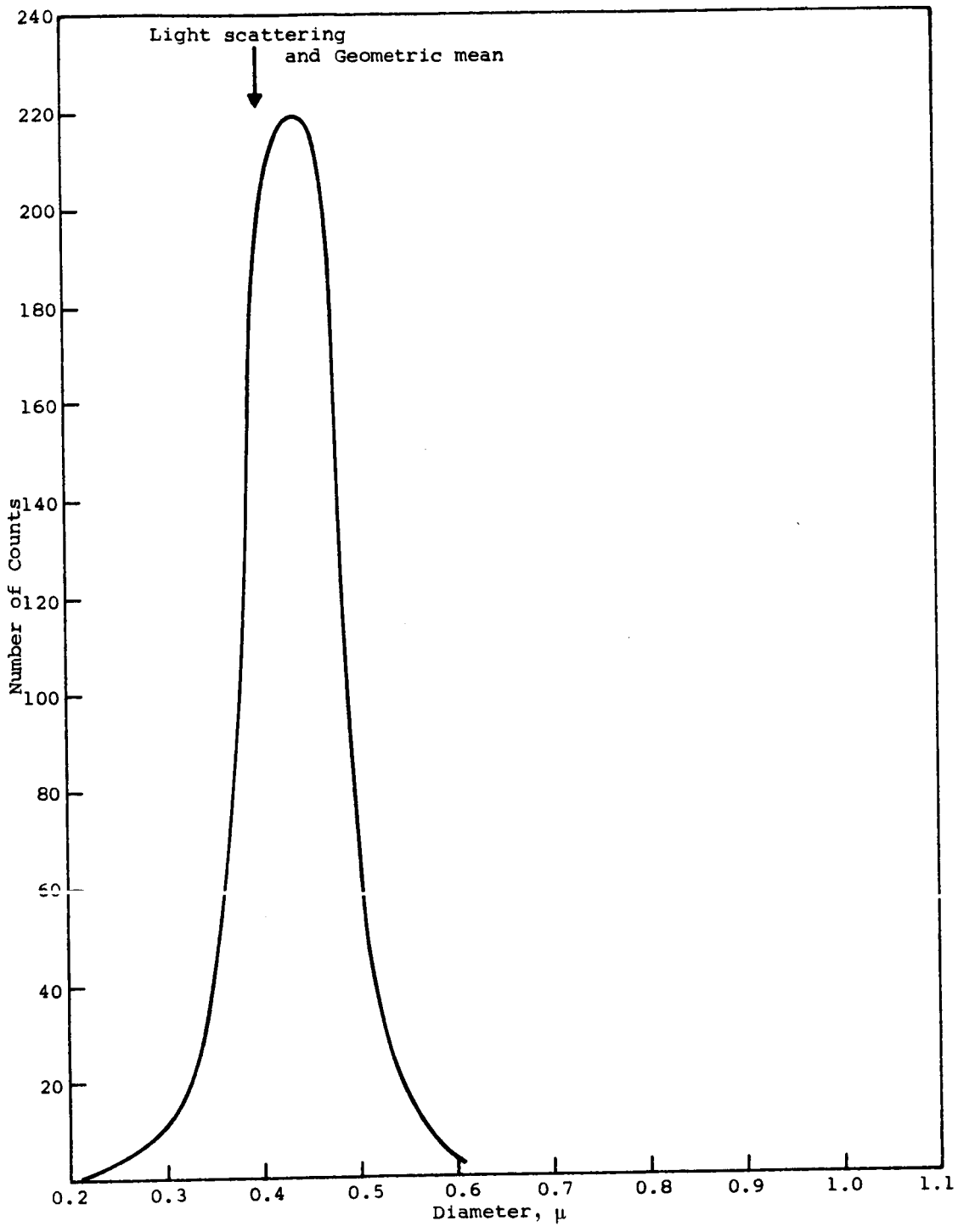

Figure 14

PARTICLE-SIZE DISTRIBUTION FOR BATCH 30

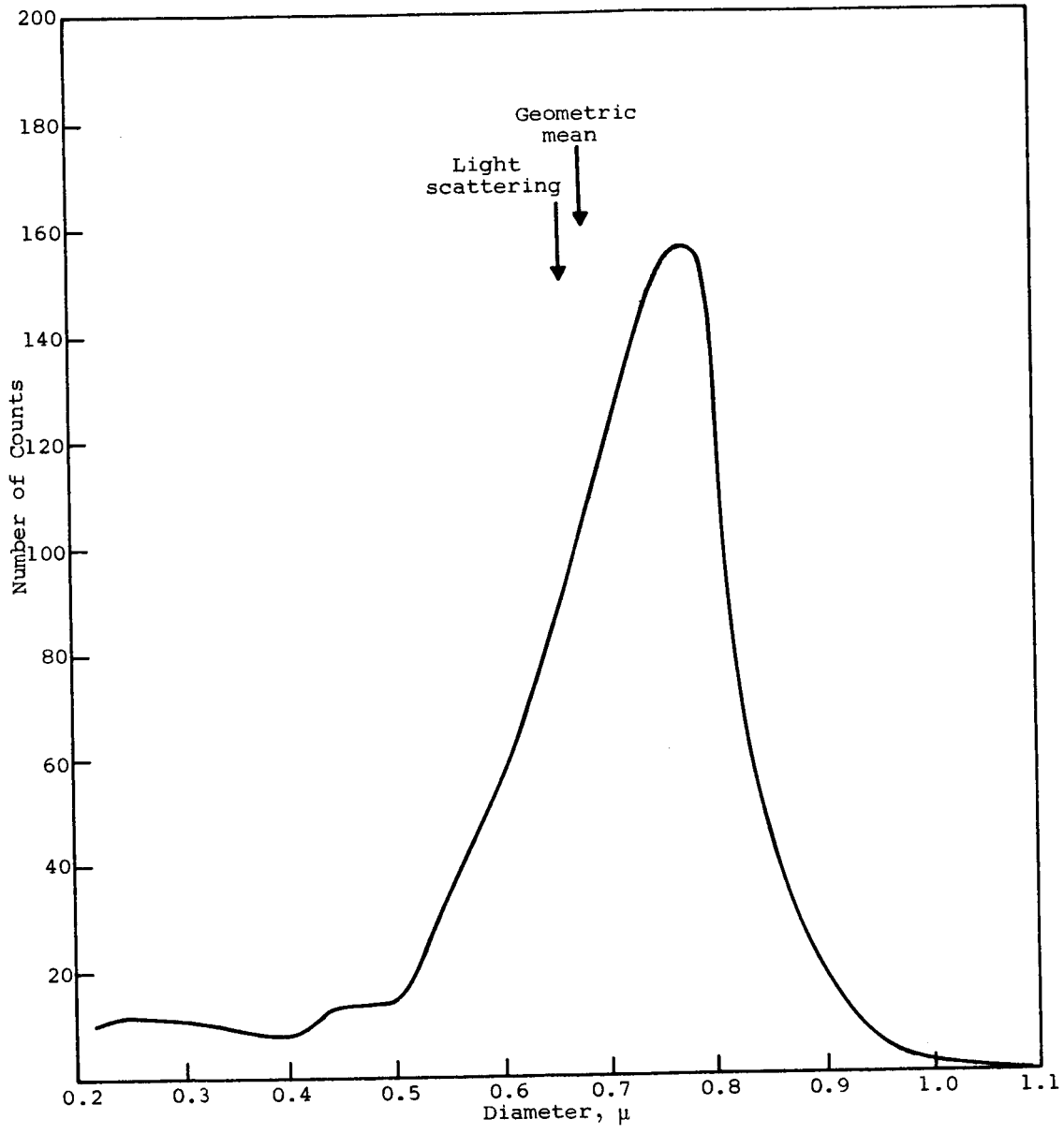

Figure 15

PARTICLE-SIZE DISTRIBUTION FOR BATCH 31

C. Results and Discussion

1. Measurements of Particle Size and Concentration

Before we could initiate a study of the optical properties of concentrated thin films, it was necessary to consider how closely the measurements under idealized laboratory conditions would approach the values predicted by the Mie theory. At this point, it may be useful to reconsider the physical assumptions implicit in the Mie theory and their relationship to experimental measurements.

Light scattering is defined as a change in the direction of a light wave after its interaction with a scattering particle. An inherent but significant assumption in experimental measurements is that the theory is valid for infintely dilute suspensions of monodisperse spheres that are illuminated monochromatically.

In traversing a dispersion of uniform spherical particles, the intensity of a parallel beam of light is reduced according to the transmission equation:

$$\frac{I}{I_0} = e^{-K\pi r^2 nL} \tag{9b}$$

or, in terms of optical density:

$$D = K\pi r^2 nL \tag{11}$$

where

K is the Mie scattering coefficient
n is the particle concentration
r is the particle radius
L is the optical path length.

The spectral transmittance curves predicted by the Mie theory are therefore oscillatory with the minima and the maxima of transmittance, which correspond inversely to the oscillations in K. Since K is a function of the size parameter, where $\alpha = 2\pi\ r/\lambda$, the minima and the maxima occur at different wavelengths for monodisperse particles of different radii.

The radii of the particles can be determined from the wavelength positions of the minima and the maxima by using spectral transmittance measurements and Equation 9b. The first transmittance minimum (measured from the long-wavelength side) corresponds to the first scattering maximum, the first transmittance maximum corresponds to the first scattering minimum, etc. The number (concentration) of scatters can be determined from absolute transmittance measurements at any given wavelength. Reciprocity of path length and concentration is assumed in Equation 9b.

Figure 16 shows the spectral transmittance curves for the majority of batches of AgBr particles used. The water suspensions contained approximately equal weights (0.707 g/ml) of AgBr particles, and a 2-cm path length absorption cell was used.

Graphical particle-size measurements from light scattering are summarized in Figure 17. The wavelength positions of the extrema were derived from the theory for a refractive index of 1.7. The effective refractive index of AgBr in water is calculated from:

$$m = \frac{m\ (\text{particle})}{m\ (\text{medium})} = \frac{2.253}{1.333} = 1.7$$

A consistent increase in measured radii at higher lobes can be seen in Figures 17. This deviation could be due to the following effects.

(a) The absorption coefficient of AgBr increases significantly at shorter wavelengths, and the effective refractive index becomes a complex number. These factors are not considered in our assumption of constant refractive index (1.7).

(b) The deviations due to nonuniformity of the particles would be significant at higher lobes.

The concentration of particles was determined from extinction measurements and was calculated independently from the weight of AgBr in suspension. All particles were assumed to be uniform, perfect spheres.

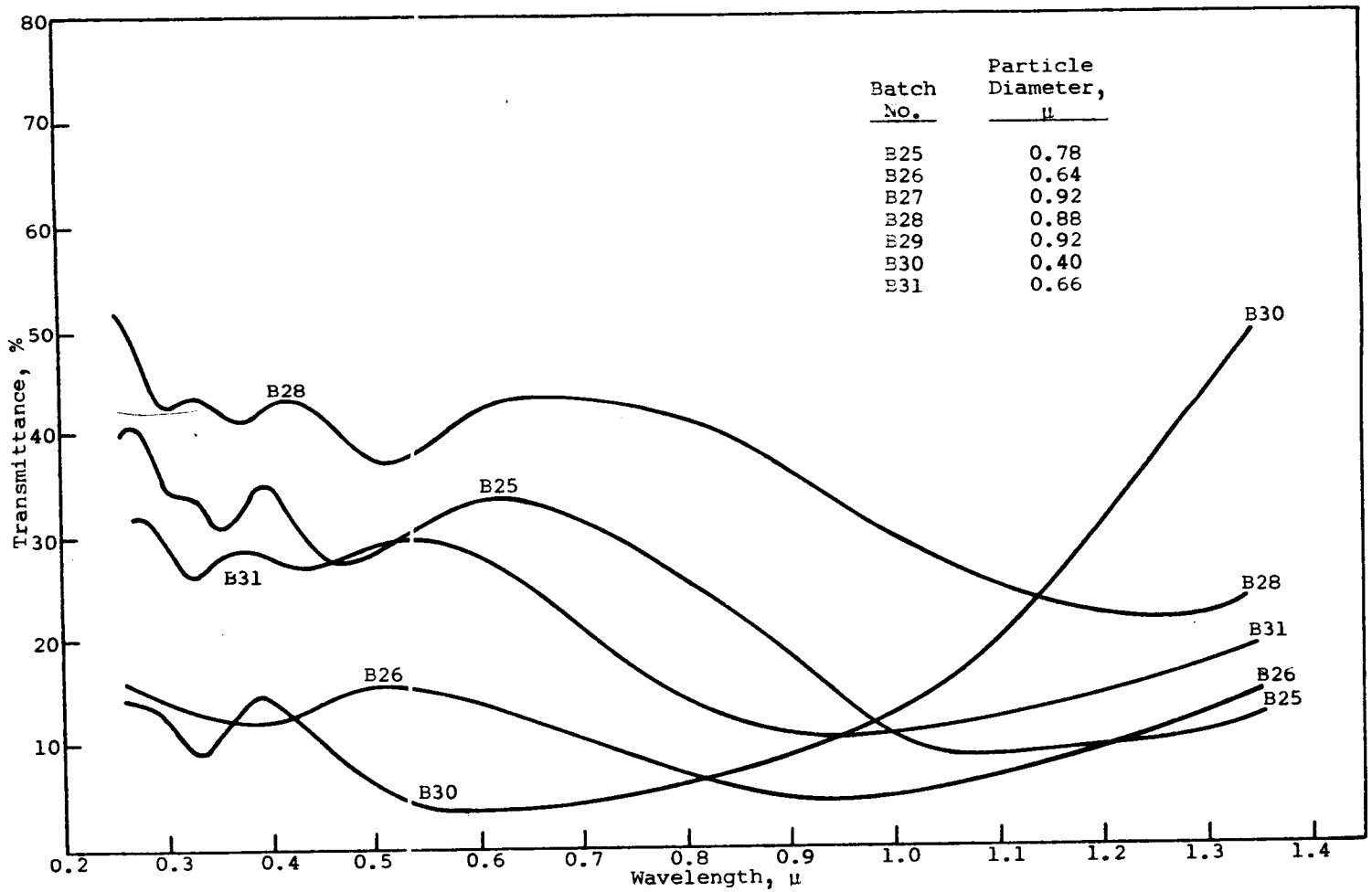

Figure 16

TRANSMITTANCE OF AgBr SUSPENSIONS IN WATER

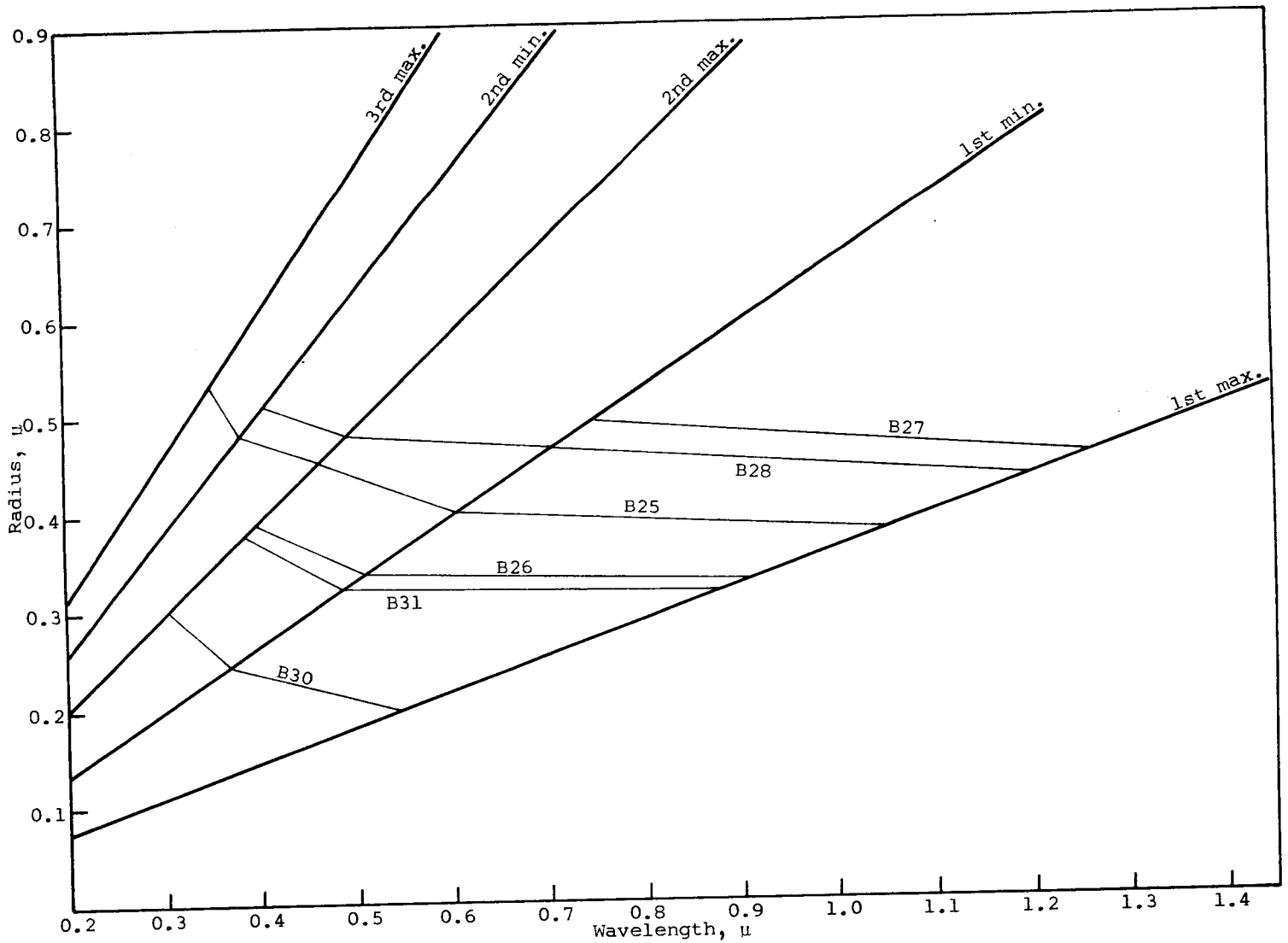

Figure 17

PARTICLE-SIZE MEASUREMENTS FROM LIGHT SCATTERING

Since the size parameter, α, is a reciprocal function of wavelength, the wavelength chosen for the concentration measurements corresponded to the midpoint of the wavelength reciprocals between the first scattering maximum and the first minimum. This wavelength was chosen because maximum deviation from the theoretical values (due to the particle nonuniformity) would be located at the wavelengths of the extrema. Also, the values of the total Mie scattering coefficient, K, tend to flatten out at approximately 2.2, which is close to the midpoint value. The concentration measurements are summarized in Table 7.

Table 7

CONCENTRATION MEASUREMENTS IN WATER SUSPENSIONS

Batch No.	Conc., particles/cm^3 x 10^{-8} Measured by Light Scattering	Calculated
25	0.594	0.586
26	1.400	1.165
27	0.271	0.358
28	0.405	0.408
29	0.271	0.358
30	3.720	3.700
31	0.840	0.870
Polystyrene (0.796)	2.170	2.239
Polystyrene (1.305)	0.522	0.531

2. Secondary Oscillations in Scattering by Polystyrene Spheres

Two samples of polystyrene spheres (Dow Chemical Co.) that were suspended in water were also included. The electron micrographs of these spheres are shown in Figure 18. The diameters reported by Dow Chemical Co. were 1.305 and 0.796 μ, with standard deviations of 0.0158 and 0.0083, respectively. The transmittance of the 1.305-μ-diameter spheres is shown in Figure 19.

In addition to major oscillations in the total Mie scattering coefficients, the theory predicts a set of minor oscillations due to interferences of the reflected, refracted, and diffracted rays of the incident light. These minor oscillations are therefore consequences of the resonance of multipoles induced by the light wave. Examination of the spectral transmittance curves obtained from suspensions of polystyrene spheres (Figure 19) reveals a set of minor oscillations at the first scattering minimum that are very similar to those predicted by the theory (ref. 3).

It has been ascertained that these oscillations (a) are not due to molecular absorption of polystyrene, (b) are independent of wavelength, and (c) are dependent on the effective refractive index. A shift in wavelength and relative positions can be easily noted by comparing the suspensions in water with those in isopropanol. These features strongly suggest that these oscillations may be due to the resonance of the multipoles.

3. Transmittance of Suspensions Containing Two Particle Sizes

To approximate a suspension containing a wider distribution of particle sizes, a series of bimodal mixtures was prepared. The spectral transmittance curves of the mixtures are compared with those of the components of the mixtures in Figures 20 through 22. The mixtures were prepared to contain 50/50 wt. % AgBr particles.

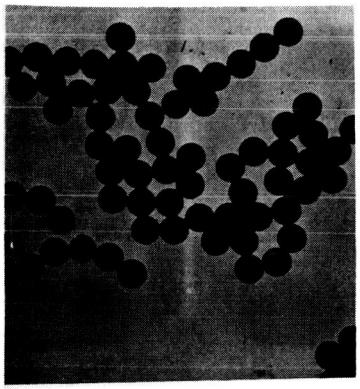

0.796-μ Diameter

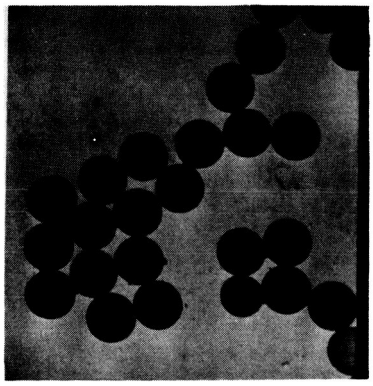

1.305-μ Diameter

Figure 18

ELECTRON MICROGRAPHS OF MONODISPERSE POLYSTYRENE SPHERES

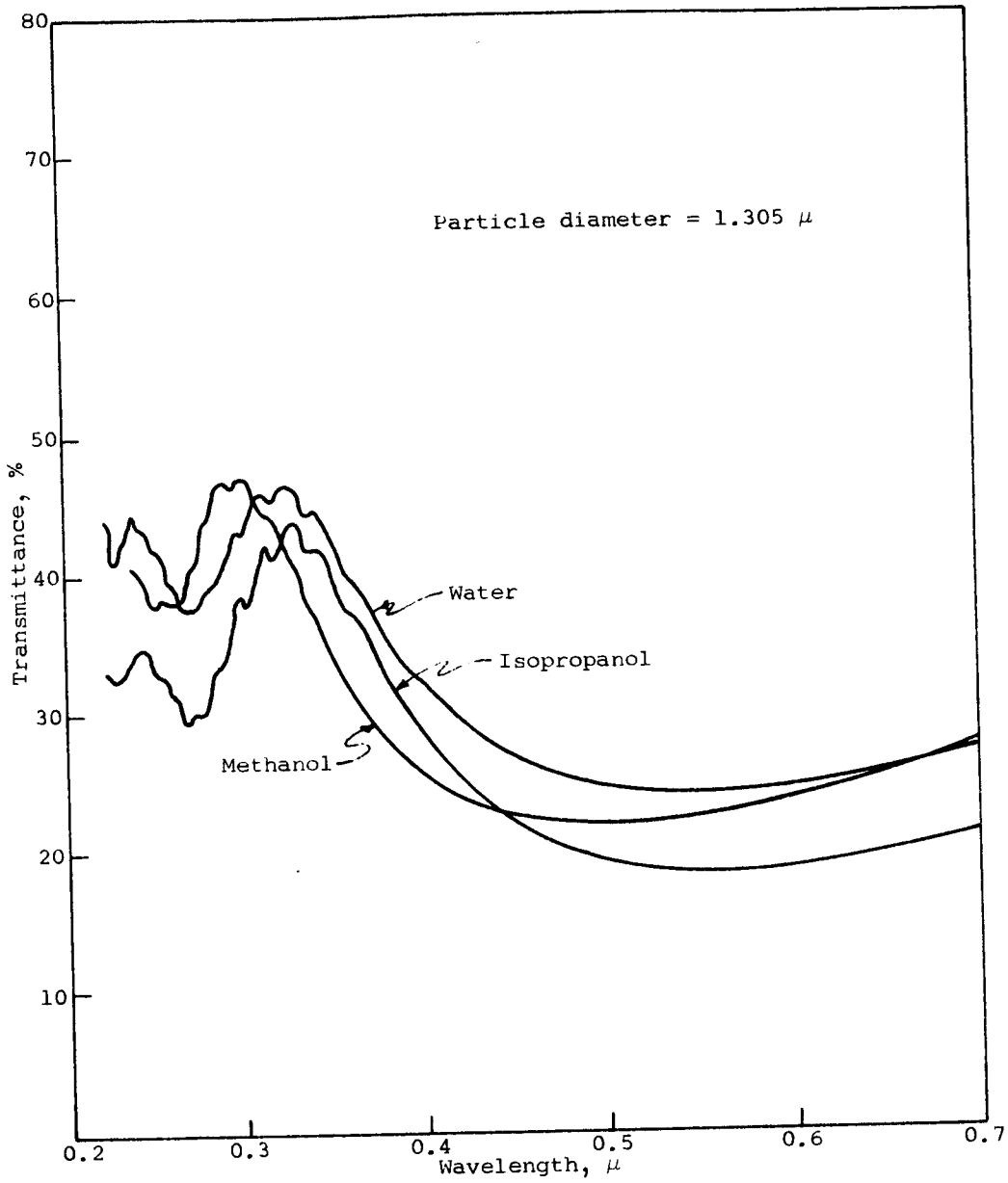

Figure 19

TRANSMITTANCE OF POLYSTYRENE SPHERES IN SUSPENSIONS
OF VARIOUS REFRACTIVE INDICES

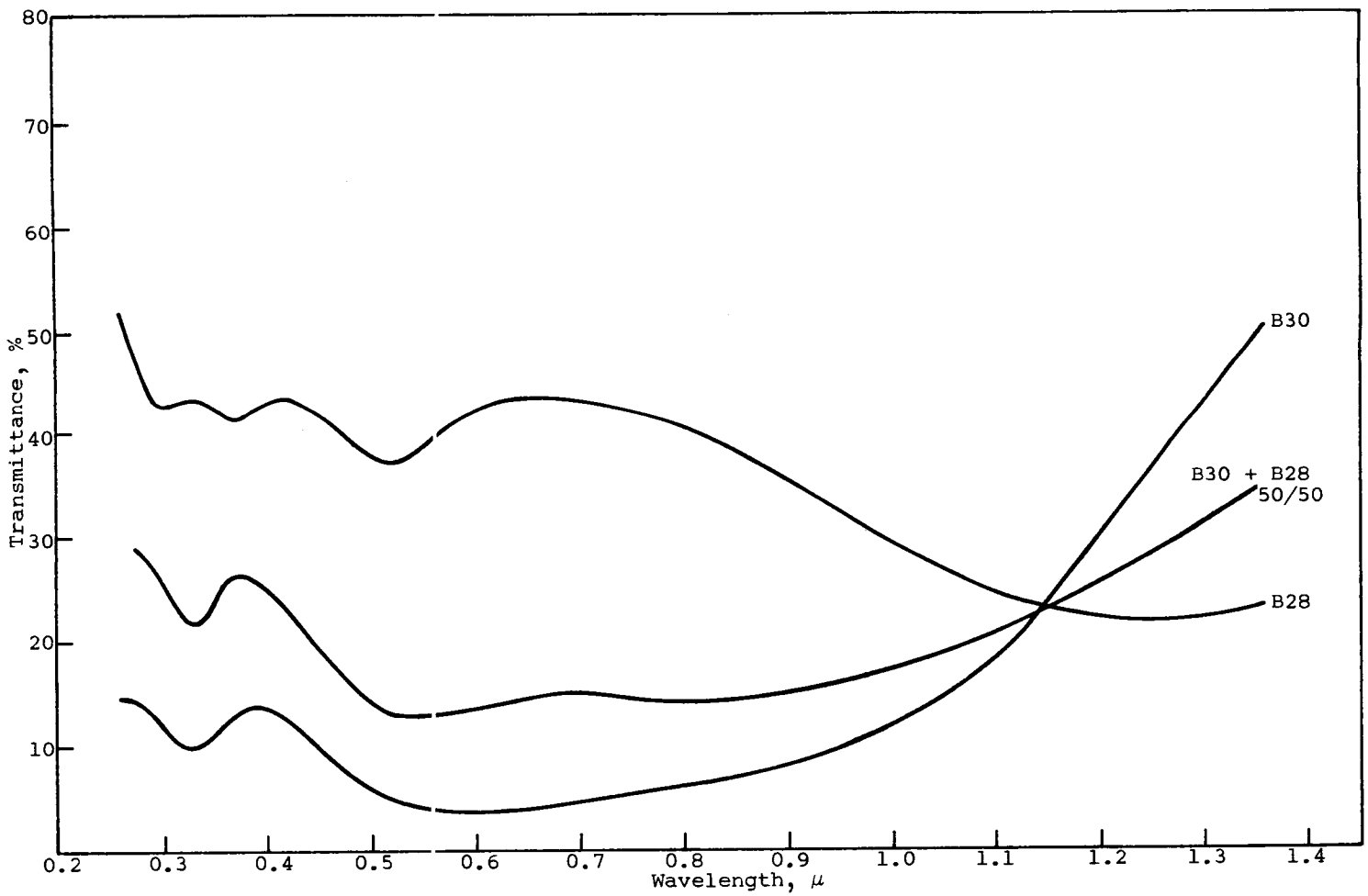

Figure 20

TRANSMITTANCE OF DILUTE SUSPENSIONS OF AgBr MIXTURES (BATCHES 28 AND 30)

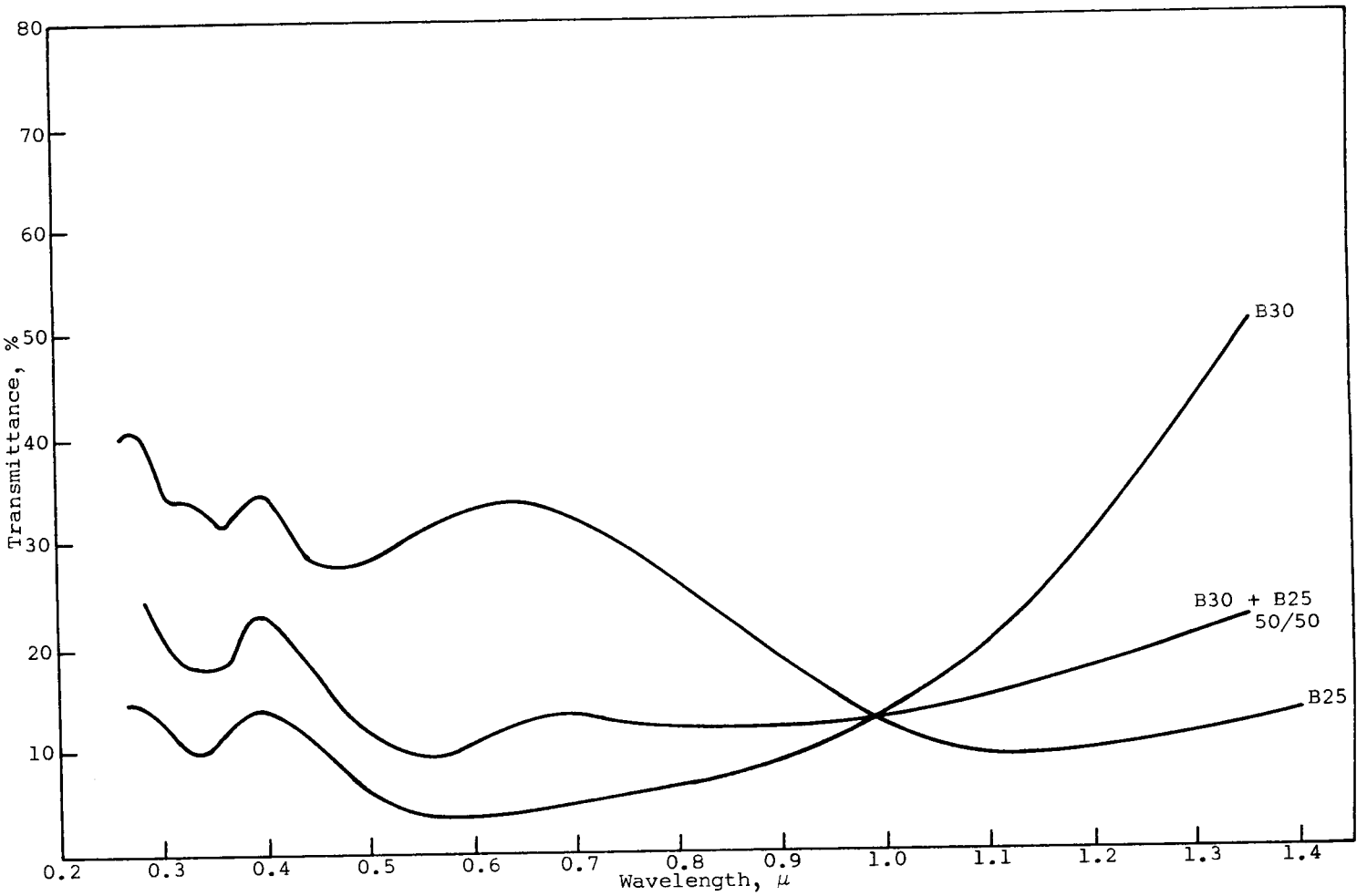

Figure 21

TRANSMITTANCE OF DILUTE SUSPENSIONS OF AgBr MIXTURES (BATCHES 25 AND 30)

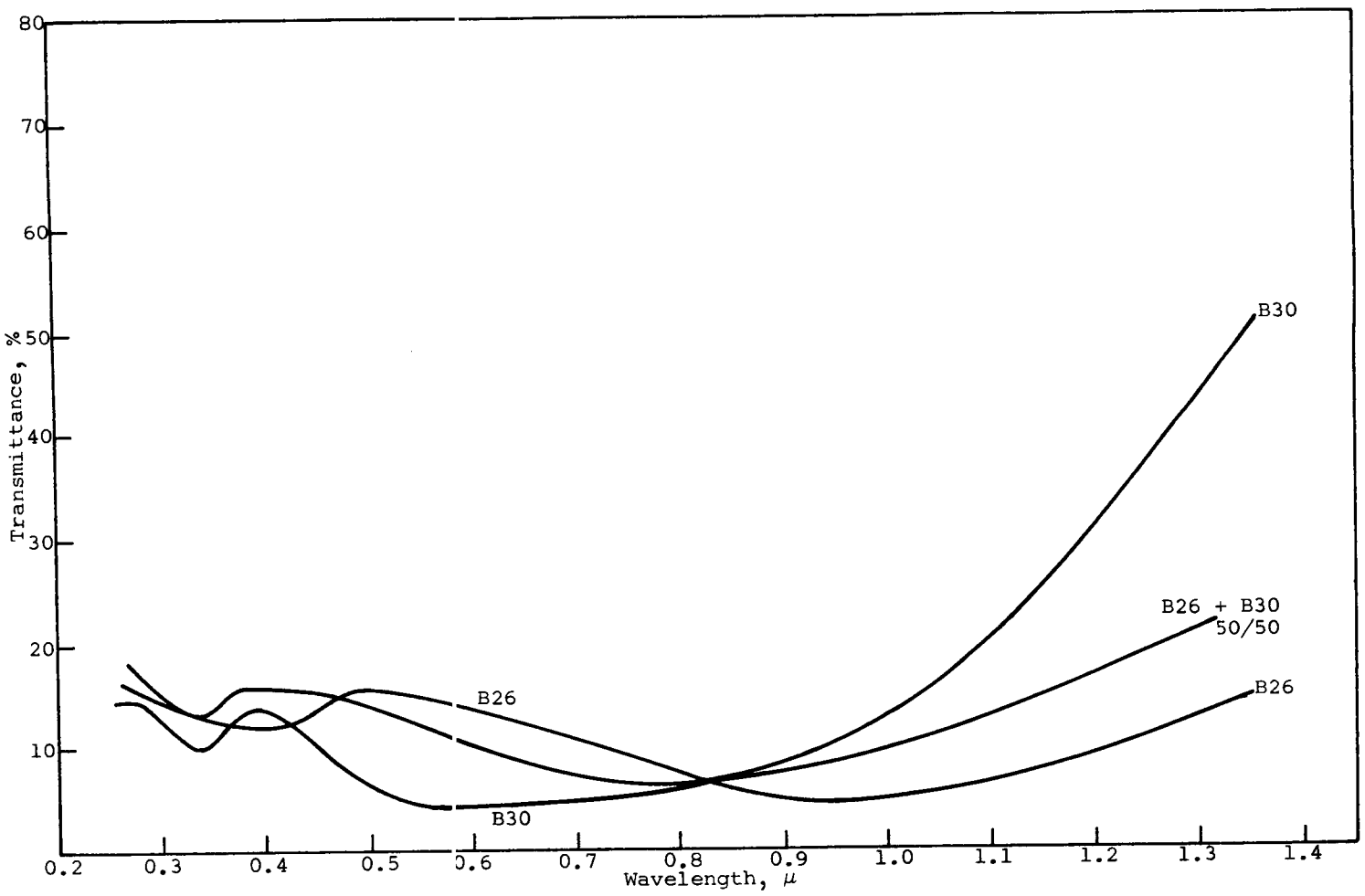

Figure 22

TRANSMITTANCE OF DILUTE SUSPENSIONS OF AgBr MIXTURES (BATCHES 26 AND 30)

The data indicate that particles of two sizes act as independent scatterers in dilute systems. The data show that independent transmittance curves for each particle size intersected with the transmittance curve of the mixture. In several cases sharp discontinuities in the transmittance of the mixture were observed at the intersection of the three curves. It can be shown algebraically from the transmission equation (Equation 9b) that the transmittance of the mixture equals the transmittances of two components at this single wavelength, although the optical densities are additive at any wavelength.

An exception can be noted in Figure 22, in which the curves do not intersect in the short-wavelength range but do intersect in the long-wavelength range. This can be explained on the basis of increasing absorption of AgBr at shorter wavelengths. The transmission equation considers the energy losses due only to scattering and not to absorption. Therefore the observed transmittance curves tend to deviate from the predicted ones at short wavelengths, when absorption effects become significant.

Thus the optical densities would be expected to be additive for each single energy-loss mechanism, e.g., scattering (transmission equation) or absorption (Beer-Lambert law). These mechanisms apparently prevail at shorter wavelengths.

4. Transmittance of Concentrated Monodisperse Suspensions in Thin Films

To obtain more closely packed suspensions that approximate real pigmented coatings, various concentrations of particles dispersed in gelatin were deposited in thin layers on quartz plates. The films were dried rapidly in a stream of hot air. The thickness of the films was varied by holding the quartz plates at various angles during the drying process. The thickness of the AgBr suspension layers was measured interferometrically by using a Zeiss model 2300 interference microscope. A clean scratch was made in the gelatin layer, and in a majority of cases three interference patterns could be detected:

(a) one due to the quartz substrate, (b) one due to the gelatin layer, and (c) a very faint one due to the particles themselves.

The most significant observations from the thickness measurements were that the particles were imbedded in the layers of gelatin, which were considerably thinner than the particles themselves, and that in a majority of cases the particles were arranged in monolayers. The manner of packing is schematically represented in Figure 23.

Since the layers are very thin (0.2 to 2.0 μ), the estimated accuracy of the thickness measured is ±15%. Also, because the particles are not completely surrounded by gelatin, the effective refractive index varies somewhat with the thickness of the gelatin layer.

In considering the transmittance characteristics of monodisperse closely packed suspensions of gradually increasing thickness, it is necessary to reconsider the physical mechanism of energy loss. It would be unreasonable to expect that the transmittance losses of parallel light in thick layers of concentrated suspensions would be similar to the losses in dilute suspensions, i.e., that they would be due only to changes in the direction of photons.

Theoretical considerations predict that, as the number of closely packed layers increases, the number of scattering events (changes in the direction of incident photons) also increases. Thus, increasing amounts of light in the deeper layers are lost by absorption and are converted to thermal and molecular energy modes. An increasing number of scattering events leads to an increasingly effective absorptive path length for each penetrating photon. Thus, even at low absorption efficiency (as is the case with AgBr), if the absorption path is long enough, the absorption mechanism of energy loss (Beer-Lambert law) predominates in the deepest layers of the suspension. As a result, a gradual decrease in the amplitude of the scattering minima and maxima and finally a transition into a continuous function are observed.

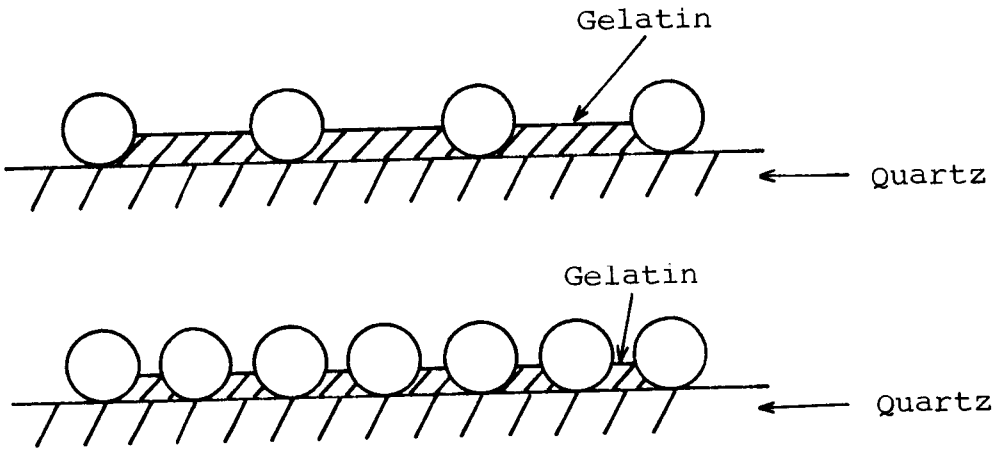

Figure 23

SCHEMATIC REPRESENTATION OF PARTICLE PACKING IN GELATIN PAYERS AT VARIOUS CONCENTRATIONS

Figure 24 shows the change in the amplitude of the scattering extrema for various film thicknesses. In the longer-wavelength region, where the scattering is minimal, the effective absorptive path length corresponds to approximately a single pass of the photon. Since there is not appreciable change in direction of the photon due to scattering, the absorptive losses are very slight, and the transmittance increases significantly.

An actual increase in transmittance at wavelengths corresponding to the first scattering maximum with increasing concentration can be observed in several intermediate thicknesses (Figures 25 and 26). This phenomenon is also thought to be caused by multiple scattering events. In the intermediate cases, the decrease in the amplitude of transmittance minima and maxima is probably the best indication of when the single-scattering mechanism begins to fail and multiple scattering and absorption becomes the dominant mechanisms of energy loss.

It was observed that only slight decreases in the amplitude of extrema occur (almost independently of concentration) when the particles are suspended in monolayers, i.e., extremely thin layers with the particles packed side by side with respect to the incident beam of light. However, in multiple layers (thick films), even with four layers the deviations become quite significant.

This observation was further confirmed by measurements of dilute suspensions in three-dimensional arrays with long path lengths. A slight but definite decrease in the ratio of extrema was observed (Table 8).

The conclusion that even extremely close packing of particles side by side in monolayers gives only very slight interactions can be explained qualitatively by considering the radial intensity distribution functions (ref. 9,19) of the scattered light. In general, the radial intensity functions approximate Figure 16 (see Figure 27), with an intensity minimum approximately 90° from the direction of the incident beam. Thus, minimal interaction is expected when the particles are packed side by side.

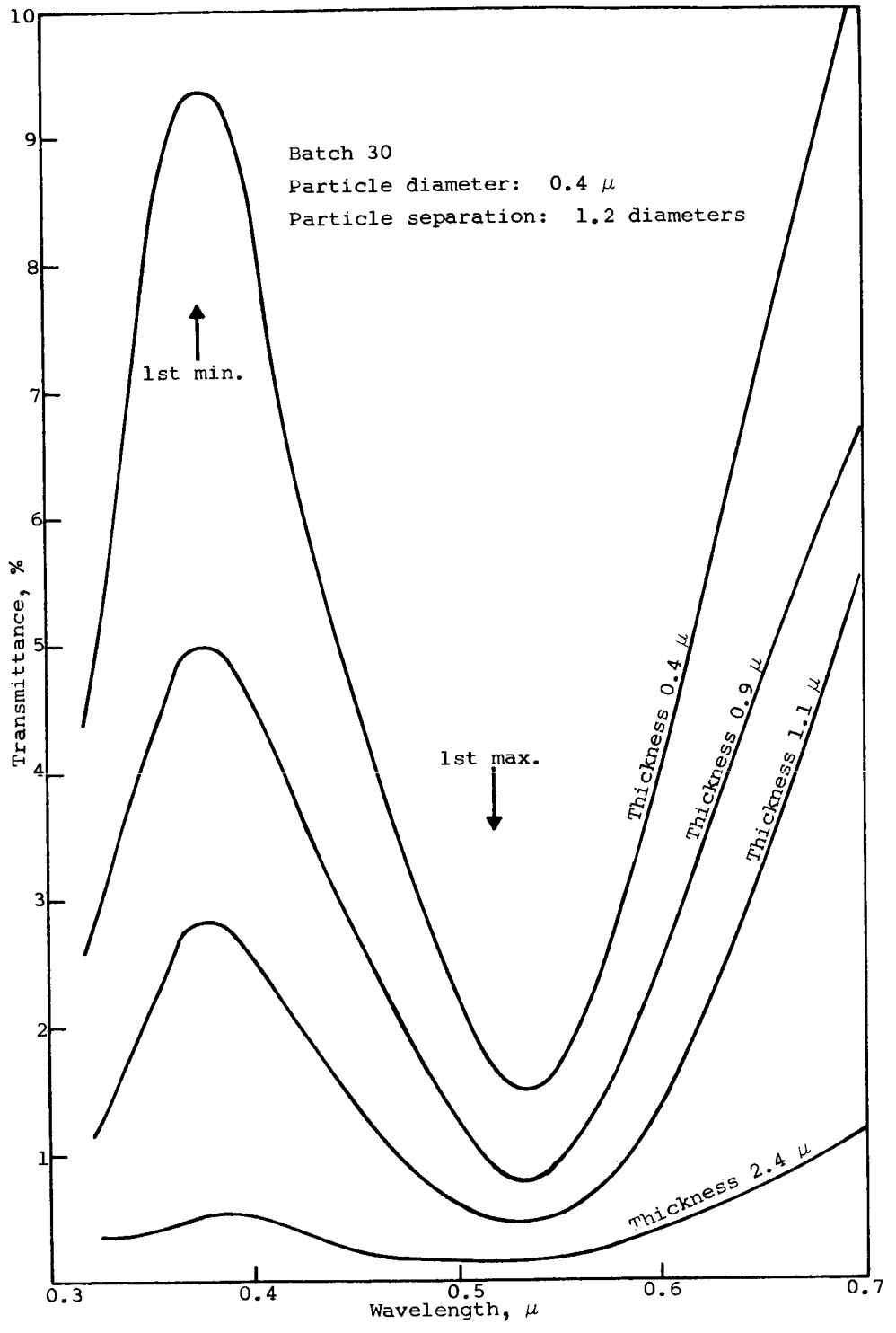

Figure 24

SCATTERING EXTREMA VERSUS THICKNESS OF GELATIN SUSPENSIONS

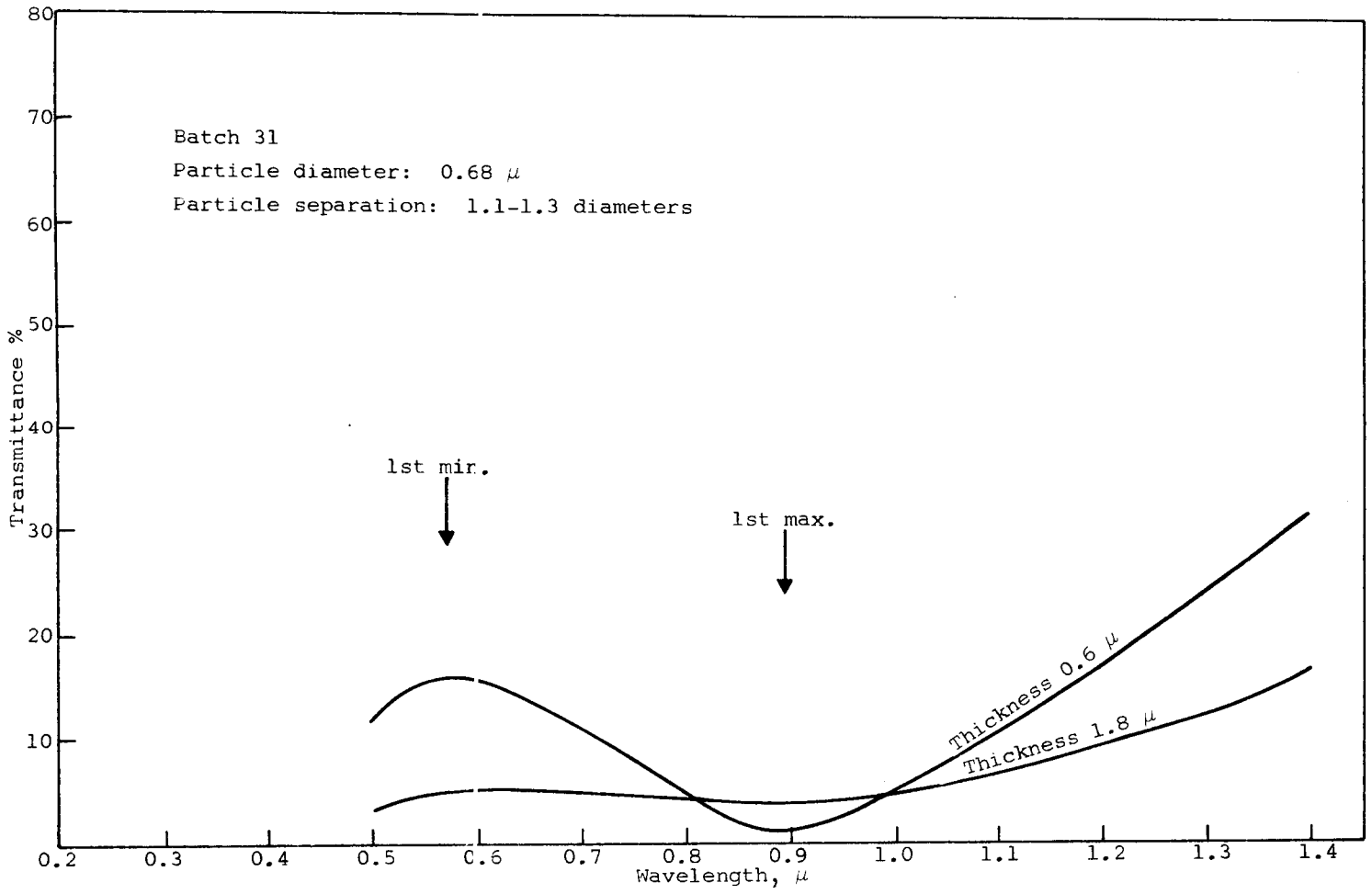

Figure 25

TRANSMITTANCE OF CONCENTRATED GELATIN FILMS

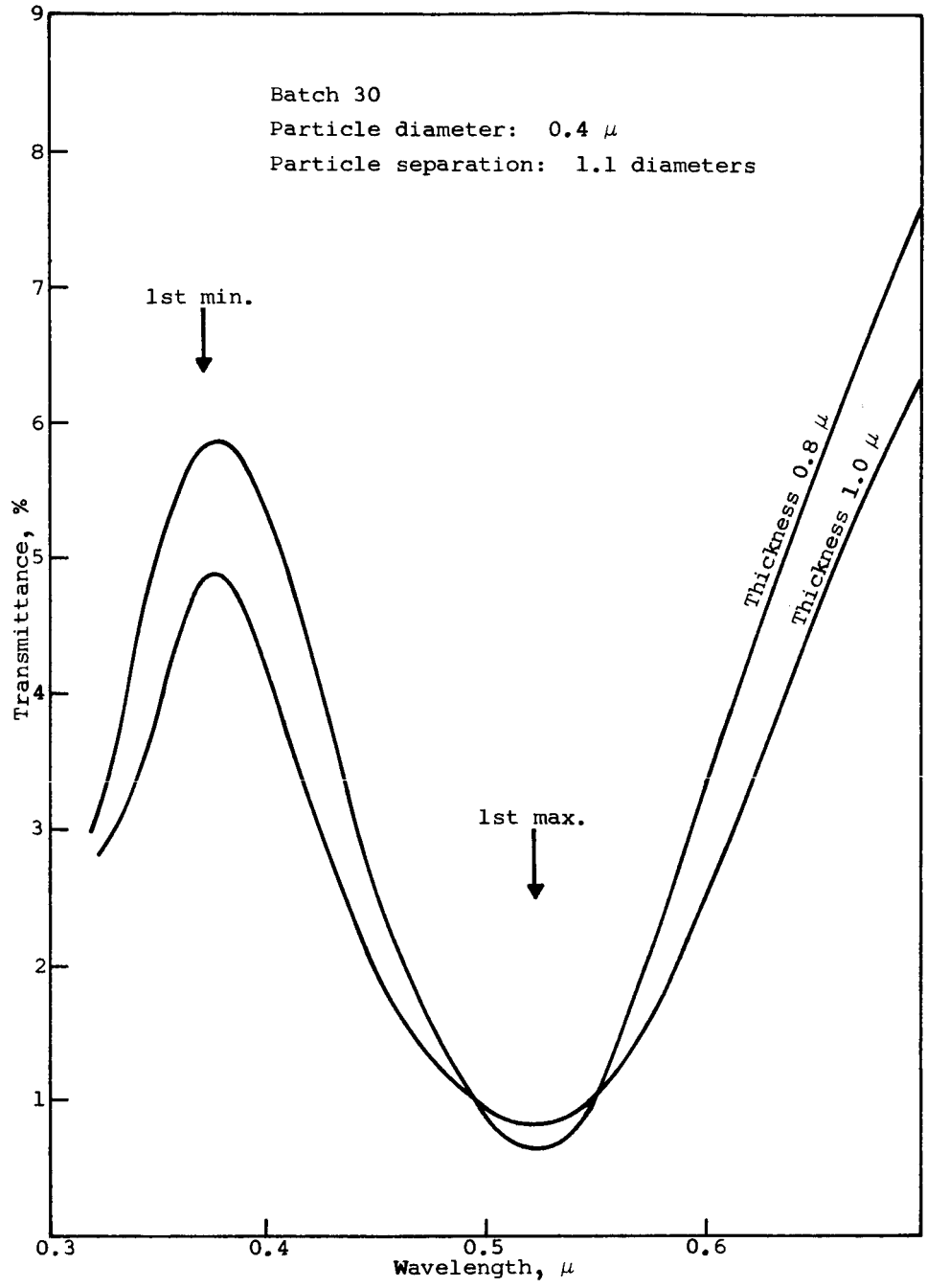

Figure 26

TRANSMITTANCE OF CONCENTRATED GELATIN FILMS

Table 8

AMPLITUDE OF THE SCATTERING EXTREMA
AS A FUNCTION OF PATH LENGTH

Batch No.	Particle Radius, r	Optical Path Length, cm	Ratio of 1st Max./1st Min.
25	0.39	2	1.85
		5	1.55
26	0.32	2	1.61
		5	1.45
28	0.44	2	1.82
		5	1.49
30	0.20	2	1.87
		5	1.60
31	0.33	2	2.09
		5	1.73
Theoretical	-	-	2.63

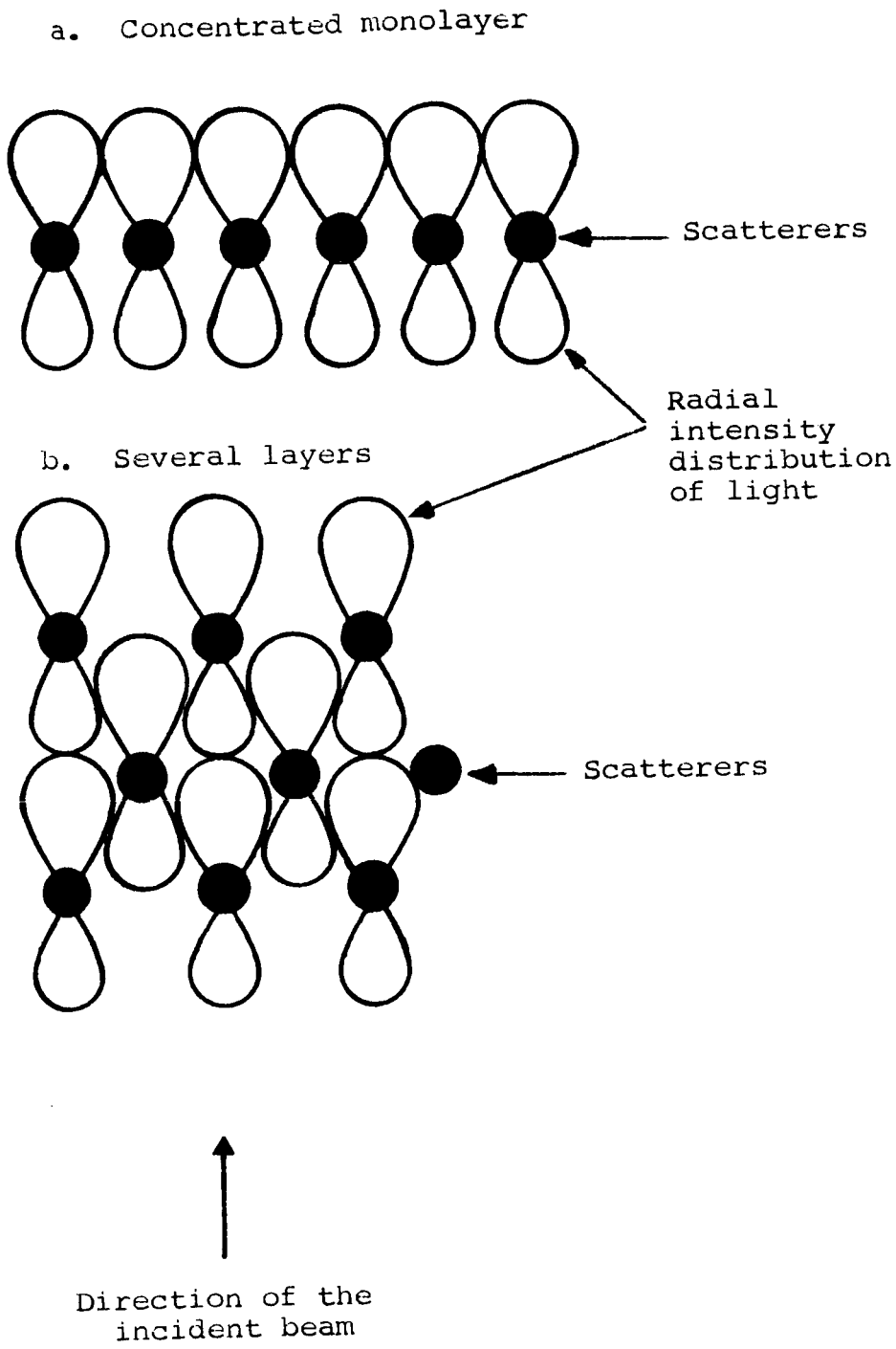

Figure 27

SCHEMATIC DIAGRAM OF THE OVERLAP OF RADIAL INTENSITY FUNCTIONS

5. Transmittance and Reflectance Properties of Concentrated Bimodal Suspensions in Thin Films

If it is assumed that the attenuation of light is due to scattering only, the optical densities for two monodisperse films are:

$$D_1 = K\pi r_1^2 n_1 L_1 \tag{11a}$$

$$D_2 = K\pi r_2^2 n_2 L_2 \tag{11b}$$

where

K is the total Mie scattering coefficient

r is the particle radius

n is the particle concentration

L is the optical path length or the thickness of the films

D is the optical density.

If the two particle sizes act as independent scatterers, the transmittance of a hypothetical sum of two monodisperse films at 50% of the original concentration is:

$$\frac{D_1 + D_2}{2} = K\pi\left[r_1^2\left(\frac{n_1 L_1}{2}\right) + r_2^2\left(\frac{n_1 L_2}{2}\right)\right] \tag{12}$$

If it is again assumed that the particles act as independent scatterers in the mixed suspension, the optical density of the mixture (at 50/50 wt. %) is:

$$D_{1+2} = K\pi\left[r_1^2\left(\frac{n_1}{2}\right) + r_2^2\left(\frac{n_2}{2}\right)\right]L_{1+2} \tag{13}$$

where L_{1+2} is the thickness of the film prepared from a mixed suspension. If

$$L_1 = L_2 = L_{1+2}$$

then

$$\frac{D_1 + D_2}{2} = D_{1+2} \tag{14}$$

In the set of experiments reported here, the thickness of each film was measured, and the optical densities of the components (monodisperse films) were normalized to the thickness of the bimodal mixtures. The thickness and concentration data are given in Table 9. A comparison of the observed transmittances of bimodal mixtures with those constructed from the measurements of monodisperse films is shown in Figures 28 and 29.

Table 9

THICKNESS AND CONCENTRATION OF AgBr FILMS

Batch No.	Radius (r), μ	Thickness (L), μ	Conc., n/μ^3	Separation, in diameters
A25	0.39	1.98	1.5	1.07
B25	0.39	1.54	1.75	1.04
26	0.32	1.68	2.63	1.14
30	0.20	1.67	9.7	1.18
A25 + 26		1.88	-	-
B25 + 30		1.76	-	-

This observation is probably not valid for more than several layers of particles. The greatest source of error in our measurements is the determination of thickness and concentration of scatterers in dry films. Since the thickness was measured interfometrically, an appreciable displacement of the observed and theoretically constructed curves can be expected.

Since a reasonable agreement was obtained between the observed transmittances of the bimodal mixtures and those constructed from observations of single particles, the above comparison was extended to include a theoretical bimodal coating constructed on the basis of Mie scattering theory. An inherent assumption in such a case is that the particles are completely uniform; i.e., there is no size distribution whatsoever for any given particle size.

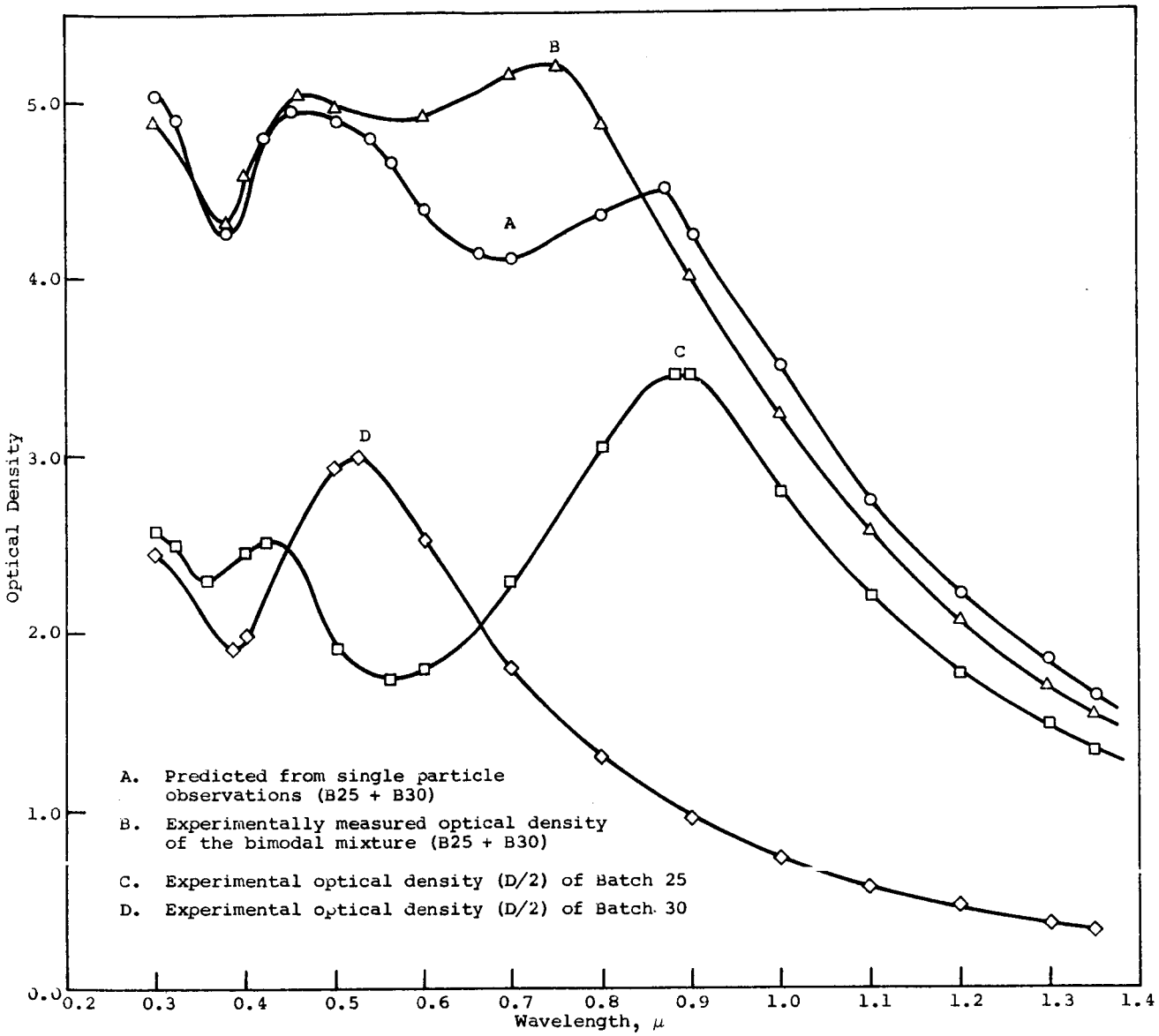

Figure 28

OPTICAL DENSITY OF AgBr SUSPENSIONS
(Batches 25 and 26)

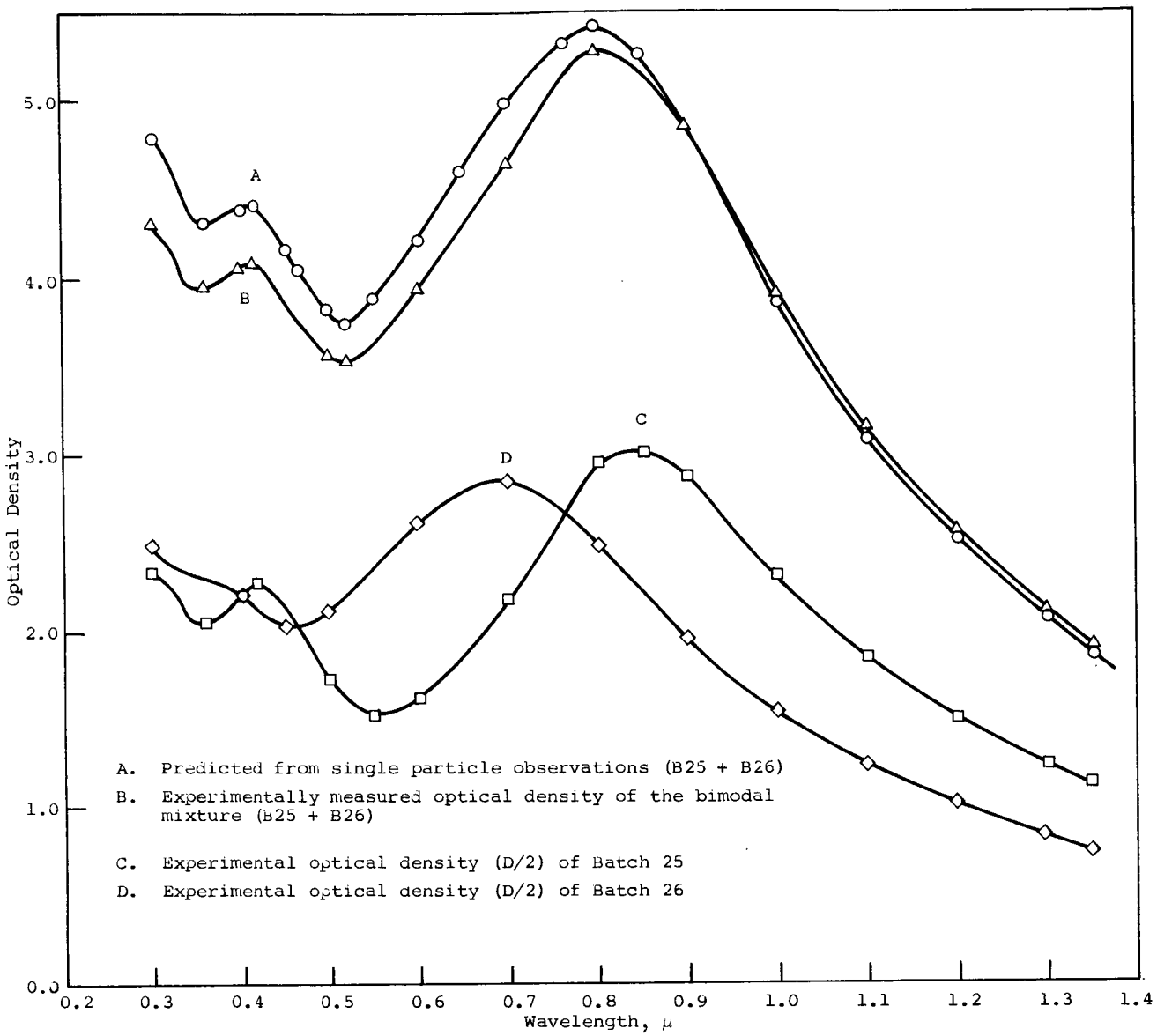

Figure 29

OPTICAL DENSITY OF AgBr SUSPENSIONS
(Batches 25 and 30)

Theoretical variations in the amplitude of minima and maxima with the width of the distribution were reported by Stevenson, Heller, and Wallach (ref. 20). Their data were used to construct the theoretical curves at the estimated concentrations of monodisperse thin films.

The graphically constructed theoretical curves for the optical density of two particle sizes are given in Figure 30. The optical densities observed and theoretical bimodal coatings are compared in Figure 31. The data indicate that although there is some loss of fine structure, the agreement between observed and calculated curves is quite good. The loss of one lobe, which was predicted by the theory, is obviously due to the width of the distribution curves of the particles used in the bimodal mixture.

The back-scatter intensity, which is represented by the reflectance measurements, is given in Figures 32 and 33. A set of films that was identical to the set transmittance measurements was used for the reflectance measurements. The back-scatter intensity is given in extinction units for a direct comparison with the transmittance (optical density) measurements:

$$\text{Back-scatter intensity} = \ln \frac{1}{100\% - \%\ \text{reflectance}} \quad (15)$$

Two modes of illumination were used in the reflectance measurements. In one case, a parallel beam of monochromatic light at near-normal incidence was used for illumination, and hemispherical reflectance was measured. In the other case, diffuse, nondispersed light was used for illumination, and the near-normal compoment of the reflected light was measured. The reflectance measurements were identical for both modes of illumination; this is expected for back-scatter due to isotropic particles. The reflectance measurements indicate that the back-scatter intensities due to each particle size are additive, and therefore in back-scattering the particles in their films tend to act as independent scatterers.

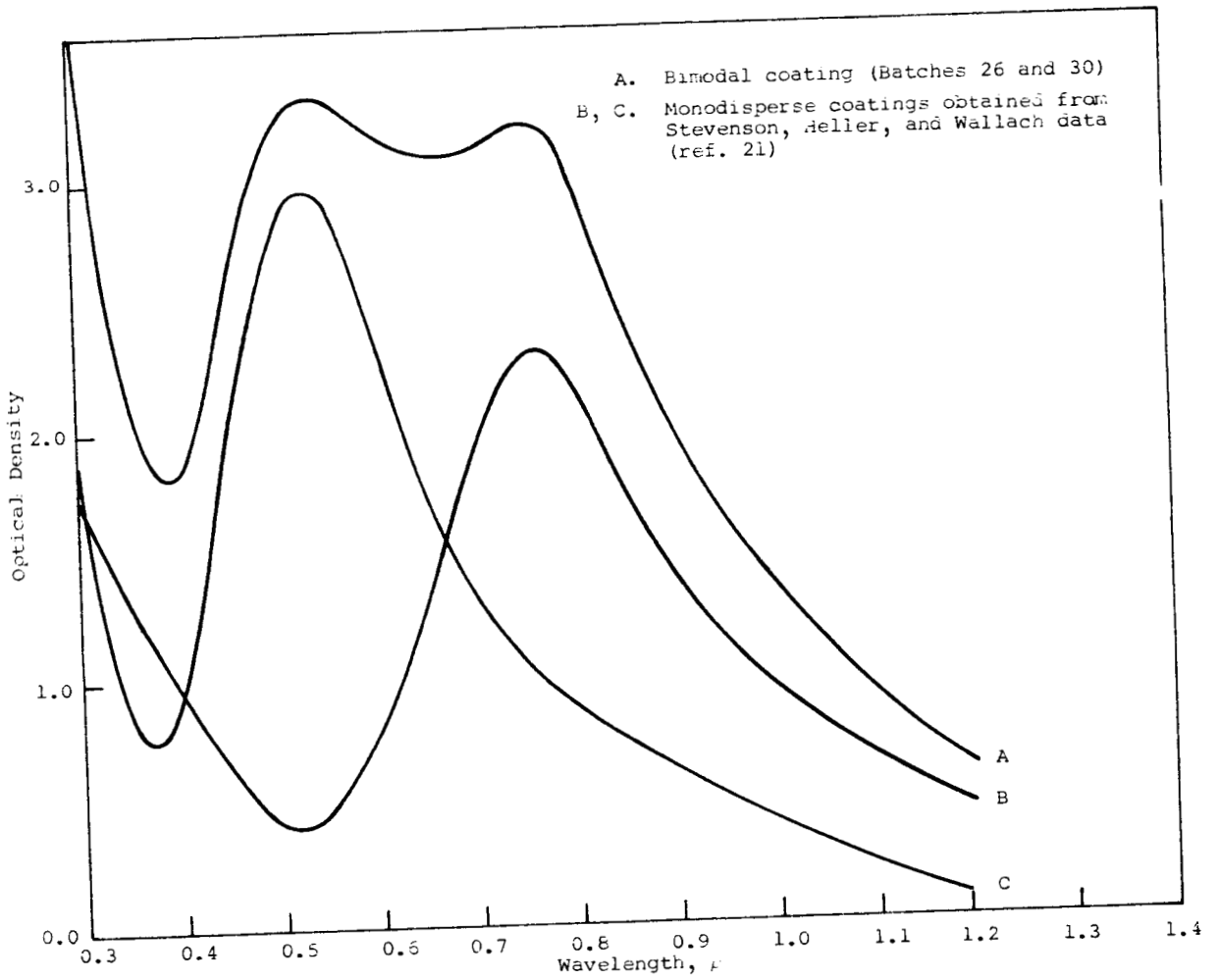

Figure 30

THEORETICAL (MIE) DENSITY OF AgBr COATINGS
(Batches 26 and 30)

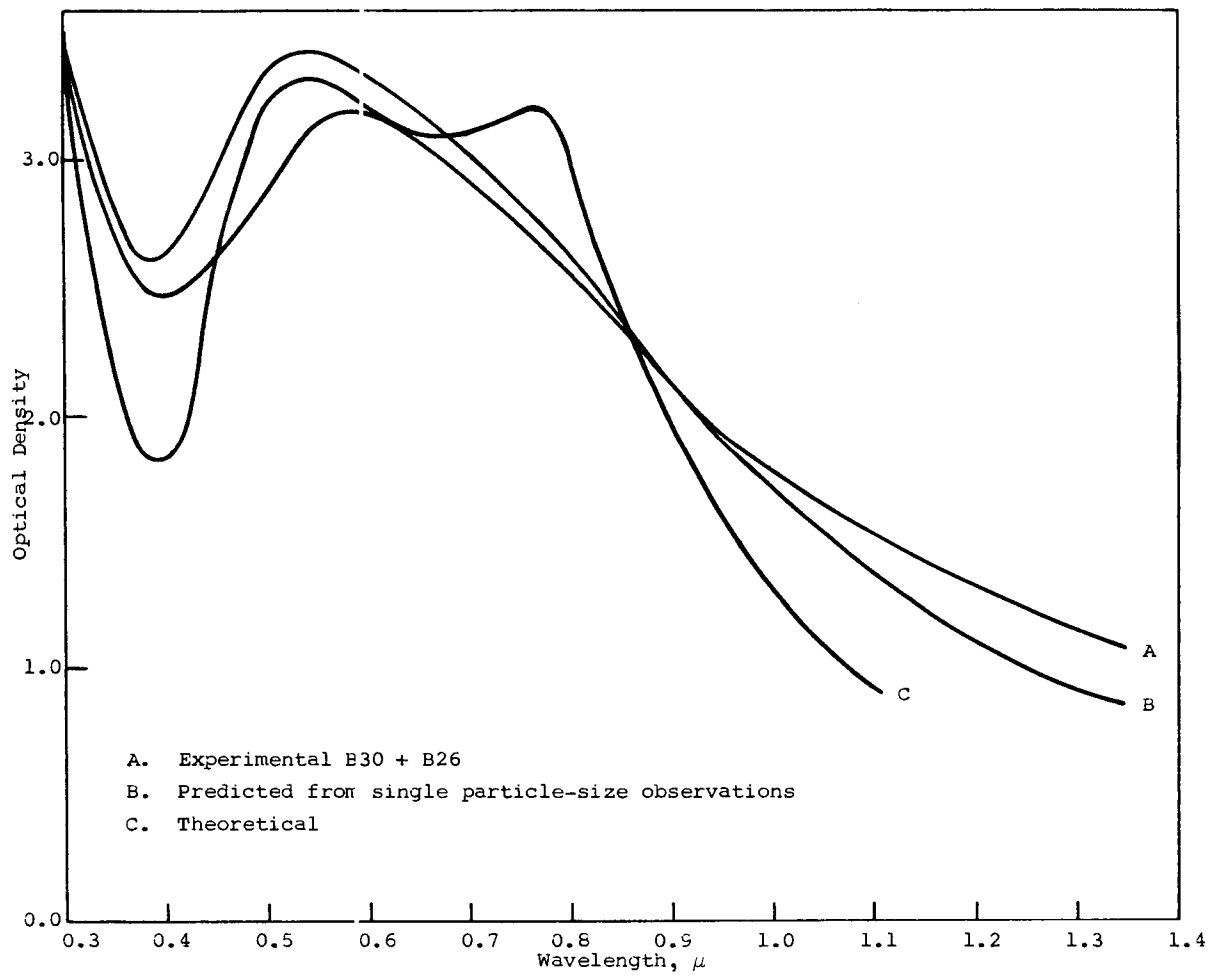

Figure 31

OPTICAL DENSITY OF A MIXTURE OF BATCHES 26 AND 30

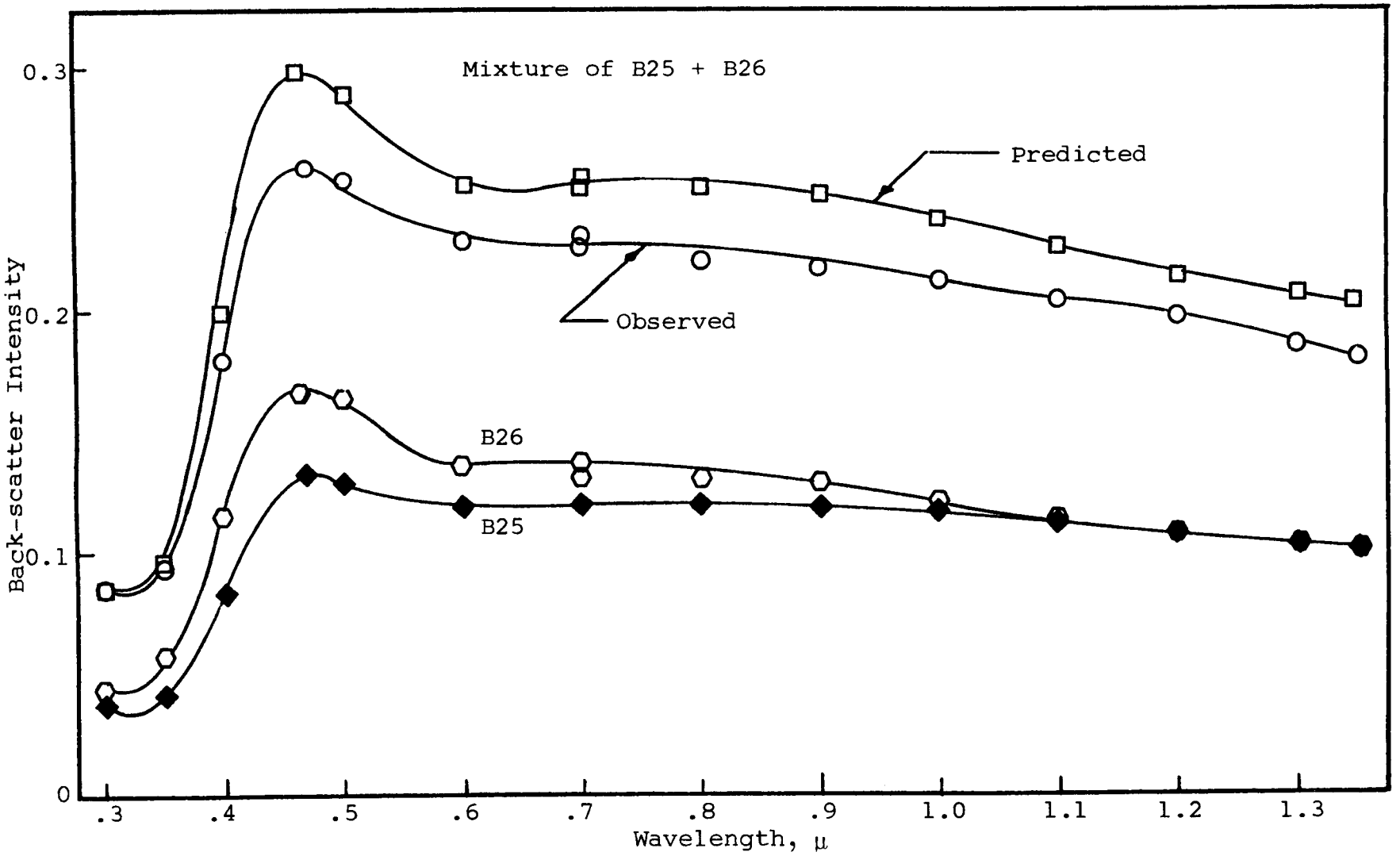

Figure 32

BACK-SCATTER INTENSITY OF AgBr SUSPENSIONS
(Batches 25 and 26)

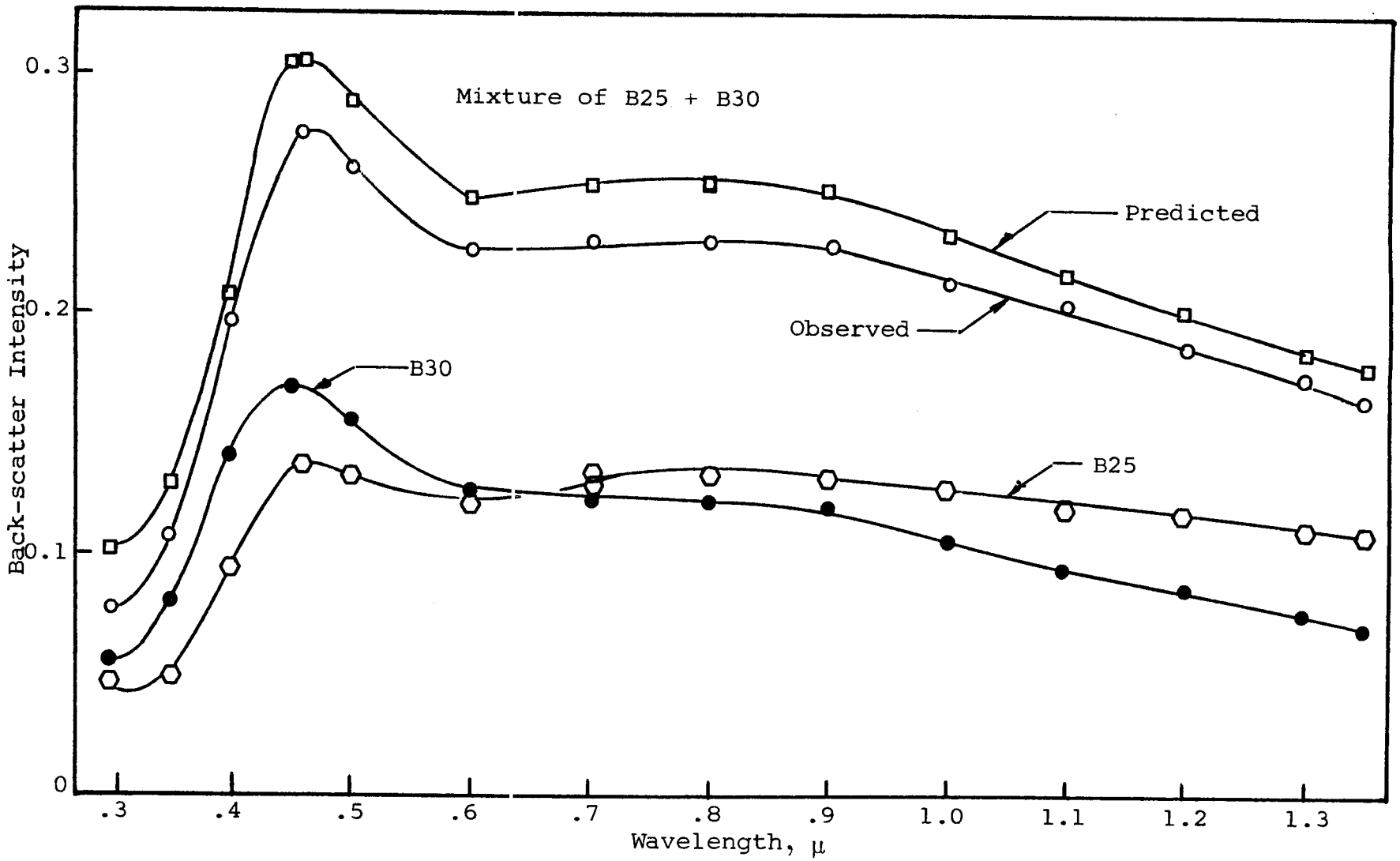

Figure 33

BACK-SCATTER INTENSITY OF AgBr SUSPENSIONS
(Batches 25 and 30)

6. Optical Properties of Films of Various Thicknesses

A set of monodisperse films of intermediate thickness was prepared first and permitted the measurement of both transmittance and reflectance. The optical densities of these films are given in Figure 34. The thickness of the films was measured interferometrically. The particle radius was 0.30 μ (batch 25). The reflectance measurements of the same films are given in terms of back-scatter intensity in Figure 35. The ratio of back-scattered energy (Equation 15) to the total scattered energy, called the "back-scatter coefficient," is shown in Figure 36.

During the reduction of the data, it was noted that a linear plot of back-scatter intensity, BI, versus ln t, where t is the film thickness, could be obtained. The data are presented in Figure 37 for the back-scatter intensity at a wavelength of 0.47 μ.

Additional experiments were performed to confirm the above observation. Two sets of films of various thicknesses were prepared. The thickness of the films was uniform throughout the area of observation. The particle radii were 0.32 μ for batch 26 and 0.20 for batch 30. The reflectances are given in terms of back-scatter intensities in Figures 38 and 39. Back-scatter intensities at 0.46 μ versus the estimated limits of the thickness measurements for batch 26 are plotted in Figure 40. Figure 41 is a similar plot for batch 30 at a wavelength of 0.45 μ.

Since Figures 37, 40 and 41 are linear plots, the following relationship between reflectance and thickness can be established.

$$\ln \frac{1}{100 - R_\lambda} = C_1 \ln t + \ln C_2 \qquad (16)$$

R_λ is the percent reflectance

t is the film thickness

C_1 and C_2 are experimental constants corresponding to the slope and the intercept.

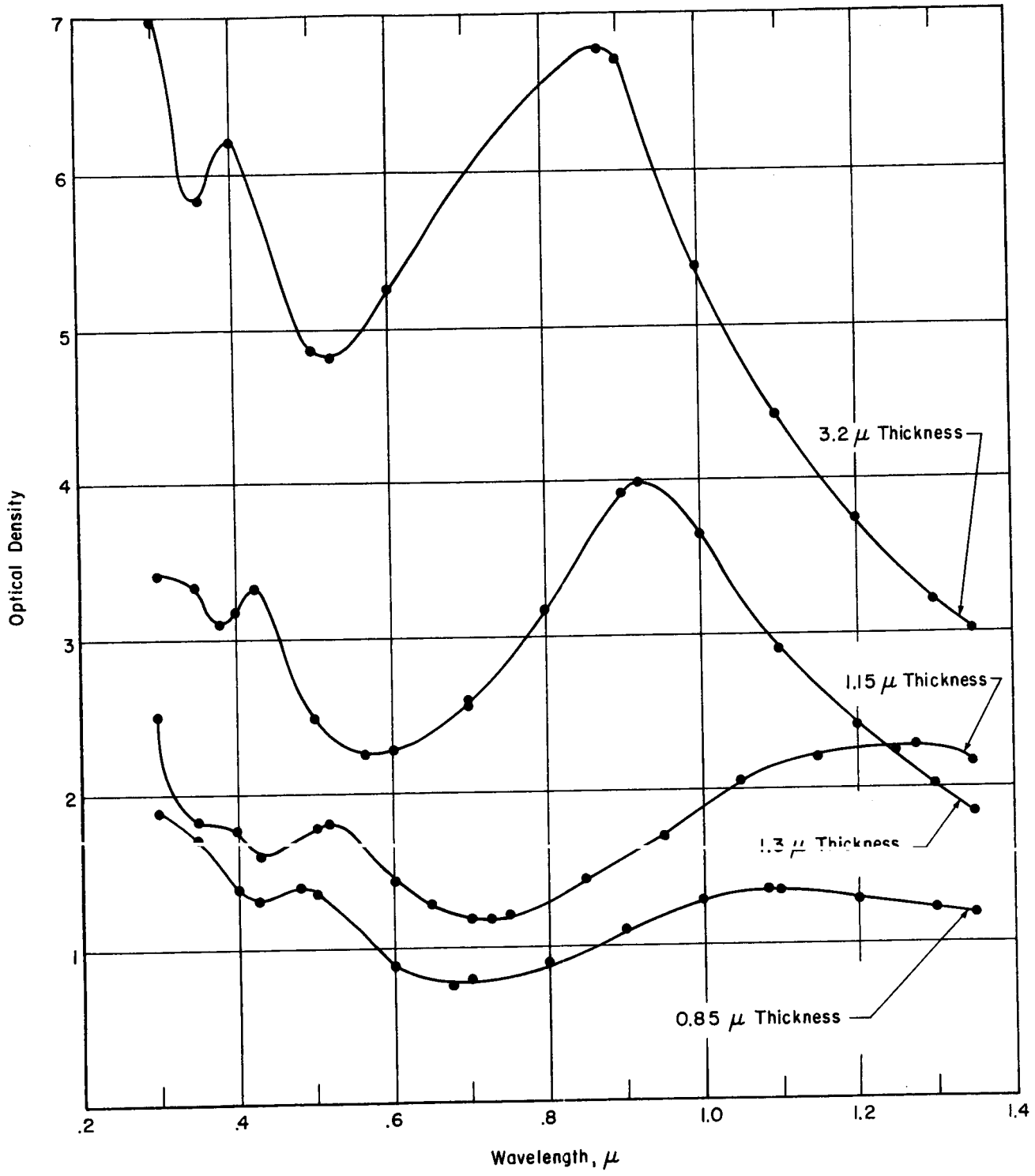

Figure 34

OPTICAL DENSITY AT VARIOUS THICKNESSES

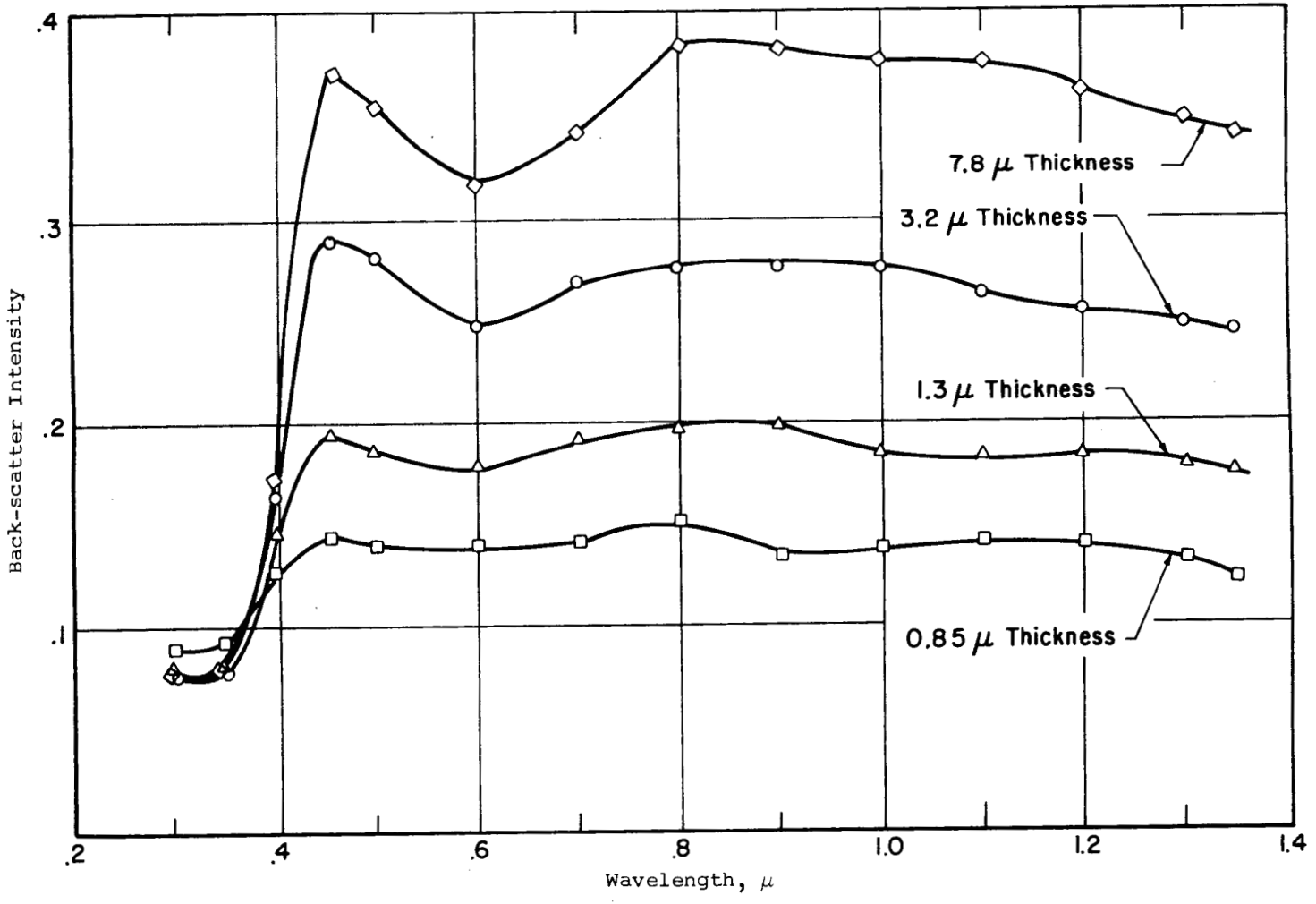

Figure 35

BACK-SCATTER INTENSITY AT VARIOUS THICKNESSES

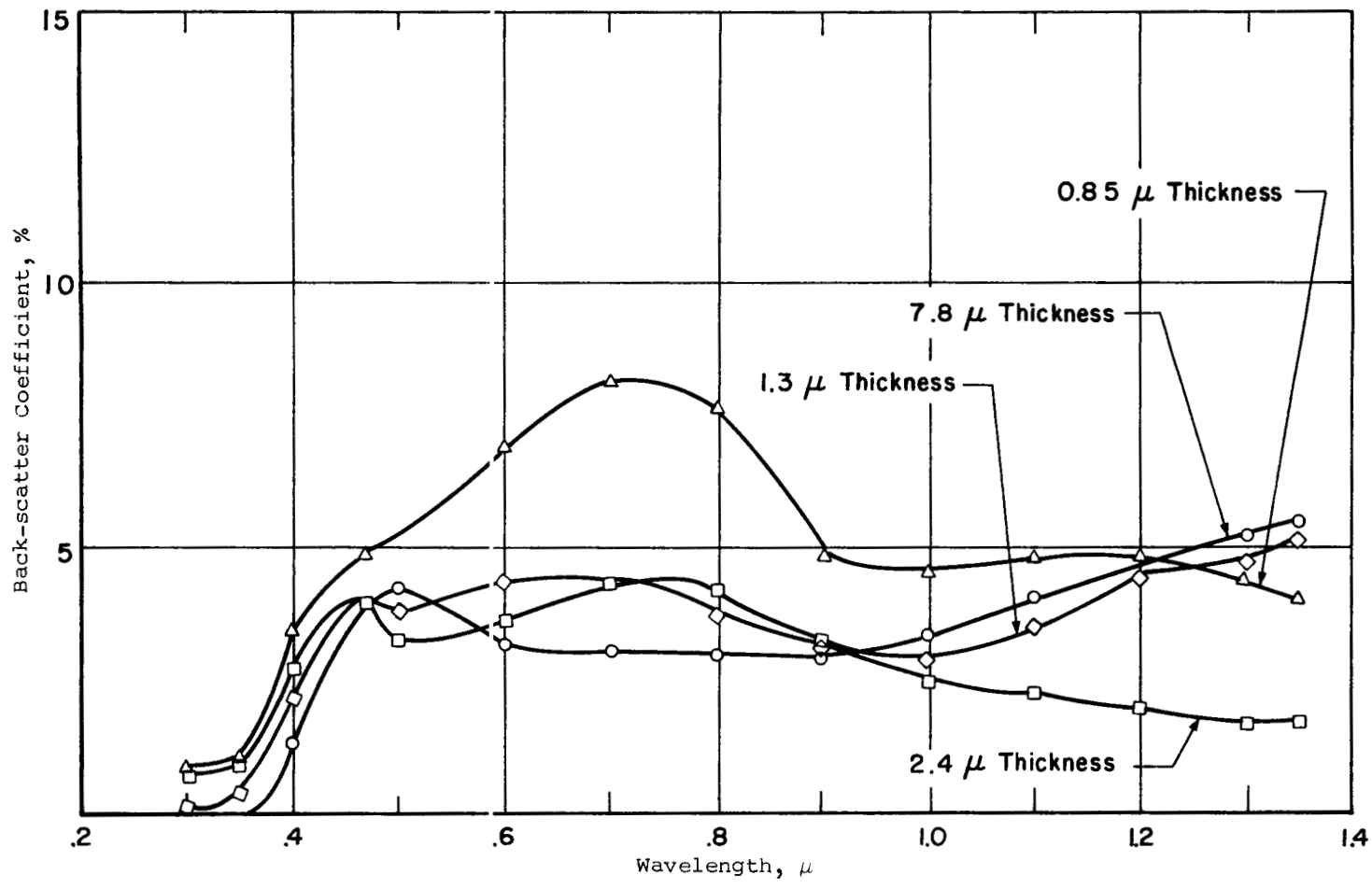

Figure 36

BACK-SCATTER COEFFICIENT AT VARIOUS THICKNESSES

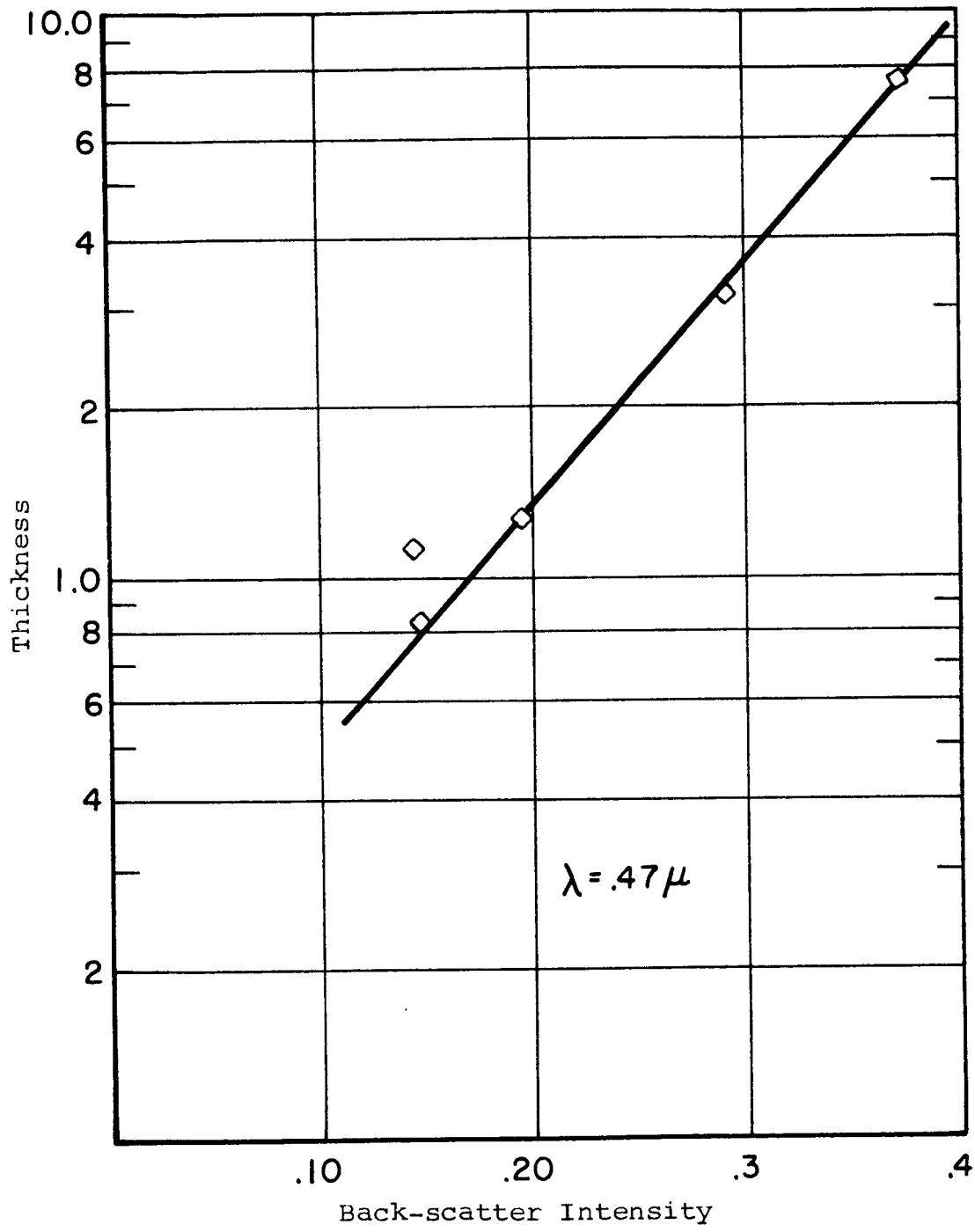

Figure 37

THICKNESS VERSUS BACK-SCATTER INTENSITY (BATCH 25)

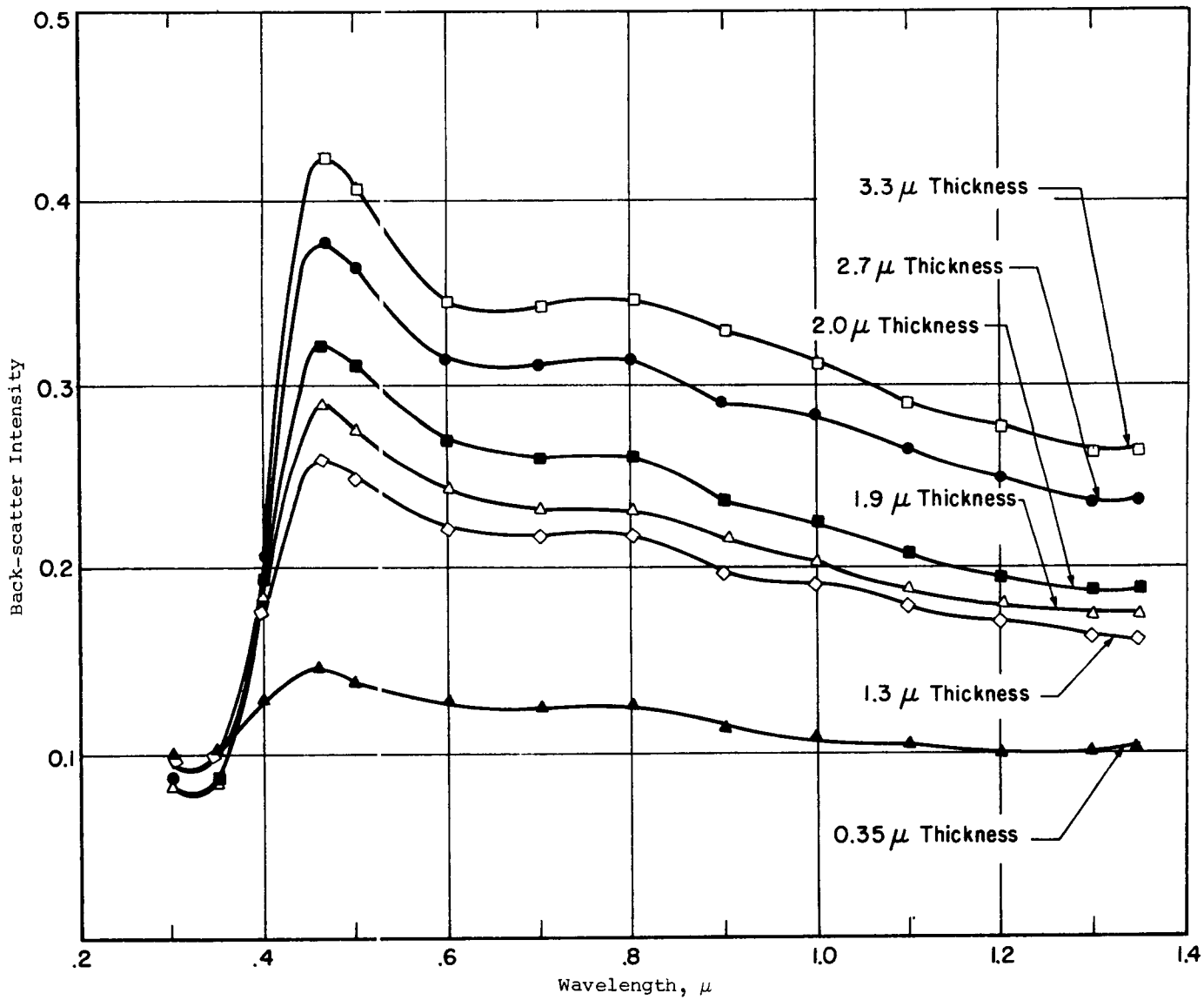

Figure 38

BACK-SCATTER INTENSITY AT VARIOUS THICKNESSES (BATCH 26)

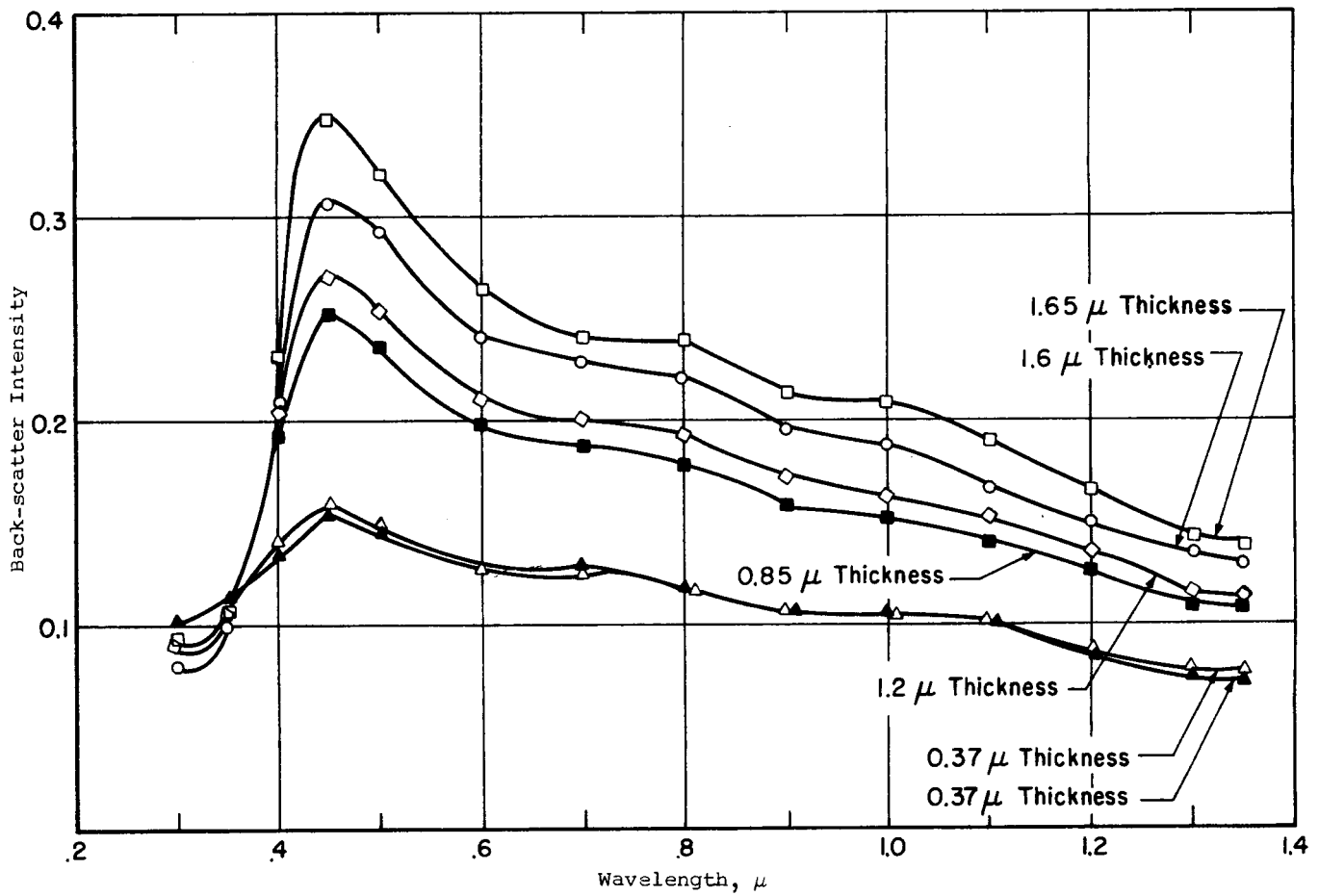

Figure 39

BACK-SCATTER INTENSITY AT VARIOUS THICKNESSES (BATCH 30)

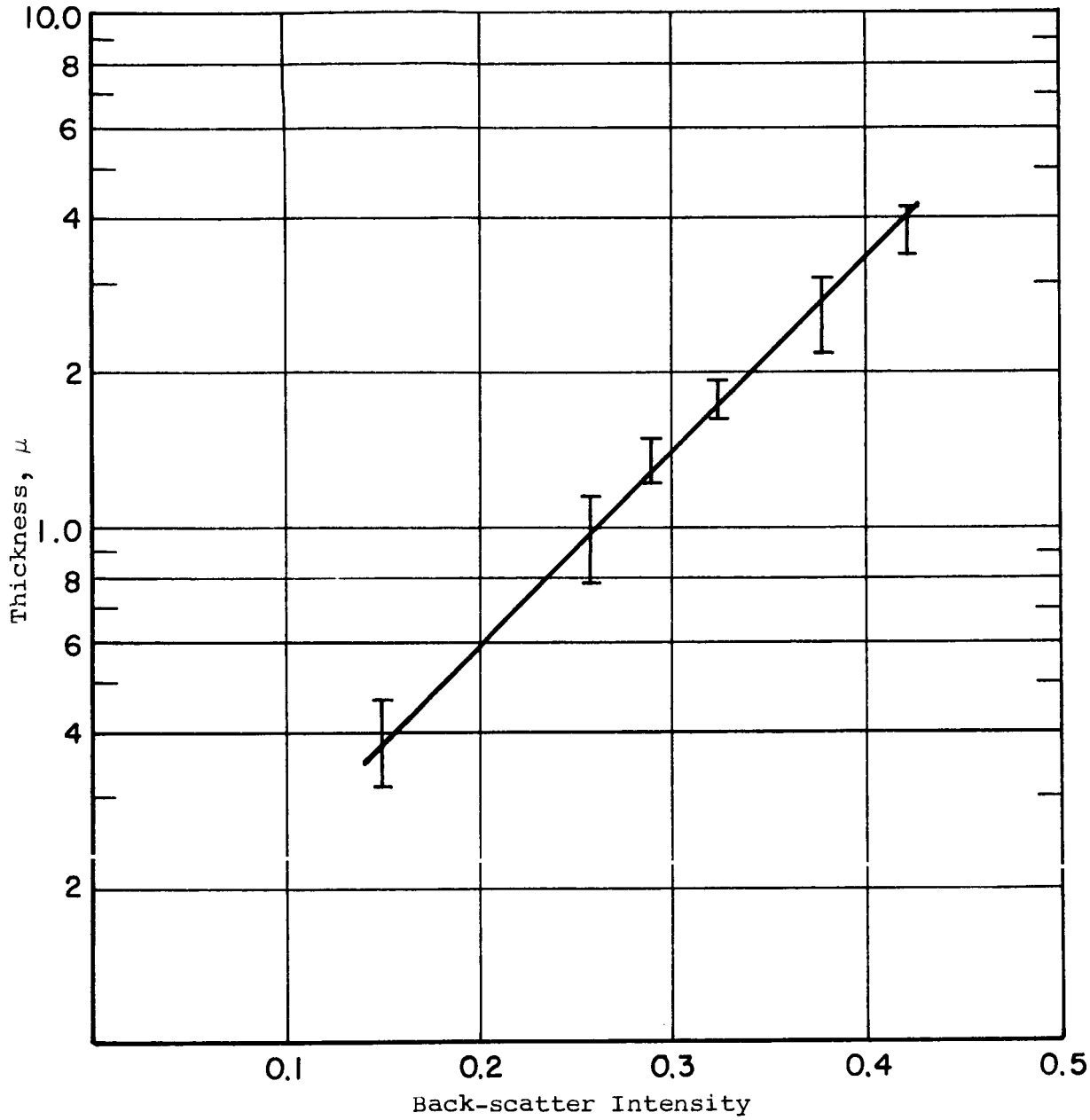

Figure 40

THICKNESS VERSUS BACK-SCATTER INTENSITY (BATCH 26)

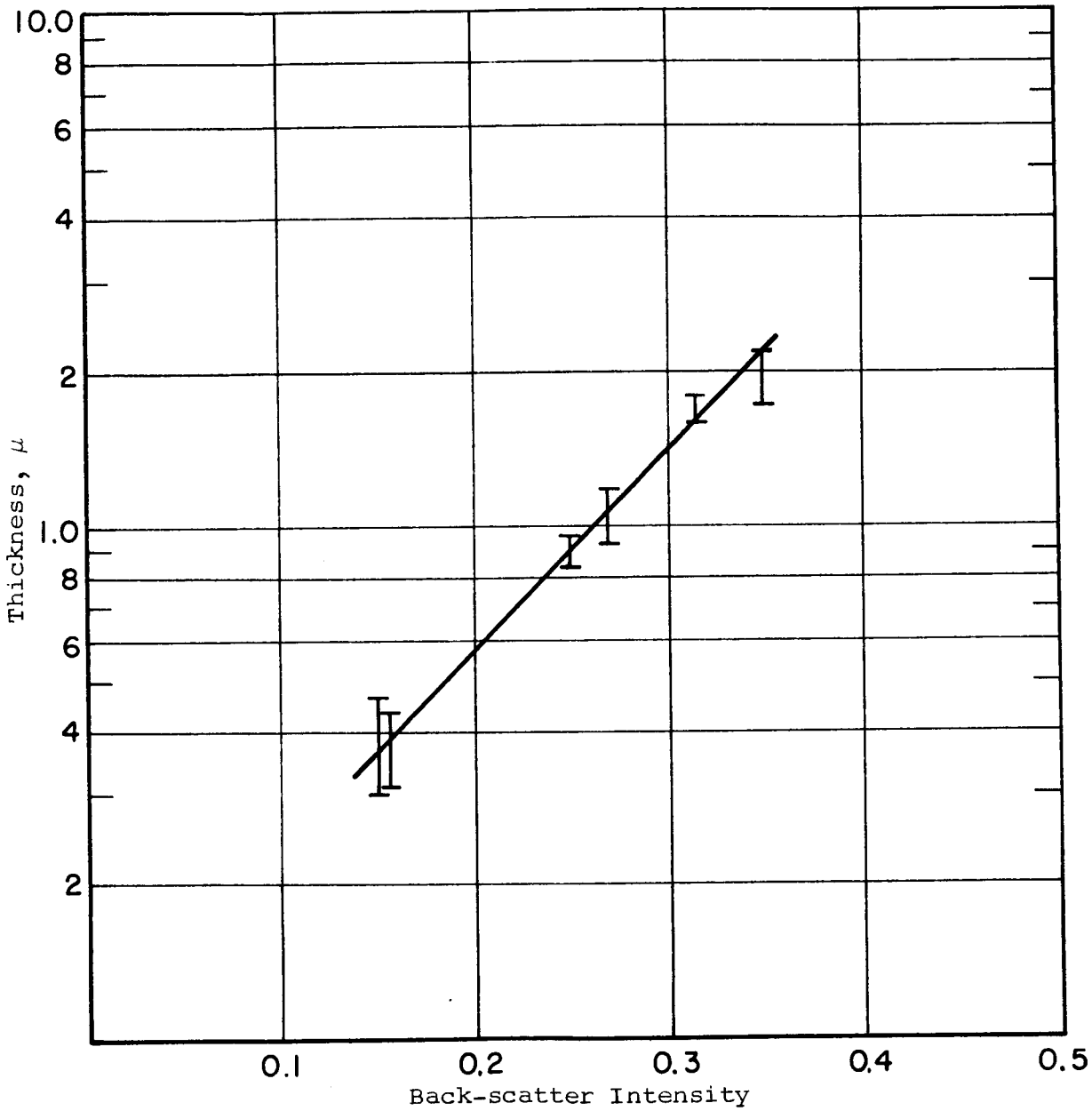

Figure 41

THICKNESS VERSUS BACK-SCATTER INTENSITY (BATCH 30)

C_1 and C_2 depend on the particle size, effective refractive index of the system, and the wavelength of measurements. All the given data are at the wavelengths of maximum reflectance (Figures 35, 38 and 39).

Equation 16 can be written as:

$$\frac{1}{100 - R_\lambda} = C_2 t^{C_1} \tag{17}$$

or, in terms of reflectance, R:

$$R_\lambda = 100 - \frac{1}{C_2 t^{C_1}} \tag{17a}$$

7. Optical Properties of Flocculated Dispersions

A set of films was prepared from a flocculated suspension of monodisperse particles. Figure 42 shows the optical density as a function of wavelength for such a dispersion. The data show that the oscillations in transmittance have almost disappeared. Also, the optical density is considerably less than for a well-dispersed suspension. Figure 43 shows the back-scatter coefficient for this suspension; it indicates a considerable decrease in back-scattering. It is therefore concluded that flucculation tends to destroy the light-scattering properties of monodisperse films.

D. Summary and Conclusions

Good agreement between theoretical predictions and experimental observations was obtained for monodisperse and bimodal dilute suspensions. Measurements of dilute suspensions were limited to a particle concentration equivalent to a particle separation of 15 diameters. Minor oscillations in the special transmittance curves of dilute suspensions of polystyrene spheres were observed. These minor oscillations were attributed to the resonance at the multipoles.

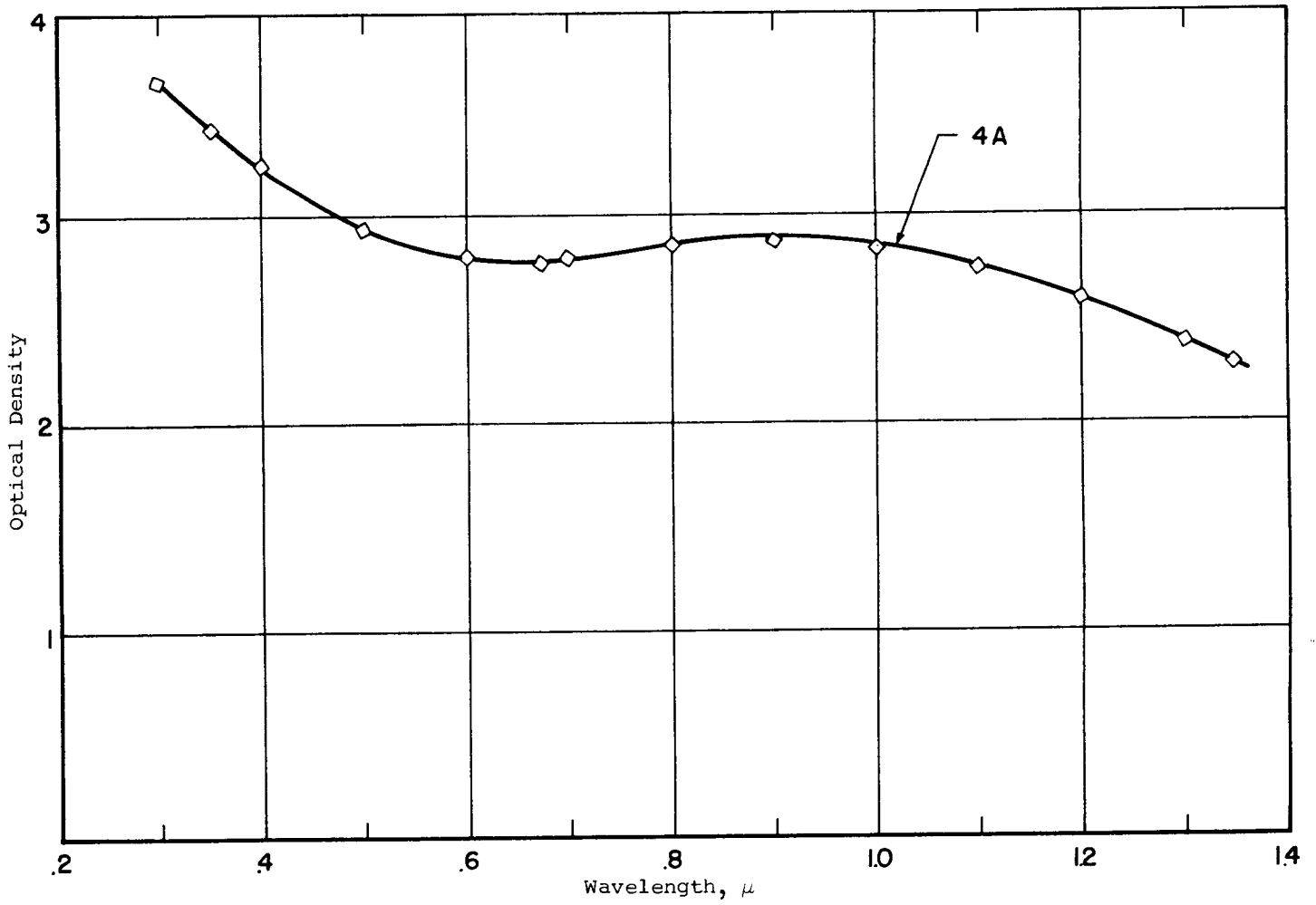

Figure 42

OPTICAL DENSITY OF A FLOCCULATED COATING

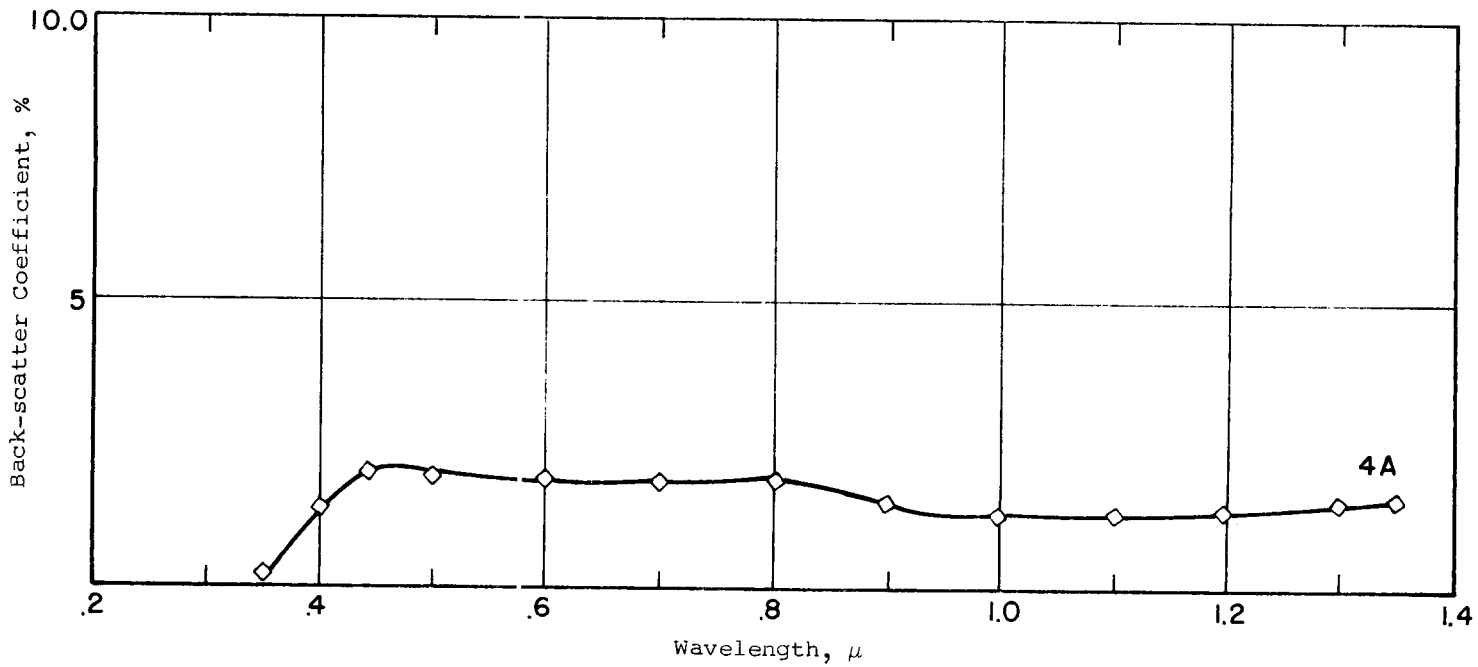

Figure 43

BACK-SCATTER COEFFICIENT OF A FLOCCULATED COATING

Within the error of the thickness measurements, agreement was obtained between the spectral transmittances and reflectances predicted from single-particle measurements and those observed experimentally on bimodal mixtures in concentrated thin films. Thus the data indicate that the particles within thin concentrated films (of up to four layers) tend to act as independent scatters.

The reflectances of thicker films were less than those of thinner films at wavelengths less than 3.5 μ. This can be explained on the basis of molecular absorption of silver bromide. Since at short wavelengths the energy-loss mechanism is absorption and not scattering, the reflectance of thick films decreases as a result of increases in the absorptive path length.

The back-scatter coefficient of thin films tend to be slightly higher than that of the thick ones. The back-scatter intensity obtained from bimodal mixtures was less than that predicted from measurements of monodisperse films. These two observations tend to support the ideal coating model proposed in the following paragraphs.

Previous experimental results indicate that a theoretical model based on the Mie scattering theory or a semiempirical model based on single-particle observations can predict the spectral transmittance properties of thin pigmented films to a fairly close approximation. The effects of absorption and interface reflection have not yet been considered directly in the experimental studies. It appears that the absorption effects are closely related to multiple scattering events. The effects of multiple scatter and absorption become quite significant in films of several layers (more than 5) of scatterers. Thus, in any real pigmented paint system some degree of multiple interactions and absorption will always be present, but these effects are minimized in thin layers of monodisperse suspensions.

Based on our experimental data, which so far consist primarily of spectral transmittance measurements, a real pigmented coating should fulfill the following set of requirements.

(a) The substance to be used as scatterer (pigment) should have a minimum bulk absorption coefficient for any given spectral band. Less radiant energy will inherently be lost and converted to thermal and molecular energy modes if the scattering particles are transmitting.

(b) The ratio of the refractive indexes between the particles and the suspension medium should be the largest available. Total scattering and especially back-scattering efficiencies increase very significantly at high effective refractive indices, with the exception of the refractive index close to infinity. In this case, the radiation can no longer penetrate the particle, and this lack of optical resonance greatly reduces the scattering efficiency.

(c) To attain minimum interactions between the scatterers, the particles should be packed in exceedingly thin layers containing particles of uniform size. The distribution of layers with respect to the incident beam should be such that each layer contains increasingly larger particles. The top layer, containing the smallest particles, will interact only with shortest wavelengths, allowing longer wavelengths to pass undisturbed in both directions. In this manner, each succeeding layer will interact with radiation of increasing wavelength. Such a coating is illustrated schematically in Figure 44.

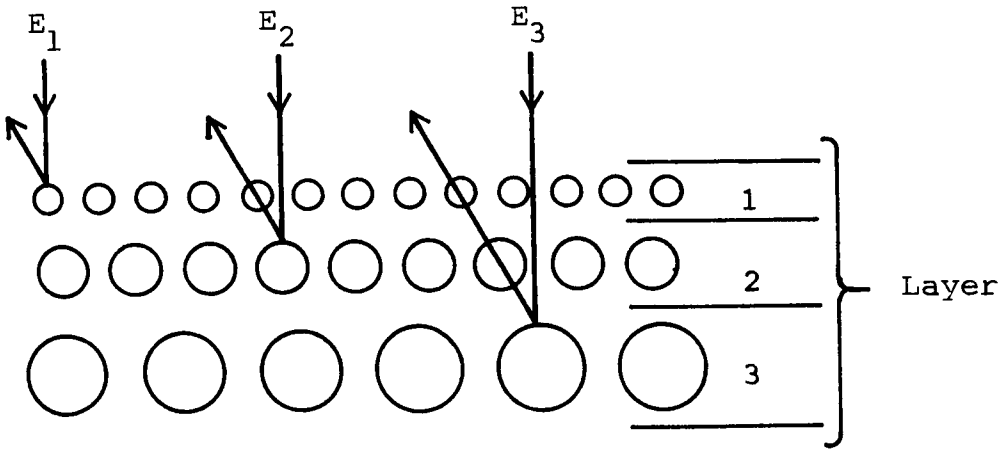

Interactions between protons and layers at increasing particle size.

$E_1 > E_2 > E_3$, or $\lambda_1 < \lambda_2 < \lambda_3$.

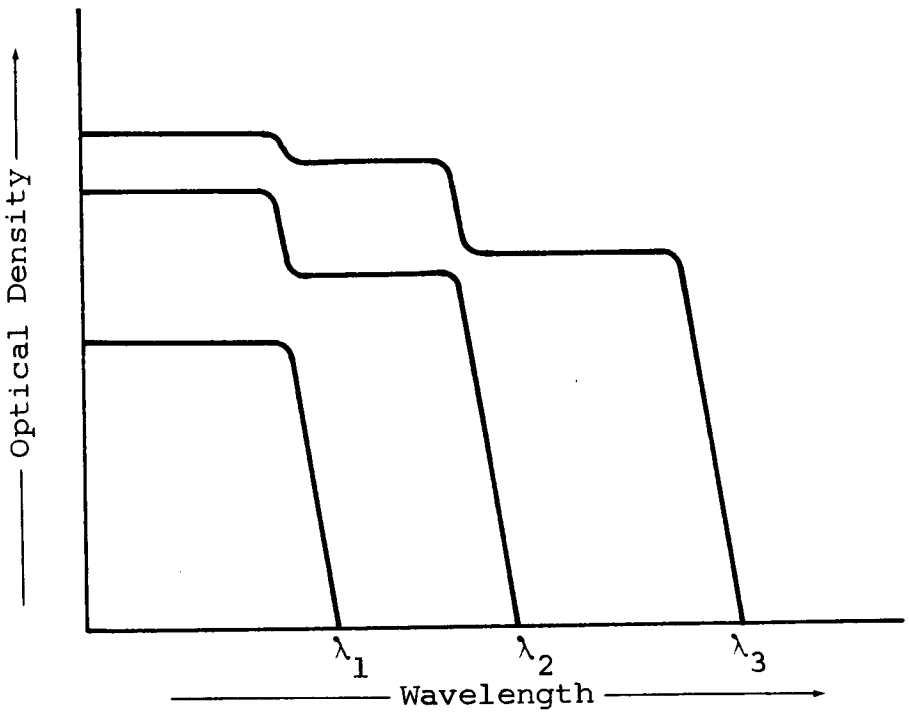

Optical density due to successive addition of layers.

Figure 44

SCHEMATIC OF MULTILAYER COATING AND RESULTANT OPTICAL DENSITY OF LAYERS

IV. VERIFICATION OF MULTILAYER MODEL OF PAINT FILM

The paint film model described in Figure 44 of Section III-D utilizes regular layers of closely sized pigment particles. The particles should be packed in exceedingly thin layers containing particles of uniform size. The distribution of layers with respect to the incident beam should be such that each layer contains increasingly larger particles. The top layer, containing the smallest particles, will interact only with shortest wavelengths and will allow longer wavelengths to pass undisturbed in both directions. In this manner, each succeeding layer will interact with radiation of increasing wavelength.

A search for closely sized uniform material with which to test the validity of this model showed that polystyrene and polyvinyl toluene latex suspensions (manufactured by Dow Chemical Co. for use as particle-size standards) were the most probable source of readily available material. Optical and electron microscope studies of these latex suspensions (ref. 21) showed the particles in any given suspension to be near-perfect spheres of uniform size. However, microscopic studies showed groups of particles in contact but failed to identify these either as tightly bound clusters or merely as separate particles in chance juxtaposition. In addition, estimation of the standard deviation of the distribution of each suspension were unreliable, since, in general, estimates were based on about 100 measurements.

In order to determine the suitability of these materials for use in studying the properties of the multilayer model, knowledge was needed of the presence and the permanence of clusters, of the standard deviation, and of mean particle size of each suspension. By using the centrifugal disc photosedimentometer previously designed, built, and proved by IIT Research Institute (ref. 22), it was shown that:

(a) The Dow latex suspensions contain tightly bound agglomerates that may be fractured by ultrasonic vibration.

(b) The smaller agglomerates are less likely to fracture than the larger agglomerates.

(c) The standard deviation of 2.956- and 1.305-μ latex suspensions were 0.12 and 0.06, respectively.

On the basis of these results, it was concluded that the latex suspensions manufactured by Dow Chemical Co. are suitable for use in verifying the multilayer model by reflectance techniques. However, visual examination showed a color difference between latex suspensions of different size; it was not possible to relate this to either the effect of light on particles of different sizes or to differences between the materials of the particle. Since the verification of the multilayer model requires consistent material in each size fraction, further work on the model was suspended.

V. CHARACTERIZATION OF OPTICAL PROPERTIES OF MIXED POWDERS

A. Description of the Reflectometer

The reflectometer used consists of a vertically mounted optical bench (Figure 45) supporting a mercury lamp and a diffuser directly above a sample holder. The light scattered and transmitted at any angle in a plane perpendicular to the sample surface is detected by a photoresistive cell that can be rotated in a circle about the sample. The light intensity is monitored on an oscilloscope as a change in the DC voltage developed across a resistance in series with the photocell.

Figures 45 and 46 show the apparatus. Figure 47 is a schematic diagram of the detection circuit.

The reflection properties of mixed powders were examined as described below.

B. Preparation of Mixed Powders

Initial attempts to make a mixture of carbon black and titanium dioxide by grinding produced a lumpy powder of uneven surface texture. Examination showed that the composition of the powder was not constant throughout the lumps. To obtain a fine powder, the lumps were broken and passed through a U.S. standard sieve No. 325. The resultant powder agglomerated rapidly when powder beds were made and yielded gross surface roughness.

Thus, it was considered impossible to obtain a constant surface texture and a uniform mixture by dry powder mixing alone. The method used in the paint industry, i.e., the powder mixture is pressed against a plate that is subsequently removed, was rejected because of the unknown pressure gradient and manner of packing immediately adjacent to the plate. These factors could affect the reflectance properties of the surface.

An alternative method was devised. Liquid suspensions of the component to be mixed were combined and filtered onto a membrane filter (Millipore HA series). The deposits had an even surface texture and color as determined by visual examination.

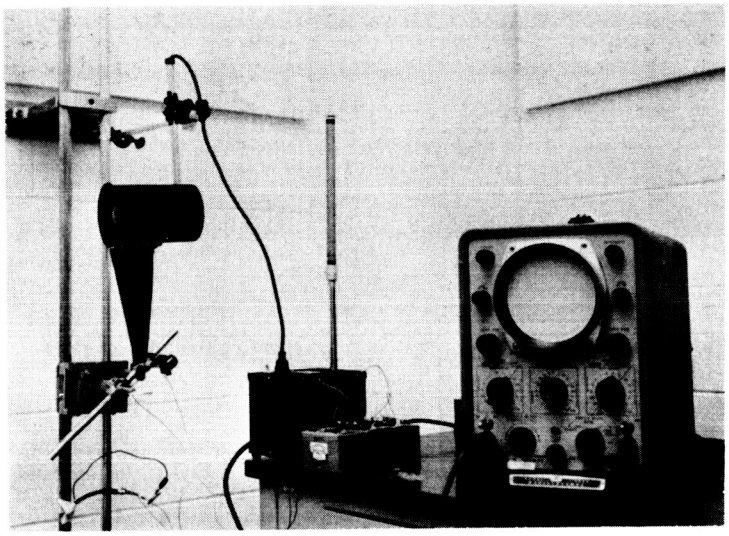

Figure 45

OPTICAL BENCH REFLECTOMETER

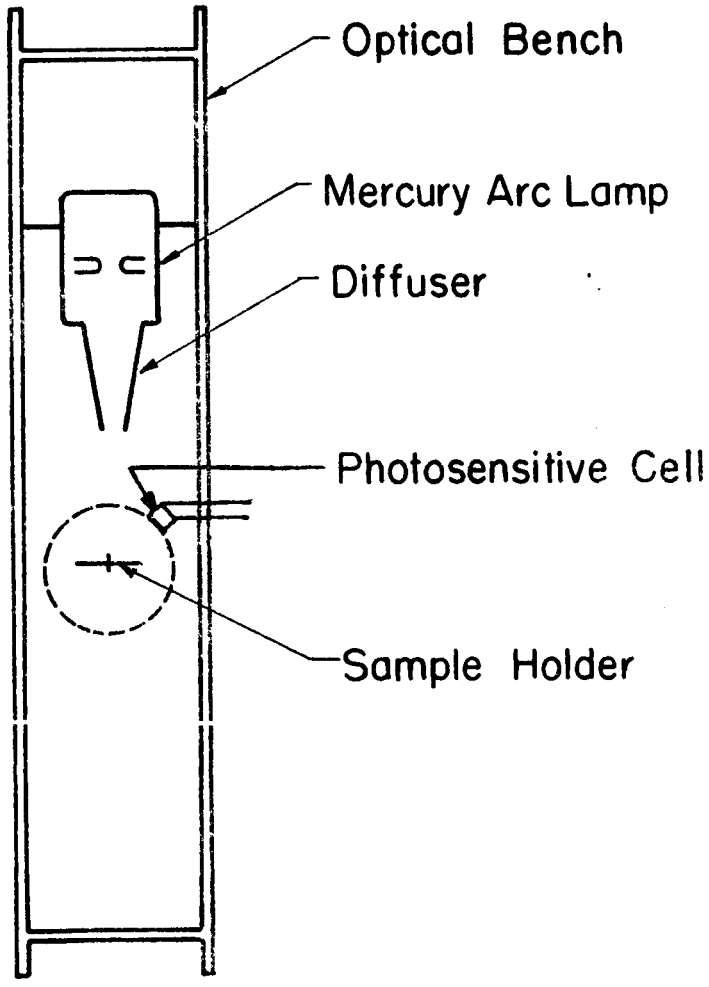

Figure 46

SCHEMATIC DIAGRAM OF THE REFLECTOMETER

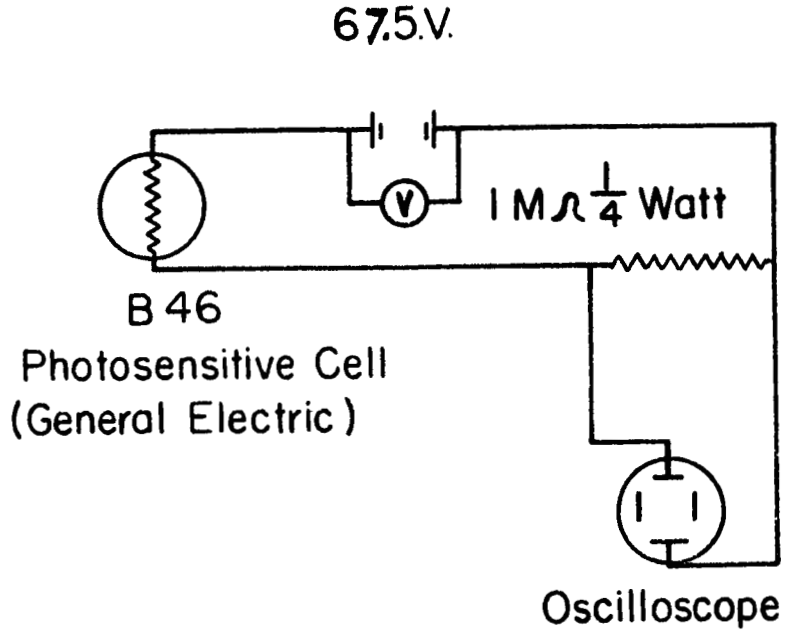

Figure 47

SCHEMATIC DIAGRAM OF THE DETECTION CIRCUIT

C. Experimental Results

A series of known volumes of 0.1 wt. % aqueous titanium dioxide suspension was deposited on separate white membrane filters. The dried filters were examined by using the photocell placed at 10° intervals from 20 to 90° to the vertical. The results are shown in Table 10. The reflected light intensity remained essentially constant for deposits of 1 cc and larger.

Table 10

REFLECTION FROM TITANIUM DIOXIDE ON WHITE FILTERS

	Reflection					
		Titania Suspension, cc				
Angle, °	Filter	0.1	0.25	0.5	1.0	2.0
20	90	80	77	78	74	74
30	82	69	68	69	67	66
40	72	58	58	58	57	57
50	60	46	50	46	48	48
60	46	36	38	33	36	36
70	31	27	24	20	23	25
80	16	13	13	13	11	13
90	7	5	4	2	5	5

Since the reflectivity of the filter and the powder was similar, further measurements were made by using black filters. The results obtained from observations on damp and dry filters are shown in Table 11.

A series of graphite and titanium dioxide mixtures was deposited on white filters, and observations were made as before. The results are shown in Figure 48, in which the intensity of the light reflected at 20° is plotted against the weight percent of graphite in the sample.

The average particle sizes of the graphite and titanium dioxide suspensions was 0.8 and 1.0 μ, respectively.

Table 11

REFLECTION FROM TITANIUM DIOXIDE ON BLACK FILTERS

	Reflection								
		Titania Suspension, cc							
Angle, °	Filter	0.1	0.25	0.5	1.0	2.0	3.0	5.0	10.0
				Damp Filters					
20	18	24	33	38	48	53	54	58	60
30	17	21	31	36	47	52	52	54	59
40	16	20	28	32	42	47	47	49	52
50	13	17	24	26	38	39	40	44	44
60	12	13	20	20	30	32	33	36	36
70	9	10	15	16	24	24	23	26	25
80	6	6	9	10	14	10	14	16	15
90	3	2	3	3	3	2	2	6	6
				Dry Filters					
20		35	45	46		60	60	63	62
30		32	39	40		56	58	60	60
40		29	33	37		51	51	60	59
50		24	31	32		41	42	48	47
60		20	26	24		32	33	38	38
70		15	19	21		25	25	25	26
80		9	12	11		17	16	16	15
90		3	3	4		6	6	5	6

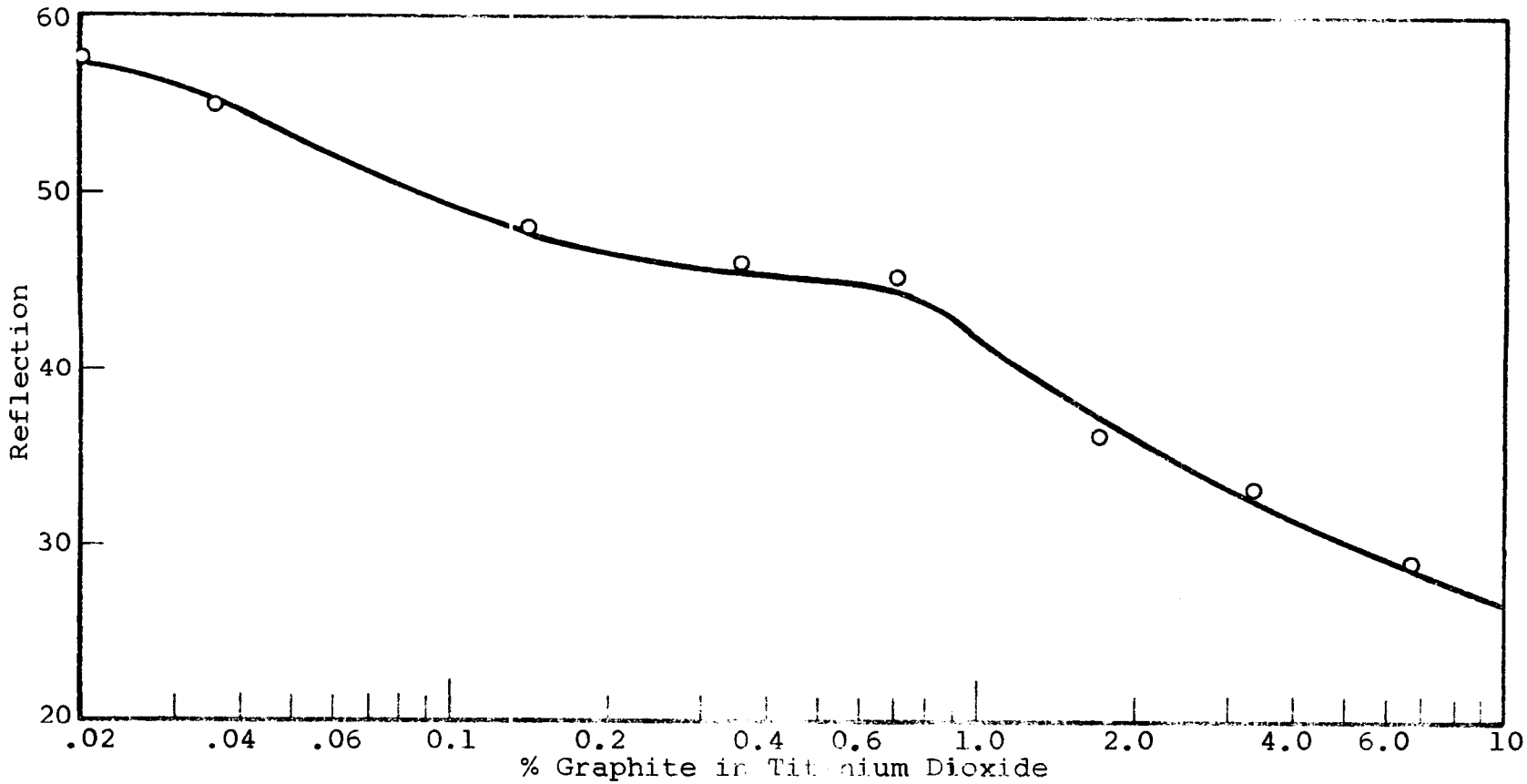

Figure 48

REFLECTANCE OF RUTILE AND GRAPHITE MIXTURES ON A NOMINALLY WHITE SURFACE

D. Discussion

Samples deposited on both black and white filters showed a constant intensity of reflected light at sample volumes greater than about 2 cc (Tables 10 and 11). Thus, all forward-directed light is scattered in penetrating a film of thickness corresponding to 2 cc.

If we assume a monosized powder of packing fraction 50%, a 2-cc sample will form a deposit about 10 particles deep. This compares well with the theoretical work discussed in Volume 3, in which 7 screens of packing fraction 50% transmitted less than 1% of the forward beam. This finding suggests that when the forward beam is destroyed, the resultant energy is present as diffuse radiation.

Tables 10 and 11 show that the intensity of the reflected light decreases as the angle of the photocell to the vertical is increased. If this were purely a geometrical effect, the plot of intensity versus the sine of the angle would be a straight line. Figure 49, which shows a nonlinear relationship, indicates that the incident beam is collimated and the reflected beam is directional. At high angles of scatter results were susceptible to tilting and bending of the filter and the deposit, presumably because of the small angle of observation. To eliminate errors resulting from these two effects, measurement should be made only at small, known scattering angles.

Table 11 shows the results for damp and dried deposits. At high observation the results are not significantly different, but at angles smaller than about 40° a systematic difference was observed. Presumably, the moisture collects by capillary action within the filter and between the particles. This could have the effect that at large angles the photocell views only the tops of particles (as an observer would see mountains from the surrounding plains) and does not consider the moisture. At smaller angles the moisture in the hollows contributes to the scattering to the photocell and results in the observed differences.

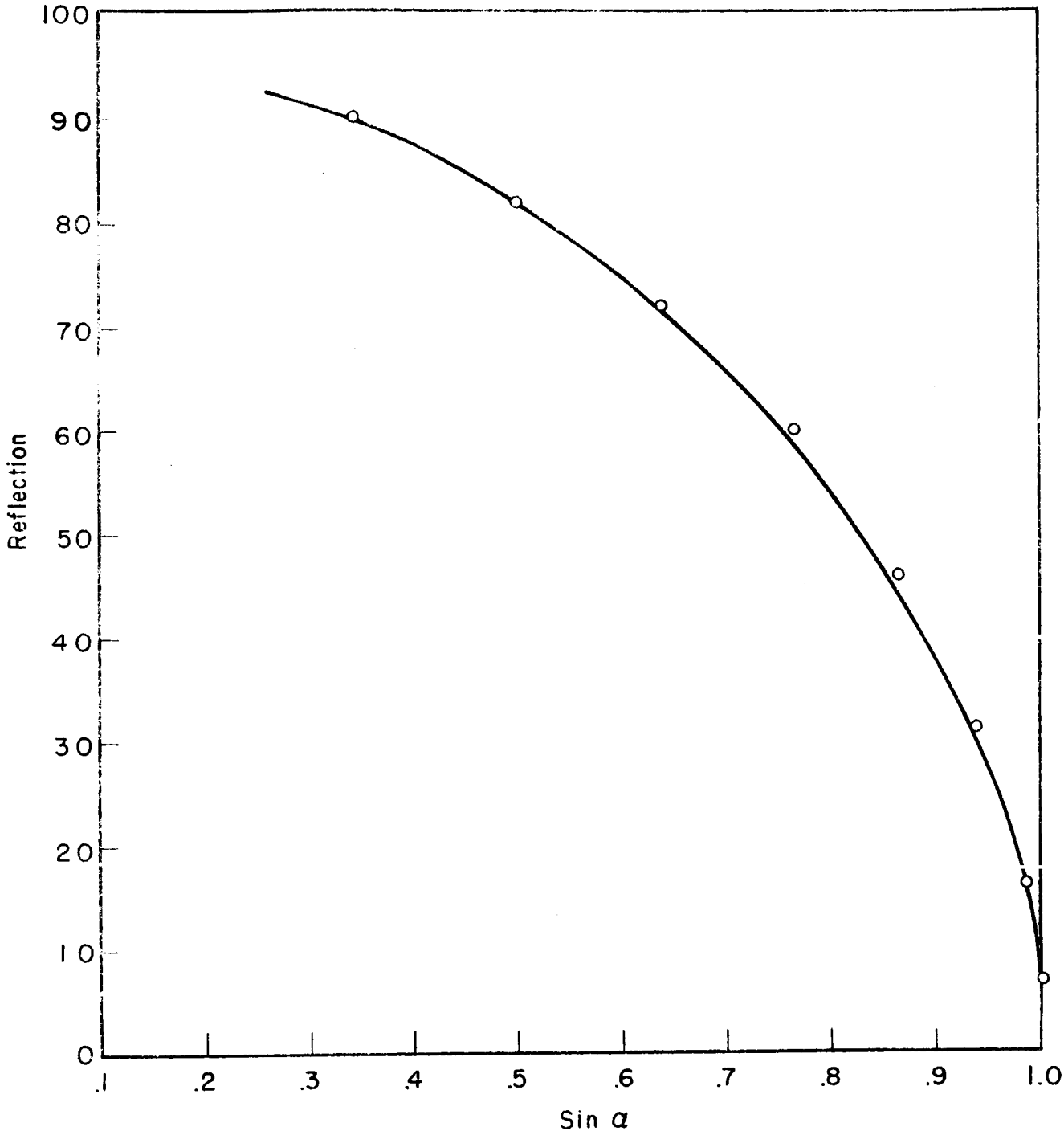

Figure 49

RELATIONSHIP BETWEEN ANGLE α OF PHOTOCELL
AND VISIBLE AREA OF DEPOSIT

Figure 49 shows a simple relationship between the concentration of black in a mixture and the intensity of reflected light. Results (not plotted) for 100% black were identical with those for 6% black, presumably because the intensity of light reflected from the crystal faces of the graphite flakes is comparable to that scattered by the less crystalline, white titanium dioxide.

REFERENCES

1. Sinclair, D. and LaMer, V. K., Chem. Rev., 44, 245, 1949.

2. Ditchburn, R. W., "Light," Interscience Publishers, Inc., pp. 441, 480, 1953.

3. Van de Hulst, H. C., "Light Scattering by Small Particles," Wiley, 1957.

4. Lord Rayleigh, "Scientific Papers," Cambridge Univ. Press, 1, 1899; 4, 1903.

5. Mie, G., Ann. Physik, 25, 1908; Stratton, J. A., "Electromagnetic Theory," McGraw-Hill, Chap. IX, 1941.

6. Penndorf, R., New Tables of Scattering Functions, Geophysics Research Papers, No. 40, AFCRC-TR-56-204(6), Parts 1-6.

7. Gumprecht, R. O. and Sliepcevich, C. M., "Tables of Light Scattering Functions for Spherical Particles," Univ. Mich., 1951.

8. Lowan, A. N., "Tables of Scattering Functions for Spherical Particles," National Bureau of Standards Applied Mathematics Series No. 4, 1948.

9. Penndorf, R., "Research on Aerosol Scattering in the Infrared," Final Report, Air Force Cambridge Research Laboratories, Technical Report RAD-TR-63-26 (Report AFCRL-63-668), 1963.

10. Johnson, J. C., Eldrige, R. G., and Terrell, J. R., Science Report No. 4, MIT Dept. Meteorol., 1954.

11. Stephens, "Total Attenuation, Scattering and Absorption Cross Sections of Water Droplets," Report AFCRL-1011, 1961.

12. Kerker, M. L., "The Size and Shape of Colloidal Particles by Light Scattering," Technical Report No. 1, Clarkson College of Technology, ASTIA Report 26048, 1953.

13. Aden, A. L., J. Appl. Phys. 22, 601, 1951.

14. Van de Hulst, H. C., "Optics of Spherical Particles," N. V. Drukkerij, J. J. Duwaer and Sons, Amsterdam, 1946.

15. Sinclair, D., "Handbook on Aerosols," Chap. VII, Atomic Energy Commission, Washington, D.C., 1950.

16. Berry, C. R., J. Optical Soc. Am., 52, 888, 1962.

17. Blumer, Z. Physik, 38, 304, 1962.

18. Berry, C. R., Marino, S. G., and Oster, C. F., Phot. Sci Eng. 5, 332, 1961.

19. Naper, O. H. and Ottewill, R. H., "Electromagnetic Scattering," The Macmillan Co., New York, 1963.

20. Stevenson, A. F., Heller, W., and Wallach, M. L., J. Chem. Phys. 34, 1789, 1961.

21. Bradford, E. B. and Vanderhoff, J. W., J. Appl. Phys. 26, 864, 1955.

22. Kaye, B. H., British Patent No. 7173/58.